Par **Changjie YIN**

Impact of diesel generator operating modes on standalone DC microgrid and control strategies implying supercapacitor

Thèse présentée
pour l'obtention du grade
de Docteur de l'UTC

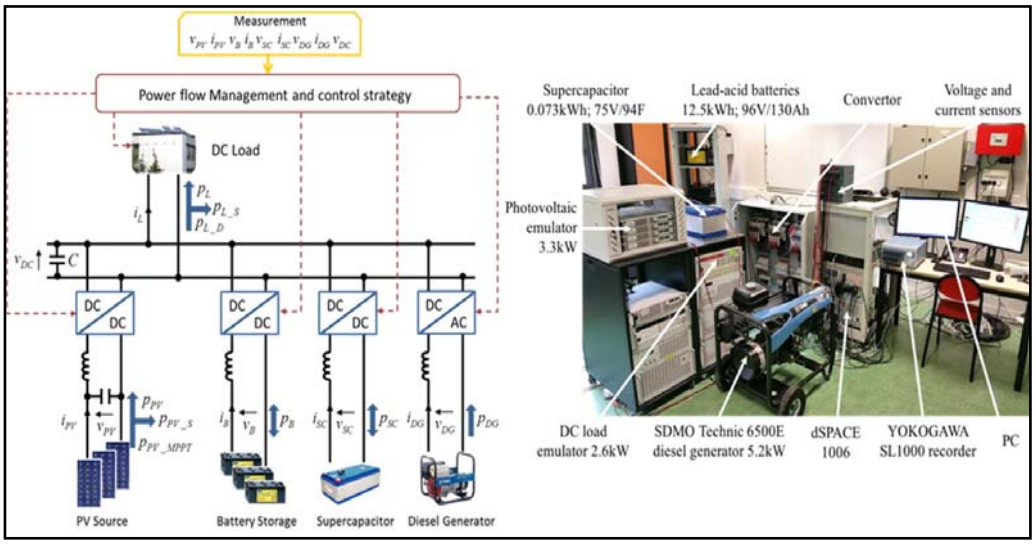

Soutenue le 23 février 2018
Spécialité : Génie Électrique : Laboratoire Avenues - GSU (EA-7284)

D2411

UNIVERSITÉ DE TECHNOLOGIE DE COMPIÈGNE

THESE

Pour obtenir le grade de

DOCTEUR

Spécialité : Génie Électrique

Changjie YIN

Impact of diesel generator operating modes on standalone DC microgrid and control strategies implying supercapacitor

Laboratoire AVENUES, EA 7284

Thèse soutenue le 23 février 2018 devant le jury composé de :

Rapporteurs :	Florence OSSART, professeure à Sorbonne Université, GeePs
	Bruno FRANCOIS, professeur à l'Ecole Centrale de Lille, L2EP
Examinateurs :	Franck BETIN, professeur à l'Université de Picardie Jules Verne, LTI
	Vincent LANFRANCHI, professeur à l'Université de Technologie de Compiègne, Roberval
Directeur :	Manuela SECHILARIU, professeure à l'Université de Technologie de Compiègne, AVENUES
Co-Directeur :	Fabrice LOCMENT, professeur à l'Université de Technologie de Compiègne, AVENUES

Université de Technologie de Compiègne - AVENUES -
Rue Roger Couttolenc, 60203 Compiègne

Abstract

The intermittent and random nature of renewable sources, such as photovoltaic and wind turbine, asks for the complement of storage, such as battery and back-up energy, such as diesel generator, especially in a standalone power system. Concerning the diesel generator, it needs some time to start up and cannot immediately offer the needed power, due to its dynamic behaviour. Hence, the power quality is lowered down during this period because of the shortage of power. Therefore, during the period of the diesel generator starting up, a supercapacitor is suggested to compensate the power balance because of its fast response and high power density. A power control strategy is proposed to achieve the coordination between diesel generator and supercapacitor. Both simulation and experimental results show that the proposed control strategy is able to regulate the DC bus voltage within the acceptable limits and supplying the load during the renewable power under generation or load step-increase situations.

In addition, the supercapacitor can be also used to overcome the electrochemical storage limits like its state of charge and maximum current. So, this thesis proposes the real time power control for a hybrid photovoltaic-battery-supercapacitor-diesel generator DC microgrid system, aiming to meet the load power demand with reliability and stabilizing the DC bus voltage. Both simulation and experimental results show that the designed control strategy improves the DC microgrid dynamic and static performances under different operating conditions.

Furthermore, in order to minimize the diesel generator energy cost, the fuel cost and fuel consumption are analysed through several experimental tests. Therefore, the optimal value of its power generation is deduced and applied in a newly proposed energy management strategy. This strategy can achieve the goal of maximizing the utilization of photovoltaic energy and taking into account the slow start-up characteristic and energy cost of diesel generator. Both simulation and experimental studies are carried out by using the real photovoltaic data to illustrate the performance and the behaviour of the hybrid system. The obtained results verify the effectiveness of this strategy. Furthermore, the comparison with the previous energy management strategy, in which the diesel generator energy cost is not considered, demonstrates that the newly proposed energy management strategy can reduce the total cost of the hybrid DC power system.

Keywords: DC microgrid; power management strategy; diesel generator energy cost; photovoltaic; supercapacitor; power balance.

Acknowledgements

First of all, I would like to express my sincere gratitude to my supervisors, Prof. Manuela SECHILARIU and Prof. Fabrice LOCMENT, for their good guidance and great efforts throughout the research and the writing of the thesis. Thanks to this teamwork and their well-organized working style, this thesis has advanced well according to the plan, which has permitted that the thesis work can be published in each stage. Thanks to Prof. Manuela SECHILARIU for the great advice and efforts in writing and revising of this thesis, as well as other publications. Thanks to Prof. Fabrice LOCMENT for the great help in the progress of my French language, as well as the experimental operations.

I also express my very gratitude to Prof. Florence OSSART and Prof. Bruno FRANCOIS, who have made detailed reports and remarks on my thesis, which help a lot in improving the quality of my thesis for both research content and presentation. Thanks also to Prof. Franck BETIN, chairman of the thesis defence committee, and Prof. Vincent LANFRANCHI for their interest in my work.

In addition, I would like to thank all the colleagues of the laboratory AVENUES and the department of GSU: Nassima MOUHOUS-VOYNEAU, Nathalie MOLINES, Carine HENRIOT, Jean-louis BATOZ, Josiane GILLES, Lydie DELETTRE, Eduard ANTALUCA, Gilles MOREL, Fabien LAMARQUE, Hipolito MARTELL-FLORES, and Cristina PRONELLO, for the good ambiance during my PhD studies at UTC and in France.

I also thank my colleagues (PhD students) and friends: Hossam AL-GHOSSINI, Leonardo TRIGUEIRO DOS SANTOS, Hongliang LIU, Walid BOUCHENAFA, Hongwei WU, Raphael ROLIN, Amine BEN DAOUED, Maroua BELFEKI, and Dian WANG, for sharing the PhD and life experience, for discussions on culture and customs, as well as on the study.

I would like to thank my friends Yongjiang LI, Kang YANG, Xuhong LI, Lei LEI, Liang MENG, Dingfu ZHOU, Lan LI, Shanggui CAI, Caiyun LIU, Yunchao PENG, Huiling LU, Rui ZHANG, and CongCong MA, and ma chérie, Gladys PAULO**,** for their help during my PhD studies and daily life.

I would like to thank the China Scholarship Council (CSC) for offering the opportunity to support my PhD study and life in France. I will treasure the experiences both academic and personal in my life.

Finally, a special bunch of thanks goes to my parents and my sister for all their love and encouragement to support me in finishing the PhD studies.

Table of Contents

Table of Contents 1

List of figures 5

List of tables 9

Abbreviations 11

Nomenclature 13

Publications associated with this PhD thesis 17

General introduction 19

Chapter I. Research background and thesis objective 25

I.1. Traditional grid and smart grid 26

I.2. AC and DC microgrid 31

I.3. Utilization of diesel generator in DC microgrid 34

I.4. Objective of the thesis 38

I.5. Conclusion 40

Chapter II. Diesel generator start-up compensation by supercapacitor 41

II.1. System modelling and description 42

II.1.1. Diesel generator system and modelling 42

II.1.2. Supercapacitor system and modelling 44

II.2. Power control strategy 47

II.3. Simulation verification 52

II.3.1. Shortage of renewable sources power 52

II.3.2. Sudden increase of load power 54

II.4. Experimental verification 55

II.4.1. Experimental platform 55

II.4.2. Shortage of renewable sources power 57

II.4.3. Sudden increase of load power 58

II.5. Conclusion 61

Chapter III. Power management of DC microgrid with DG load following mode 63
III.1. Description of hybrid system and its components..... 65
III.1.1. Photovoltaic array 66
III.1.2. Electrochemical storage 66
III.1.3. Supercapacitor and diesel generator 67
III.2. Power management strategy design 68
III.2.1. PV power is equal to the required load power 69
III.2.2. PV power is less than the required load power 69
III.2.3. PV power is higher than the required load power 71
III.3. Simulation results 72
III.4. Experimental verification 77
III.4.1. Experimental platform 77
III.4.2. Twelve experimental cases 78
III.4.3. One-day experimental test 84
III.5. Conclusion..... 87
Chapter IV. Power management of DC microgrid with DG economical mode 89
IV.1. Fuel consumption and cost analysis through experiment 90
IV.1.1. Electrical scheme and experimental platform..... 91
IV.1.2. Diesel consumption and cost optimization analysis 92
IV.1.3. DG operation and maintenance cost 95
IV.2. Power management strategy design 95
IV.2.1. System configuration 96
IV.2.2. Definition of energy tariff of each element 97
IV.2.3. Power management strategy 99
IV.3. Simulation results..... 102
IV.3.1. Simulation 1..... 103
IV.3.2. Simulation 2..... 109
IV.3.3. Simulation 3..... 112
IV.4. Experimental verification..... 115

IV.4.1. Test 1 116
IV.4.2. Test 2 121
IV.4.3. Test 3 123
IV.5. Economic analyses 125
IV.6. Conclusion 125
General conclusions and perspectives 127
References 133
Appendices 141
Appendix 1: Parameters of Solar-Fabrick series SF 130/2 143
Appendix 2: Parameters of Sonnenschein Solar: S12/130A 145
Appendix 3: Parameters of Maxwell 75V modules: BMOD0094 P075 B02 147
Appendix 4: Parameters of SDMO Technic 6500E AVR 153
Appendix 5: Parameters of programmable electric load PL-6000-A Puissance+ 155
Appendix 6: Parameters of IGBT module SEMIKRON SKM100GB063D 157
Appendix 7: Parameters of industrial driver (SEMIKRON SKHI22A) for IGBT 159

List of figures

Figure 1. Smart grid topology [11]. 31

Figure 2. General microgrid scheme [12]. 32

Figure 3. DC microgrid structure. 38

Figure 4. (a) Start-up voltage curve of DG without load and (b) the voltage curve between 4s and 5s 43

Figure 5. DG model. 44

Figure 6. Start-up voltage curve of real DG and of the DG model 44

Figure 7. SC model. 45

Figure 8. Profiles for different constant current discharge curves. 46

Figure 9. Voltage charging and discharging curve of experiment and simulation. 46

Figure 10. Configuration of the power system. 47

Figure 11. Control block diagram for the renewable source dominant mode. 48

Figure 12. Control block diagram of the supercapacitor dominant mode. 49

Figure 13. Control block diagram of the SC/DG cooperative control mode. 50

Figure 14. Control block diagram of the DG dominant mode. 51

Figure 15. Status of DG and SC in the conversion process. 51

Figure 16. Dynamic response of shortage of renewable power. 52

Figure 17. Detailed dynamic response curves of microgrid parameters before and after SC connection in the case of renewable power shortage. 53

Figure 18. Dynamic response curves of microgrid parameters 54

Figure 19. Detailed dynamic response curves of microgrid parameters before and after the SC connection in the case of sudden load power increase. 54

Figure 20. Experimental platform. 56

Figure 21. Dynamic response of shortage of renewable power. 57

Figure 22. Detailed dynamic response curves of microgrid parameters before and after SC connection in the case of renewable power shortage. 57

Figure 23. Dynamic response curves of microgrid parameters. 59

Figure 24. Detailed dynamic response curves of microgrid parameters before and after the SC connection in the case of sudden load power increase. 59

Figure 25. DC microgrid power system configuration [71]. 65

Figure 26. SOC of SC during the self-discharging. 67

Figure 27. Flow chart of the power management strategy when PV power is less than the required load power. 69

Figure 28. Flow chart of the power management strategy when PV output power is more than the required load power. 71

Figure 29. Solar irradiance and PV cell temperature on 16th April 2015. 73

Figure 30. Load power demand and PV MPPT power. 73

Figure 31. Power evolution. 75

Figure 32. *SOC* evolution of batteries. 76

Figure 33. *SOC* evolution of supercapacitor. 76

Figure 34. Evolution of DC bus voltage. 76

Figure 35. Image of experimental platform 78

Figure 36. Power evolutions. 79

Figure 37. *SOC* evolution of batteries. 79

Figure 38. *SOC* evolution of supercapacitor. 79

Figure 39. Evolution of DC bus voltage. 81

Figure 40. Power evolutions. 82

Figure 41. *SOC* evolution of battery. 82

Figure 42. *SOC* evolution of SC. 82

Figure 43. Evolution of DC bus voltage. 84

Figure 44. Power evolutions. 85

Figure 45. *SOC* evolution of batteries. 86

Figure 46. *SOC* evolution of supercapacitor. 86

Figure 47. Evolution of DC bus voltage. 86

Figure 48. The figure of experimental platform. 91

Figure 49. Three tests of declining curve of weight of fuel in 12 minutes experiment. 93

Figure 50. Declining curve of weight of fuel of different output power. 93
Figure 51. The diesel consumption rate along with the output power. 94
Figure 52. DG generation tariff along with the output power. 94
Figure 53. Topology of proposed off-grid DC microgrid system. 96
Figure 54. Flow chart of the power management strategy. 100
Figure 55. Solar irradiance and PV cell temperature. 104
Figure 56. Load power demand and PV MPPT power. 104
Figure 57. DC microgrid power evolutions. 105
Figure 58. *SOC* evolution of electrochemical batteries. 106
Figure 59. *SOC* evolution of supercapacitor. 106
Figure 60. DC bus voltage. 106
Figure 61. DC microgrid power evolutions. 107
Figure 62. *SOC* evolution of electrochemical batteries. 108
Figure 63. *SOC* evolution of supercapacitor. 108
Figure 64. DC bus voltage. 108
Figure 65. Solar irradiance and PV cell temperature. 109
Figure 66. Load power demand and PV MPPT power. 109
Figure 67. DC microgrid power evolutions. 110
Figure 68. *SOC* evolution of electrochemical batteries. 111
Figure 69. *SOC* evolution of supercapacitor. 111
Figure 70. DC bus voltage. 111
Figure 71. Solar irradiance and PV cell temperature. 112
Figure 72. Load power demand and PV MPPT power. 112
Figure 73. DC microgrid power evolutions. 113
Figure 74. *SOC* evolution of electrochemical batteries. 114
Figure 75. *SOC* evolution of supercapacitor. 114
Figure 76. DC bus voltage. 114
Figure 77. Off-grid DC microgrid experimental platform. 115
Figure 78. DC microgrid power evolutions. 117

Figure 79. *SOC* evolution of electrochemical batteries. 118
Figure 80. *SOC* evolution of supercapacitor. 118
Figure 81. DC bus voltage. 118
Figure 82. DC microgrid power evolutions. 119
Figure 83. *SOC* evolution of electrochemical batteries. 120
Figure 84. *SOC* evolution of supercapacitor. 120
Figure 85. DC bus voltage. 120
Figure 86. DC microgrid power evolutions. 121
Figure 87. *SOC* evolution of electrochemical batteries. 122
Figure 88. *SOC* evolution of supercapacitor. 122
Figure 89. DC bus voltage. 122
Figure 90. DC microgrid power evolutions. 123
Figure 91. *SOC* evolution of electrochemical batteries. 124
Figure 92. *SOC* evolution of supercapacitor. 124
Figure 93. DC bus voltage. 124

List of tables

Table 1. Differences between traditional grid and smart grid. 30

Table 2. Parameters of diesel generator. 43

Table 3. Parameters of supercapacitor. 45

Table 4. Elements detail for experimental test. 56

Table 5. Arbitrary values and limits. 74

Table 6. Elements detail for experimental test. 77

Table 7. Elements detail for experimental test. 91

Table 8. The diesel consumption rates. 93

Table 9. Arbitrary values, tariffs, and constraints. 103

Table 10. Elements detail for experimental test. 116

Table 11. Costs comparison of the different DG mode: duty cycle and load following. 125

Abbreviations

AC	Alternate Current
DC	Direct Current
DG	Diesel Generator
EDF	Electricité de France
HVDC	High-Voltage Direct Current
I/O	Input/Output
IGBT	Insulated Gate Bipolar Transistor
NOx	Nitrous Oxide
MPPT	Maximum Power Point Tracking
O&M	Diesel Generator Operation and Maintenance
PC	Personal Computer
PCC	Point of Common Coupling
PI	Proportional-Integral controller
PI_bus	PI Controller of DC Bus Voltage
PI_DG	PI Controller of Diesel Generator Current
PI_RS	PI Controller of Renewable Sources Current
PI_SC	PI Controller of Supercapacitor Current
PI_V_SC	PI Controller of Supercapacitor Voltage
PV	Photovoltaic
PWM	Pulse Width Modulation
RS	Renewable Sources
SC	Supercapacitor
STC	Standard Test Conditions

Nomenclature

a_{DG_1}	Coefficient of a linear fuel consumption function
a_{DG_2}	Coefficient of a quadratic fuel consumption function
b_{DG_1}	Coefficient of a linear fuel consumption function
b_{DG_2}	Coefficient of a quadratic fuel consumption function
c_{B_Ageing}	Batteries bank energy tariff (€/kWh)
c_{DG}	Diesel generator power production tariff (€/kWh)
$c_{DG\_O\&M}$	Diesel generator average O&M cost per hour (€/h)
c_{DG_2}	Coefficient of a quadratic fuel consumption function
c_{L_S}	DC load shedding tariff (€/kWh)
c_{PV_S}	Photovoltaic shedding energy tariff (€/kWh)
c_{SC_Ageing}	Supercapacitor energy tariff (€/kWh)
C	DC bus capacitor (μF)
C_B	Total Capacitor of batteries bank (kWh)
C_{B_Ageing}	Batteries bank aging cost (€)
$C_{DG\_O\&M}$	Diesel generator O&M cost (€)
C_{DG_Fuel}	Diesel generator fuel cost (€)
C_{L_S}	DC load shedding cost (€)
C_{SC_Ageing}	Supercapacitor aging cost (€)
C_{PV_S}	Photovoltaic shedding cost (€)
C_{Total}	Total energy cost (€)
C_{SC}	Capacitor of supercapacitor (F)
E_{SC}	Supercapacitor stored energy (kWh)
F	Diesel generator fuel consumption ((L/kWh)

f_{DG}	Diesel generator voltage frequency (Hz)
i_B	Batteries bank current (A)
i_B^*	Batteries bank current control reference (A)
i_{B_MAX}	Upper limit of batteries bank current (A)
i_{B_MIN}	Lower limit of batteries bank current (A)
i_{DG}	Diesel generator current (A)
i_{DG}^*	Diesel generator current control reference (A)
i_L	DC load current (A)
i_{RS}	Renewable sources current (A)
i_{RS_MAX}	Maximum current of renewable sources
i_{PV}	Photovoltaic current (A)
i_{PV}^*	Photovoltaic current control reference (A)
i_{SC}	Supercapacitor charging or discharging current (A)
i_{SC}^*	Supercapacitor charging or discharging current control reference (A)
I_{DG_RATED}	Diesel generator rated output current (A)
K_I	Integral gain of DC bus voltage controller
K_P	Proportional gain of DC bus voltage controller
p_B	Batteries bank power (W)
p_{DG}	Diesel generator output power (W)
p_{DG_MAX}	Diesel generator maximum output power (W)
p_{DG_RATED}	Diesel generator rated output power (W)
p_L	DC load power (W)
p_{L_D}	DC load demand power (W)
p_{L_S}	DC load shed power (W)
p_{PV}	Photovoltaic power (W)

p_{PV_MPPT}	Photovoltaic power by MPPT algorithm (W)
p_{PV_S}	Photovoltaic shed power (W)
p_{SC}	Supercapacitor power (W)
R_1	Equivalent series resistor of supercapacitor (Ω)
R_2	Equivalent series resistor of supercapacitor (Ω)
$Rate$	Diesel generator fuel consumption rate (gram/s)
SOC_B	State charge of batteries bank (%)
SOC_{B_init}	Initial state of charge of batteries bank (%)
SOC_{B_MAX}	Upper limit of state charge of batteries bank (%)
SOC_{B_MIN}	Lower limit of state charge of batteries bank (%)
SOC_{SC}	State charge of supercapacitor (%)
$SOC_{SC\_MAX\_MAX}$	Maximum value of the maximum state charge of supercapacitor (%)
$SOC_{SC\_MAX\_MIN}$	Minimum value of the maximum state charge of supercapacitor (%)
$SOC_{SC\_MIN\_MAX}$	Maximum value of the minimum state charge of supercapacitor (%)
$SOC_{SC\_MIN\_MIN}$	Minimum value of the minimum state charge of supercapacitor (%)
t	Continues time (s)
t_0	Initial time instant (s)
t_F	Final time instant (s)
T_{DG_run}	Diesel generator running time (h)
v_B	Batteries bank voltage (V)
v_{DC}	DC bus voltage (V)
v_{DC}^*	DC bus voltage control reference (V)
v_{DG}	Diesel generator Voltage (V)
v_{PV}	Photovoltaic Voltage (V)
v_{RS}	Renewable sources voltage (V)

v_{SC}	Supercapacitor voltage (V)
v_{SC}^{*}	Supercapacitor voltage control reference (V)
v_{SC_init}	The initial voltage of supercapacitor (V)
v_{SC_RATED}	Supercapacitor rated voltage (V)
V_{DG_peak}	Diesel generator amplitude voltage (V)
V_{DG_RATED}	Diesel generator rated output voltage (V)

Publications associated with this PhD thesis

The works presented in thesis are validated by several publications which have been accepted or submitted in journals and conferences. The details of them are listed as below:

Article in international refereed journal:

C. Yin, H. Wu, F. Locment, M. Sechilariu. "Energy management of DC Microgrid based on Photovoltaic Combined with Diesel Generator and Supercapacitor". *Energy Conversion and Management*, 2017 (132): 14–27.

Article in the process of submission for international refereed journal:

C. Yin, H. Wu, M. Sechilariu, F. Locment. "Diesel generator energy cost applied into the off-grid DC microgrid energy management". *International Journal of Electrical Power and Energy Systems*, 2018.

Articles in proceedings at international conferences:

C. Yin, H. Wu, M. Sechilariu, F. Locment. "Energy management of standalone DC microgrid". *ELECTRIMACS 2017 (International conference on theory and application of modeling and simulation in electrical power engineering including electric machines, power electronic converters and power systems)*, 4th-6th, July 2017, Toulouse, France.

C. Yin, M. Sechilariu, F. Locment. "Diesel Generator Slow Start-up Compensation by Supercapacitor for DC Microgrid Power Balancing". *ENERGYCON 2016 (IEEE International Energy Conference)*, 4th-8th, April 2016, Leuven, Belgium.

General introduction

Energy is the basis for human survival and society development. The rational use of electricity is like creating a sun in the night, bringing great convenience to mankind. However, the conventional fossil energy (such as coal and petroleum), which provides the driving force for generating electricity, is drying up gradually all over the world. At the same time, the problem of environmental pollution (such as climate change and greenhouse gas emission) caused by the use of fossil fuels is attracting increasing attention around the society and the governments around the world. As a result, governments are paying more and more attention to the development of renewable energy resources. Although the traditional power system network is still served as the main role of power supply, it can incorporate with the renewable energy resources, which are in the form of distributed generation sources and served as the necessary complement to the traditional electricity generation.

The distributed generation technology makes use of various dispersive energy sources, including green renewable energy (such as wind energy, solar energy, geothermal energy, biomass energy, tidal energy and small hybrid energy) and the local easily-accessible fossil fuels (such as natural gas, coal gas and diesel), in the form of single power generation unit and connect them to the traditional power grid to improve the environmental friendly degree. The capacity of small distributed generation system is within tens of kilowatts while the large one can be more than one megawatt. The use of distributed power generation technology helps to make full use of the rich clean and renewable energy around the users and to provide users with green power. It is an important measure to energy saving and emission reduction. Flexibility, economy and environmental protection are the main features of distributed power

generation technology. However, due to the intermittent and random nature of renewable energy sources, it is difficult to meet power balance by relying solely on their own regulatory capacity. Therefore, other power supplies are often required, such as the utility grid and the storage sources. Hence, according to its relationship with the main grid, distributed generation system can be classified as:

- Grid-connected system

  The distributed generation resources imply a total and permanent power injection into the main grid.

- Off-grid system

  The system can not only run together with the grid, but also run in off-grid mode when there is main grid failure or when it is needed to disconnect the main grid. Back-up power, like diesel generator (DG) and storage, is used together with the distributed sources.

- Standalone system.

  The system runs alone to support the users' demand and balance the power, mostly seen in remote areas or islands. Back-up power is strongly required in these cases.

As an effective complement to centralized power generation, distributed generation technology is becoming more and more mature. Along with the liberalized electricity market as well as the strong support of relevant government policies, the relevant technology is becoming more and more widely used nowadays.

However, the increasing number of distributed power supply into the utility grid also puts forward a new challenge to the operation of the utility power system. Unlike the hundred megawatts coal-fired generator or nuclear generator, which can be controlled directly by the power system operators, a large number of distributed small-capacity distributed power generation are often 'invisible' to the main power grid operators, some of which are even uncontrollable and less controllable. Just as large-capacity wind farms and high-capacity photovoltaic (PV) power plants have a lot of impact on the safe and stable operation of the transmission network, when the distributed power generation system achieves a higher proportion in the low-voltage distribution system, the power balance and reliable operation will be difficult to the personnel workers of operation. The existing structure and operation of conventional power distribution system is not well adapted to large-scale access demands of the distributed generation system. The increased development leads to the grid-connection incidents, which became true technical constraints. This is due to the hardly predictable and intermittent characteristics of the renewable power generation given its dependency on the environment and weather conditions, which is not participating in ancillary services (technical regulation of frequency and voltage) in current alternating current (AC) system. They behave like passive electric generator. Therefore, when there are fluctuations in both users' demand and renewable power generation, it is the conventional generation units to balance the power between generation and demand and to ensure the power quality. In face of these technical problems, research works are paying attention on grid integration and control of renewable decentralized

generation or developing new power system structure, energy and power management strategy, and real time power control.

A lot of research works have proposed the microgrid structure, which is a small generating and distributing power system. It includes low voltage distribution lines, distributed energy sources, power conversion devices, controllable loads, monitoring, and protection devices, which is an autonomous system being capable of self-control and self-management. Under this definition, the power is generated by itself and also absorbed by itself. Microgrid is regarded as a small power system, which has a very good energy management capability and can effectively maintain the energy balance and energy optimization within itself, providing power quality to the end user as well as increasing renewable energy penetration. It can also be defined as a group of interconnected loads and distributed generation units within clearly defined electrical boundaries that act as a single controllable entity with respect to the grid. Under this definition, microgrid is considered as a "virtual" power supply or load and connected to the larger outer power system at the point of common coupling (PCC). Through the coordinated control of the distributed renewable output power in the microgrid, it can play the role of load shedding, utility grid power valley filling and peak shaving. The influence of the fluctuation of the power generation on the external distribution network and the surrounding users is decreased and it also effectively reduces the difficulty of the control operation.

As aforementioned, the microgrid generally refers to the local power system connected to the utility grid, which can operate both in grid-connected mode and off-grid mode. In the grid-connected mode, the microgrid can receive power from the utility grid. On the contrary, excess power can be returned back to the utility grid. The microgrid and the outer medium voltage distribution network support each other to achieve the two-way flow of the energy. In the case of external power grid failure, the microgrid can be turned into independent operation mode, continuing to supply the important users within the grid.

As a special case of the conventional microgrid, the standalone microgrid is not connected to an external distribution network, which is always working in off-grid mode, fully utilizing its own distributed power generation to meet the load demand. This microgrid is generally equipped with energy storage system to suppress the power fluctuations of renewable energy, in the full use of renewable energy on the basis of meeting the needs of different loads in the different periods of time. On the other hand, it is possible that the energy storage is used up because of the long-term bad weather. Therefore, back-up power, like DG, is very important to start up to continue to supply the users. To meet the basic requirements of the user's electricity, this type of microgrid is generally used in islands, mountains and remote areas where the conventional power distribution system is difficult to reach and/or very expensive.

According to this context, this thesis intends to make a further contribution on the real time power control of the standalone microgrid. This study presents a direct current (DC) microgrid consisting of PV sources, an electrochemical storage system (batteries), a supercapacitor (SC), a DG, and a DC load (electric appliances of buildings and houses). As the main back-up power, DG is studied to understand its start-up characteristic. A local rules-based power management for the real time control is designed to start up the DG accordance with the SC, to meet the load demand and stabilize the DC bus voltage. Then, the diesel consumption status is obtained through experiments. Based on the DG production tariff under different output power value, another rules-based energy management strategy for the real time power control is proposed to further enforce the power supply reliability and power system stability. The economic criteria are chosen and the energy cost of system in one day is calculated. The results show that the latter strategy is more cost saving than the former strategy. Both of the energy management strategies are verified through the experiments, the results of which showing that the proposed strategies are able to balance the power and maintain the DC bus voltage stable.

The thesis is organized in four chapters. After the general introduction, Chapter I firstly gives the research background and thesis objectives. By comparing the traditional grid and smart grid, the thesis summarises the driving force of the smart grid and answers the question why the human needs to develop the smart grid. As the local level of smart grid, microgrid is regarded as one of the promising solutions to construct the smart grid. According to the form of power transmission, AC microgrid and DC microgrid are compared. It points out that, with the development of technology and the consideration of the energy conversion stages efficiency, DC microgrid is a better choice in the future power system. Therefore, this study focuses on DC microgrid, consisting of PV sources, batteries storage, DG, SC, and DC load. Chapter I gives also the relevant review of the utilization of DG in the DC microgrid. At last, this chapter outlines the objectives of the thesis.

In Chapter II, SC is used as compensatory energy to overcome the sluggish dynamic behaviour of DG while starting up. Firstly, based on the experimental results and technical notice data, simplified DG and SC models are presented. Then, a power control strategy is proposed to achieve coordination between DG and SC, to resist against the shortage of renewable power or the sudden load power surge. The individual control schemes are coordinated through the proposed control coordination approach to maintain the DC bus voltage stable and the system's power balance. The control strategy is verified by simulation and experiment. The results show that the proposed control strategies are able to regulate the DC bus voltage within the acceptable limits and supplying the load during renewable power under generation or load step-increase situations.

Based on the study of SC/DG coordinating control strategy, Chapter III further develops a whole power management strategy for the real time control, which controls the operation of an off grid and standalone DC microgrid, consisting of PV source, battery storage, SC, DG and DC load. It implements the SC/DG coordinating control strategy into the following rule based energy management strategy. SC and DG operate together to balance the DC power and stabilize the DC bus voltage, during the period of

starting up DG. On the other hand, SC is used to supply/absorb power when the needed batteries power is out of the range of its discharging/recharging power. Thus, this section firstly presents the hybrid system including PV, batteries, SC and DG. Then, an energy management strategy is proposed to achieve coordination between these sources. Simulation with a real PV profile is done for validation of this strategy, which consists of twelves cases. Then, controllable experimental cases are operated to verify all the twelve possible cases. In addition, a one day experiment is operated to verify the feasibility of implementing the energy management algorithm in a real environment, based on the real weather data. The results show that the proposed control strategy is able to regulate the DC bus voltage within the acceptable limits, balance the power, and supply the DC load.

At the beginning of the chapter IV, the experimental analysis of DG is done to understand its energy cost and fuel consumption. Based on several tests a precise fuel consumption function contributes to the research of the optimal operating mode of DG and the calculation of total energy cost of the whole power system. The environmental temperature influence on the operation of DG is also studied by means of experimental methods. Then, the diesel fuel consumption rates under different DG output power values are also obtained by several experiments. Therefore, a precise DG power production tariff is deduced, which are used in the following parts. According to the instruction manual of its manufacture, DG operation and maintenance cost is also defined in this part. And then, considering the DG energy cost, an improved energy management strategy for the real time power control is newly proposed. The aim of this strategy is to provide a continuous supply to the building with a low energy cost under relevant constraints. The simulations are firstly done to verify the control strategy theoretically. Then, an experimental platform is set up and the power management strategy is implanted into the real-time control system. The experimental tests, for both DG duty cycle mode and DG load following mode, are carried out with the experimental platform. To analyze DC microgrid validation and its technical feasibility, three test studies, corresponding to three types of solar irradiance evolution, are proposed and discussed following the two DG operating mode: duty cycle and load following. Given the obtained experimental results, the feasibility of DC microgrid control with the power management strategy, in real operation with respect to rigid constraints, is validated. In addition, the energy tariff of each element is defined and the total cost of the whole system is calculated. Compared with the DG load following mode, the fuel cost is reduced in the newly proposed strategy with a reasonable operation mode of DG (duty cycle), which is good from economic point of view and environmental point of view (reducing the emissions).

General conclusions and perspectives of the proposed off-grid DC microgrid research are given in the end.

Chapter I. Research background and thesis objective

After entering into the 21st century, the governments and research institutes evidently pay close attention to the energy and environmental problems, such as increasing growth of energy demand, depletion of fossil energy, the emission of greenhouse gas, global warming, the promotion of ecological civilization awareness and the requirement of the power supply reliability. With the proposition of Paris Agreement at COP21 [1], the world-wide countries will take further measures to realize the goal of reducing the risks and impacts of climate change and global warming. Concerning the field of electrical power system, it asks for the change and improvement of the existing power grid system: the smart grid has come into the field of researchers' vision [2,3]. As the basis of smart grid, microgrid that combines distributed energy resources and loads is believed as an effective and promising approach to achieve high level renewable energy penetration into smart grid [4], in which the power is generated and absorbed by themselves so that to decrease the influence on the utility grid. With communication technology [5,6], microgrid can interact with smart grid in order to assist grid power balancing by an advanced energy management and so to reduce the cost and to improve power quality. In microgrid, the output power of many distributed generation sources is in the form of DC form, such as PV power generation and fuel cell power generation. With the development of society and technology, the DC load is increasing largely in our daily life, such as electric vehicles, solid state lighting systems, and motors speed variation systems. Therefore, DC microgrid attracts more and more attention both in industry field and academic circle. However, the intermittent and uncertain characteristics of renewable energy

sources give rise to the requirement of backup power, such as DG and gas turbine generator. DG, or bio-diesel generator, is a good choice because of its ease-removability and ease-accessibility. This chapter gives a review of issues about research background, places DC microgrid concept and its comparison with AC microgrid, and the application of DG.

I.1. Traditional grid and smart grid

In the 21st century, the power industry is facing enormous challenges. In order to meet the new needs of economic and social development and to upgrade the existing power system, many countries and governments gradually form and finally propose the smart grid as the core content of development planning of electrical power system, in accordance with their national energy resources and current power system characteristics.

In United States of America, electric power research institute has proposed the future development power grid concept, which is called as Intelligrid [7]. In April 2003, senior experts from the power companies, power equipment manufacturers, federal and state government officials, universities and national laboratories, gathered together to discuss the future of the united states power system. After the meeting, in June 2003 on behalf of the meeting, the United States Department of energy transmission and distribution office published a report named "Grid 2030 - power of the next 100 years of national vision" [8]. This report can be described as a programmatic document of the US electricity reform, depicting the future of the United States power system vision, and to determine the various stages of research and development and experimental work objectives. At the beginning of 2009, the former President Obama signed the American Economic Recovery Investment Act (2009) [8] and made the construction of the smart grid the main content of the United States economic revitalization plan. He took smart grid as the core of the energy development strategy, actively responding to global warming, the international financial crisis and the United States economic revitalization, which makes the concept of smart grid, gradually get the attention of national research institutions and power companies.

European countries have different modes of grid operation and the demand for electricity is gradually saturated. The energy policy of Europe emphasizes the protection of the environment and the development of renewable energy generation and the low carbon economy. At the same time, the European power companies are subject to competition from the open electricity market pressure, needing to improve the quality of power supply services, to improve customer satisfaction, and to win more customers. Therefore, improving operational efficiency, using more renewable energy, lowering down power prices and strengthening customer interaction have become key issues to construct the European smart grid. In 2005, the European Commission for the first time proposed the concept of "smart grid" and established the "Smart Grids European Technology Platform", the goal of which is to transform the traditional grid into the user and operator interactive service network, to improve the

European transmission and distribution system efficiency, security and reliability, as well as to remove the barriers to the access of large-scale distributed generation power. In 2006, the Forum published two important documents: "The Vision and Strategy of the Future Grid in Europe" [8] focuses on the vision and needs of the future European power grid; the "Strategic Research Agenda (SRA) for Europe's Electricity Networks of the Future" [9] focuses on the priorities of research and highlights the development priorities and routes of the European smart grid, which is updated in 2012 [10]. The two documents describe detailed the European Smart Grid development roadmap, to carry out related projects and to promote the realization of smart grid. According to the European grid strategy in the future requirements, by 2020 the proportion of renewable energy sources in Europe well increase by 20%, energy efficiency will increase by 20%, greenhouse gas emissions will decrease by 20%, therefore known as the 20/20/20 plan. On September 16, 2009, the European proposed in the "Energy Technology Development Strategy": 30 cities will be selected as the smart grid pilot cities, in order to become the world leader in green technology competitions.

On May 21, 2009, the ex-chairman of the board of State Grid Corporation of China, Liu Zhenya announced the development strategy of building a strong and smart grid in China, at the 2009 international conference on extra high voltage transmission technology. It clearly stated that based on the special high-voltage grid as the backbone grid, by using the advanced communications, information and control technology, the strong smart grid will be constructed. It can realize flexible access and convenient use of diverse power users and different characteristics. It can greatly improve the ability of power network optimization and configuration, greatly enhance the service capability of power grid, and promote the power industry and other industries. This technology upgrade is to meet China's economic and social development requirements, coordinated and sustainable development requirements. This major strategic decision will be a strong impetus to China's smart grid research and construction, especially in this special period of the current financial crisis, which has seriously affected the China's economy.

The countries all over the world are researching on smart grid. But it does not have a definite and doubtless concept, and the worldwide experts in various fields elaborate on the connotation of the smart grid from different angles. With the depth of research and the understanding of practice on smart grid, it will be redefined and be enriched in the contents.

Broadly speaking, smart grid, which is essentially defined as intelligent, is based on integrated, high-speed two-way communication network, through the application of advanced intelligent sensing and measurement technology, communication technology, information processing technology, and decision support system technology application, to achieve the safety, reliability, economy, efficiency of the environmentally friendly electrical power system. According to the development of smart grid around the world, the driving force of the smart grid will be summarized as follows in several aspects:

(1) Energy depletion and environmental pressures.

With the rapid growth of global energy demand, the reliability of energy supply and national energy security has put forward a severe test to the world; global warming and environmental pollution problems are increasingly serious, making the environmental constraints more stringent. Resource-saving and environment-friendly development objectives require the power industry to shoulder the energy-saving emission reduction, the development of low-carbon economy, safeguard the economic and social development. To develop wind energy, solar energy, biomass, and other renewable energy has become an inevitable choice. These renewable energies, both large-scale and small-scale or individual local plants, have to be connected with the utility grid to supply the users. As the generation of wind power, PV power is also greatly affected by the weather conditions. Their intermittent and uncontrollable characteristics will increase the power mismatching in the utility grid and cause fluctuations in voltage and frequency, or even blackout. So, the power grid is required to be stronger and more compatible to solve these large-scale renewable resources development, access and consumption, to truly realize the effective use of green energy. Therefore, the research on smart grid, which is to protect energy supply security and to ease the pressure of resources and environment, is of great significance.

(2) Power grid security and a wide range of electricity demand.

With the rapid development of modern power grid and the gradual formation of interconnected power grid, ultra-high voltage, long-distance transmission, AC-DC hybrid, large power supply side and large power demand side, diversification of power generation forms and other characteristics become increasingly obvious. Power grid operating conditions are more complex. So, how to effectively resist all kinds of serious faults and how to reduce the risk and harm of accidents put forward great challenges to the planning, operation and management of power system. The future power grid should have integrated coordination and management level, a high degree of flexibility and reliability to enhance the ability to control the safe operation of large power grids. The large power grid can be flexibly dispersed into small microgrid. At the same time, with the improvement of people's living standards, the demand for power supply reliability, power quality and power services, is increasing. In addition, with the progressive development of small wind power, PV power generation, small hydropower, electric vehicles, and other distributed power sources, the distribution network has to meet the two-way trend (from power generation to the users and inversely). So, there is an urgent need for intelligent power technology to support these requirements.

(3) The global financial crisis.

Before the global financial crisis, the scholars have begun to imagine the future of power grid, which should have a variety of intelligent functions, and put forward the idea of smart grid which did not attract enough attention at that time. The outbreak of the financial crisis prompted many countries to introduce the economic stimulus plan. As the basis for economic development industry, the upgrading of the power

grid not only influences the people's livelihood but also promote the development of related industries (information industry, materials, equipment manufacturing, renewable energy etc.). Smart grid is not only conducive to promote economic growth, but also ease the employment pressure. Therefore, the financial crisis has become an iconic event to forcedly drive the rapid development of smart grid. Especially after the United States Obama government proposing smart grid development strategy, the idea of smart grid gradually gets the world recognition and attention.

(4) The demand of economic operation under electricity market environment.

Facing the need of resource-saving and environment-friendly social development, the grid is necessary to fully improve energy efficiency, but also energy-saving and environmental protection and to achieve economic operation. Therefore, to promote the use of energy efficient power generation and transmission equipment, to improve power generation scheduling and to strengthen demand side management, are the future developments of the power grid requirements. On the other hand, if all the generators can run near optimal output, the installed capacity can be greatly reduced, which can save social resources and reduce greenhouse gas emissions. What is more, under the environment of liberalized market competition, power generation enterprises, transmission enterprises and distribution enterprises should also optimize the utilization of equipment, reduce the costs and absorb more customers as much as possible.

(5) The new technologies and new equipment are widely used.

New technologies and new equipment, such as information, communication, network, computer, renewable energy, energy storage, and power electronics and so on, have been widely used in the power system. They provide technical support to the operation and control so that the smart grid is possible to achieve.

Therefore, compared with the operation mode of traditional power grid, the smart grid is a complete enterprise-class information framework and infrastructure system. It can achieve continuous monitoring of customers, the assets of electric enterprise and the power operation, so that to improve management level grid reliability and the users' service level. The energy resources are not properly configured in the traditional way of electricity distribution, resulting in energy and wealth losses, but smart grid can eliminate such waste, by temporarily selling the unused power to other People who need electricity according to the power resources market. In addition, the smart grid can combine the centralized generation and a large number of "plug and play" distributed power generation. It is a flexible architecture by intelligently reorganizing the system's structure and optimizing the grid control at all levels, to get the best system performance configuration. According to the above analysis, the specific differences between the traditional grid and the smart grid are shown in Table 1.

Table 1. Differences between traditional grid and smart grid.

	Traditional grid	**Smart grid**
Power sources	Dominant centralized power generation	Centralized power generation assisted by a large number of "plug and play" distributed generation
Renewable energy	Difficulty on absorbing the power generation of large-scale renewable energy	Support the access and integration of large-scale renewable power generation
Power quality	Power outages are concerned but rarely care about power quality.	Both power reliability and power quality are guaranteed
Self-healing	Cut off users to protect the electrical assets and equipment if there is an emergency, natural disasters or even terrorist attack	Prevent power failure, reduce the ill impact, resist attack, have fast recovery capabilities.
Information flow	Rarely concern about the user needs, one-way information stream and power flow	Interact with the users and two-way information exchange
Electricity price	Constant electric price with few changes	Time-of-use tariff

As the local level of smart grid, microgrid is regarded as one of the promising solutions to construct the smart grid. The power is generated locally and consumed by the local users. The microgrid can participate in the global smart grid interaction with a bidirectional information communication, which is based on proper routers and protocols. Several microgrids can be organized together through a dedicated adaptive controller and they are connected to the traditional utility grid by the PCC. A microgrid can also operate in islanded operation mode through the intelligent switches, if there is power failure and electricity fault either in the utility grid or in the microgrid itself.

AVENUES laboratory has been working for more than nine years on the DC microgrid as the main body of smart grid, in order to optimize the local energy sources and users' demand and to pursue the power quality. The research aspects include the human-machine interface, power prediction, the design of the energy management strategy, and the detailed operation and control of the distributed sources. The smart grid topology presented in Figure 1, shows the vision of the smart grid structure and the role of microgrid.

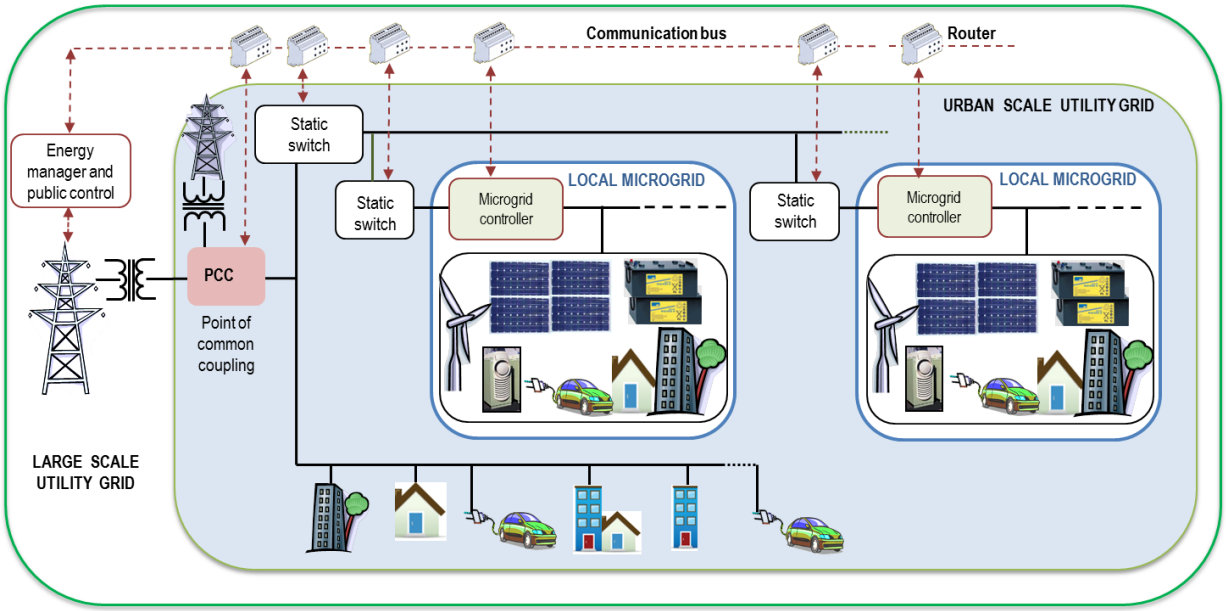

Figure 1. Smart grid topology [11].

I.2. AC and DC microgrid

Different countries and different organizations have different definitions of microgrid and the microgrid structure also varies according to different applications and projects. But after synthesizing these researches and studies, microgrid can be generally considered as a small low-voltage system, which composes of distributed generation resources, energy storage device, load and its monitoring and protection devices. The internal power supply of microgrid is mainly clean energies, which are connected to the main bus by power electronic devices. These electronic devices are controllable to balance the power within the grid and the operation mode (grid-connected mode and off-grid mode). Compared to the external utility grid, microgrid can be expressed as a single autonomous control unit: if the external utility grid is in the normal state, microgrid operates as a controllable and dispatch unit, reducing the effects of the influence of intermittency and uncertainty of distributed generation on large power grids; when the large power grid fails or the power quality does not meet the requirements, the microgrid can operate independently as an autonomous system to increase the flexibility and reliability of the power supply to the internal load of the system.

Concerning microgrid approach, several main advantages can be given: improving renewable energy penetration level, better energy supply for remote areas or islands, power balancing at local level with self-supplying possibility, and maintaining load supply during standalone operation or off-grid mode. Figure 2 displays the general microgrid scheme.

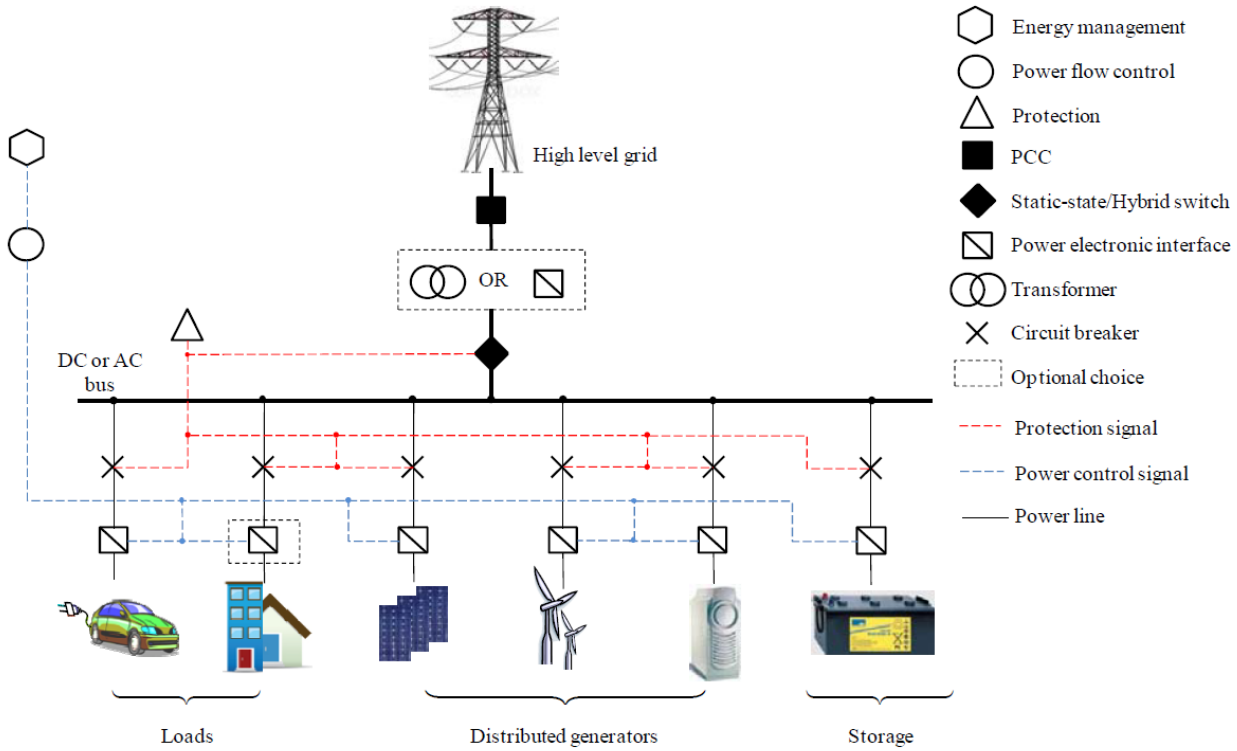

Figure 2. General microgrid scheme [12].

According to the form of power transmission within the microgrid, it can be divided into AC microgrid [13,14], DC microgrid [15,16] and hybrid AC/DC microgrid [17,18]. In the DC type microgrid, a large number of distributed power and energy storage systems directly supply the DC load through the DC main grid; and for AC load, the use of power electronic converter device will convert DC power into the AC form. In the AC microgrid, the output of all distributed power and energy storage systems is first converted to AC power to form an AC backbone network and then directly given to AC load; and for DC load, AC power is converted to DC power by means of power electronic invertor. In the hybrid microgrid, either the DC load or the AC load can be directly supplied from the microgrid without the power conversion between AC and DC. That is to say, the renewable sources (RS) that generate DC energy, and the DC loads are connected directly in the DC bus while the AC loads and the AC power sources are connected on the AC bus.

As for the present, the microgrid mainly adopts AC microgrid structure, because the electrical form of utility grid is AC form and the AC loads are still the principal loads. But more high-voltage direct current (HVDC) transmission lines have been built in MW level [19], while DC grid has already been used for years, such as telecommunication systems, data centres [20]. In addition, with the access of a large number of DC loads, like light-emitting diode lighting, electrical vehicle and variable-frequency drive machines (refrigerators, heaters, air conditioners, washing machines), and the large-scale application of renewable energy sources, it is the extension of DC to future appliances and to those that were traditionally operating on AC backbone that will make a true difference.

Compared with DC configuration of microgrid, AC microgrid has advantages in the following two aspects. Firstly, increasing or decreasing AC voltage is easy and economical by the transformer while DC transformation needs specific power electronic devices. But with the development of high-power converter technology [21], the DC transformation has already become easy and convenient. Secondly, the technology of AC circuit breaker is much more mature than DC and breaking the high current rating of DC circuit is much more difficult. After all, the present electrical AC power supply systems are the invention of a long-term technological development which started at the end of 19th century. However, ABB's Hybrid HVDC Circuit Breaker has partly solved this 100 year old dilemma [22,23].

Even though there are some problems in DC system, its advantages gain more than its shortcomings and these merits are not available in AC power grid.

1) The output form of the most renewable energy sources is the DC form. PV generation and fuel cells can be easily connected to DC microgrid with a DC/DC converter stage while it needs a more DC/AC invertor stage to transform the DC power into AC power in AC microgrid. So, the AC microgrid requires at least double commutation devices, resulting in, on the one hand an increase of system investment, on the other hand the poor reliability and flexibility of system.
2) There is no need for thinking over the synchronization. The varieties of distributed AC sources in DC microgrid, such as wind turbine, DG and micro gas turbine, are integrated into DC bus through the AC/DC rectifier. The control is relatively simple and there is no longer need to consider the output voltage frequency, phase synchronization and other issues. In addition, between DC microgrid and large power utility grid, it needs only a bidirectional flow DC/AC converter.
3) There is no reactive power in DC bus. Since no reactive power is present in DC bus, the AC sources could run with only active power so that the power efficiency and power transfer ability are increased. In addition, the DC bus voltage is the only parameter that characterizes the power balance in DC microgrid. It is the only control goal of DC microgrid. That is to say, the power balance of each unit in the DC microgrid system can be realized as long as the stability of the bus voltage is ensured. The control of the power flow in the grid can be realized directly by controlling the current flow direction.
4) The power quality is improved. As DC/DC conversion significantly reduces the distortion and clutter of current which often are introduced by the AC/DC conversion process, the DC microgrid can significantly improve the quality of power supply. The AC/DC converter between DC microgrid and AC utility grid can effectively isolate the disturbances caused by the large-scale power grids. DC microgrid can be cut off from the large power grids in the event of a large power grid failure. This improves the quality and reliability of the power supply.
5) Higher efficiency. With the development of technology, a large number of DC load springs up in the family house and office buildings [24]. But conversion from AC to DC often loses energy.

6) In the reality of a variety of DC microgrid projects, the system design is easier. DC systems do not suffer from skin effect, so thinner cable can be used with improved material efficiency. The line cost can be controlled in an acceptable range.

To sum up, compared with AC microgrid, DC microgrid is easy to realize the coordination of distributed sources and energy storage within the grid. The power control management is simple and reliable to achieve the power flow and the energy scheduling, to improve the power quality and the supply reliability, to obtain a higher efficiency and lower expense. Under the traditional large grid structure of AC transmission, DC microgrids show good adaptability to distributed generation and micro source of renewable energy, especially the sources in DC output form. Because of its internal use of DC transmission, there is a series of outstanding advantages. In the new energy power generation and smart grid development trend, the DC microgrid has broad prospects in the future.

I.3. Utilization of diesel generator in DC microgrid

Even though renewable energy is gradually taking up the main power sources in DC microgrid, the traditional fossil energy source, like gas turbine and DG, still acts as a component connected into the DC bus in some DC microgrid structure, especially for standalone microgrid. This is because of the intermittent and uncertainty characteristics of renewable energy. In the PV power dominant DC microgrid, it is possible that there is no power output in the daytime if it is overcast and it is sure that there is no power output in the night. In the wind power dominant DC microgrid, obviously, there is no power output or insufficiency if the wind forth is not enough. Therefore, when operating in standalone or off-grid mode, DC microgrid needs backup energy to deal with the intermittent feature of renewable energy. However, bio-diesel generator may be also considered.

When the microgrid operates in grid-connected mode, the outer utility grid is a better choice than DG to supply the users' demand when the renewable source is not enough. This is because that the prize of electricity of utility grid is evidently lower than the energy cost of DG. Taking the company Electricité de France (EDF) as an example, the prize of peak hours is 0.1593 euros/kWh, while in the off-peak hours, the prize is 0.1252 euros/kWh [25]. However, the prize of diesel is 1.25 euros/litre [26]. When the diesel prize is converted into the electricity prize, the energy cost of DG is much higher than the electricity bought from the DEF. The energy cost and fuel consumption of DG will be analysed by experiments in detail in the beginning of Chapter IV. Therefore, this thesis mainly discusses the standalone DC microgrid or DC microgrid in off-grid mode, which needs the back-up sources.

For a small-scale PV generator as the main renewable source, the lead-acid battery is commonly utilized as energy storage because of the comparatively low cost with respect to its good performance [27]. Due to the size and economic constraints, the capacity of battery storage is limited [28]. Therefore, it is possible that there is not enough power supply after battery storage is used up.

In conclusion, the plug and play backup power resource (like gas turbine and DG) is very important for off-grid microgrid to guard against the deficiency of RS and storage. On the other hand, the power supply from traditional DG is controllable and independent of weather and climate conditions [29]. DG can be a good choice for using as backup power due to its several advantages, such as low investments, ease of move and compatible combination with other energy sources and storage system in hybrid configurations [30]. The integration of a DG into a renewable energy generation based on DC microgrid system enhances the regulation of DC bus voltage and power support.

According to the operational mode of DG and the research work of others scholars, DG can be operated in continues-running mode to participate in maintaining the power balance of the whole system as one of the main power sources, or is regarded as backup energy which is used when needed. Once the DG is stated up, it can also operate in load-following mode (only supply the load) and in duty-cycle mode (not only supply the load but also recharge the storage).

Several energy management strategies and control methods of DC microgrid have been proposed. In [31], the control strategy uses DG as back-up power to study the multi-objective optimization of a stand-alone PV–wind–diesel DC power system with batteries storage, by using the HOGA software. The optimization results show that in many cases the DG is a good option to be added in the hybrid system. In addition, the DG is a backup source of electrical energy that is independent of the meteorology. In [32], a power control and energy management for an hybrid standalone diesel-wind-battery system is investigated through experimental methods. The system is managed by the developed controller which ensures the automatic start and stop of the emergency DG as needed and instant control of the battery charge state. The principal role of the developed controller is to continuously supervise the input power and load demand and to optimize the diesel operation under all working conditions. In the PV-DG-battery DC microgrid presented in [33], DG serves as the backup energy source and only operates to supply the power in the case of insufficient PV power and battery storage. A nonlinear adaptive backstepping controller is proposed to balance the power and stabilize the voltage of DC bus. In [34], the power from PV system and DG is controlled by the designed linear quadratic regulator controller in a PV based DC microgrid. The DG is only started up to supply the power when the PV power is not enough and battery storage is exhausted. In [35], backup diesel generation is used when there is shortage in electricity. Both a centralized and a decentralized demand-response multi-agent control and management system are devised to minimize the operational cost and inconvenience of electricity consumers. In [36], the pumped-storage hydroelectricity is used to store or release energy when the PV and wind turbine generating power is sufficient or short. If all of them cannot response the load energy requirement, DG would serve as the last resort. In [37], both the load following control strategy and cycle-charging dispatch control strategy are considered and compared in the proposed PV-DG-battery power system. Two tests using real metrological data and load demand have been done to validate the proposed hybrid system.

Different from the above research work, in the paper [38], the DG is operating all the time to participate in the power balance of an isolated DC microgrid, which includes wind turbine, PV panels and battery storage. A discrete Fourier transform method for the coordinated dispatch of battery and DG is proposed in this paper to compensate the power fluctuations and lower the fuel consumption of the system. In [39], battery and SC are used to improve the performance of wind-DG generation by absorbing disturbances due to wind speed variations. But in this power management, DG is operated continually to replenish the deficient power and regulate the bus voltage. So, if there is no deficient power, the DG is still operating to stabilize the bus voltage, which is not indeed economical. In [40], two control strategies (continuous operation control and on/off control) are applied to the PV-DG-battery hybrid system. Continuous control has more fuel saving while on/off control achieves more DG daily operating time reduction. However, the pros and cons of long running time and several starts and stops are not clearly investigated in this paper.

However, the fuel combustion efficiency and power generating efficiency are proved to decrease in case of low load operating mode [41], especially for small size DGs. Thus, there are some works which study variable speed control method of DG to reduce fuel consumption and greenhouse gas emission [42]. One notes that the commercial DG is often fixed speed synchronous generator. Thus, for a small size DG in a small-scale microgrid, DG would be better to be regarded as backup energy source which is involved only when needed.

Even though DG is a good choice as backup energy source to support a long-time operation in off-grid DC microgrid, it cannot output power immediately as needed because it takes several seconds, even several minutes, depending on the machines' capacity, to output the stable power [43]. In [44], it is also considered that fuel-based generators needs a warm-up period for a certain length of time to reach a safe operating temperature and to stabilize the output power before being connected it to the grid. Power interruptions during the DG start-up can cause the interruption of the entire microgrid power system. The power interruptions are very costly and unacceptable to the critical power consumers, such as hospital, data centre and security system, etc.

Thanks to its rapid power response and high-power density, SC is a solution that may solve the discontinuity problem of power supply during DG start-up. The research work in [45], uses SC to improve the dynamic characteristics and to compensate the sluggish dynamic behaviour of a variable speed commercial diesel engine in an isolated system. In [46], SC is applied to improve the sluggish dynamic response of the diesel engine for hydraulic mining shovels, to make the diesel engine a nearly constant speed while keeping the DC bus voltage stable. In [47], the evolution of specific fuel consumption versus the specific DG generating power is presented. The proposed energy management of PV-battery-DG hybrid system can get evident savings in the fuel cost (-7.8%), compared to the case of using only DG. In [48], it presents an optimal energy management for PV-DG-battery hybrid off-grid power system, to minimize both fuel costs and battery wear costs. The DG runs in load-following

strategy to only supply the load, so that there is no fuel cost comparison with the duty cycle mode in which DG also recharges the battery.

The handbook of manufacturers gives generally the basic information about DG, such as the rated power and the root-mean-square value of output voltage, but the situation of fuel consumption is not clearly addressed, especially in low power situation. To overcome this issue, in the papers [49,50] the linear regression function is used for fuel consumption calculation, based on its rated power P_{DG} and the actual output power p_{DG} of the DG. According to other research work [51,52], the specific fuel consumption, noted F (L/kWh), can be formulated as a quadratic function of the corresponding generated power.

$$F(p_{DG}) = c_{DG\_2} p_{DG}^2 + b_{DG\_2} p_{DG} + a_{DG\_2} \tag{1.1}$$

where c_{DG_2}, b_{DG_2} and a_{DG_2} are the coefficients of fuel consumption function and can be found by curve fitting by the Approximate Diesel Fuel Consumption Chart given by different manufacturers [53].

In the research work [54], a similar third order polynomial fuel consumption cost function is also obtained by being fitted to this fuel consumption chart. However, this chart shows an estimate of the fuel consumption of a DG based on the size of the generator and the load at which the generator is operating. As various factors can alter the fuel consumption, this chart is not an exact figure; it is based only on consumption per hour. Therefore, the exact fuel consumption should be known by experiments.

After concluding the control problems and the energy cost description of DG in the above context, the lake or shortage in the recent research about the utilization of DG in DC microgrid can be summarized in three aspects:

1) Most of the research works do not consider the start-up time of DG in the hybrid standalone power system.
2) The fuel cost and fuel consumption of DG is not clearly addressed, which is not precise.
3) The impact of DG operating modes on standalone DC microgrid is not studied thoroughly, especially in the economical aspect and the energy cost analysis.

Therefore, in order to solve the shortcomings in the above, the objectives of this thesis will be explained in the next section.

I.4. Objective of the thesis

By aggregating loads and multi-source, renewable and traditional, microgrid can operate in both off-grid and grid-connected configuration, but the self-supply tendency increases (cost competitive micro-source technologies). Microgrid could be able to control RS instead of direct injection and interacts with smart grid in order to assist the utility grid power balancing by an advanced energy management. The AVENUES project research focuses on DC microgrid whose supervision implies intelligent control strategies as well as smart grid communication. The proposed DC microgrid structure, consisting of various sources and energy management strategy, is proposed in Figure 3.

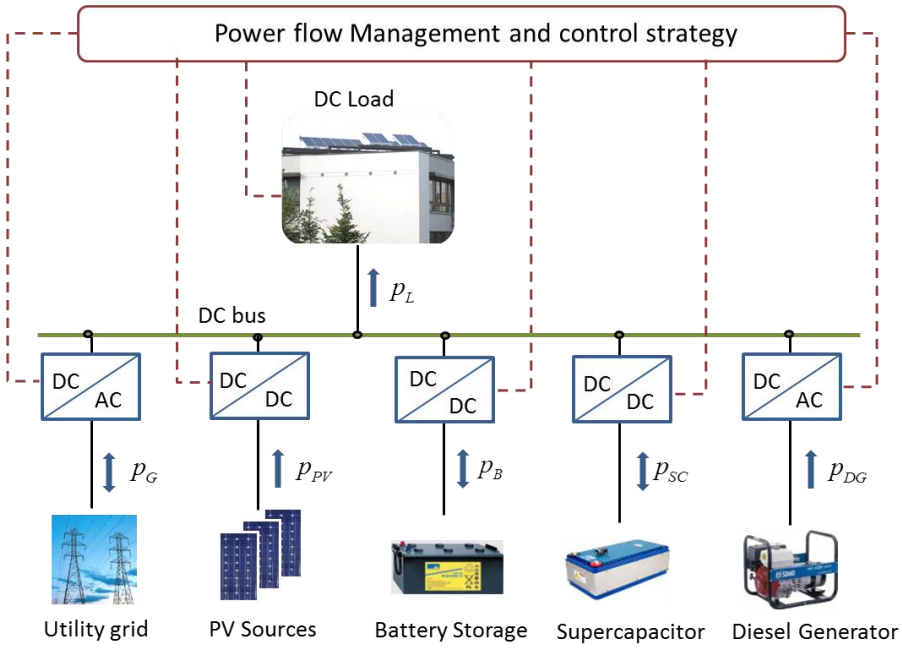

Figure 3. DC microgrid structure.

Before establishing a microgrid, the energy sources must be sized according to the load, to the electricity consumption, to the environmental conditions, and to the solar irradiation, within the technical specifications of the desired microgrid. This is the problem of sizing of microgrid [55–57]. This thesis focuses on the power management and the real time control of a standalone DC microgrid without consideration on the sources sizing. One of the reason why the sizing is not considered here lies in the fact that the research work is validated by experimental tests based on test benches already available in our laboratory. One notes that the experimental equipment is gradually purchased, depending on experimental conditions and funding.

The research, through this thesis, aims to study, analyze and evaluate the best setting parameters of the DG set that could lead to a global energy efficiency and cost optimization of the DC microgrid taking into account its different operating modes (load following mode and duty cycle mode). The main research work and objectives are as follows:

1) How to start up DG and how to connect the DG into DC bus is the first research point. If it needs to utilize the DG, its characteristics should be understood at first and then the power control of DG should be studied.

2) After the DG will being controlled, its economic features and fuel consumption conditions should be known so that it can be used in the most economical and optimized way. This is good for fuel saving and decreasing the harmful exhaust gas.

3) At last, the power management strategy for the real time control of DC microgrid including DG, needs to be proposed. Under this condition, the actual power system can have application in industrial field and in the human life.

Therefore, this thesis focuses on the impact of DG operating modes on standalone DC microgrid and aims to design the necessary control strategies with respect to the economic analysis.

Compared to the research works mentioned above, this thesis is distinguished by the integration of two complementary systems, DG and SC and by applying the DG energy cost into the power management strategy, in order to balance the power, i.e. to stabilize the DC bus voltage, as well as to reduce the energy cost for the end users. The most original scientific contributions of this thesis concern:

1) DG is compensated by SC during the DG start-up stage. When the microgrid needs to start up DG and the DG output is not yet stable, SC outputs power to support the microgrid bus during this short period. Therefore, the microgrid system is steady and the DC bus voltage is stable.

2) DG fuel cost function is found according to the experimental results, which is much more precise then the past research work. In addition, the research work takes into account the environmental temperature influence on the DG start-up.

3) Impact of DG operating modes on standalone DC microgrid has been studied. DG different operating modes (load following and duty cycle) are analysed and compared. The fuel cost of DG and the total cost of the whole power system are calculated, so that the optimal DG running mode of DG has been found.

4) The power management strategies for the real time control have been proposed for the standalone DC microgrid, which can keep the bus voltage stable as well as reduce the energy cost.

Regarding the technical contributions, the work of this thesis built up several experimental test benches for standalone microgrid based on PV sources emulator, which allows the repeatability conditions and reproducibility (the comparisons of different DG operating modes under the same solar irradiance and air temperature conditions). Numerous experimental tests were carried out and allowed the validation of the proposed concepts and power management strategies. Therefore, the ideas and innovations are validated not just by simulation in the computer, but also by the experiments, which can have applications in real environment and in industrial field.

I.5. Conclusion

Brief description about the traditional grid and smart grid has been introduced in this section, especially the summarization of the driving force of the smart grid. The comparison between AC and DC microgrid gives the conclusion that DC microgrid gains more than the AC microgrid in several aspects such as the efficiency, the coordination with the renewables sources and so on, so that the DC microgrid has broad prospects in the future. Therefore, this thesis focuses on the standalone DC microgrid system, which consists of PV sources, battery storage, SC, DG and DC load. Facing to the state of the art of the utilization of DG in DC microgrid, the thesis summarises the shortcomings and inadequacies in the current research. Under this academic and industrial circumstance, it describes the research purposes, motivations, and research contributions. The first objective of this thesis, DG start-up compensation by SC, is given in the next chapter.

Chapter II. Diesel generator start-up compensation by supercapacitor

Regarding the DC microgrid, the use of DG enhances the regulation of the DC bus voltage and power support. Thus, for off-grid operating mode or standalone microgrid, power balance is performed by adjusting DG power and storage for voltage stabilization. Although DG large capacity backup power can provide long-term support, its response speed is slow and the starting time lasts several seconds even tens of seconds to reach stable output power. Therefore, due to the slow dynamic behavior of the DG, the DC microgrid power balancing needs compensation for sudden load power increase or sudden renewable power decrease. On the other hand, storage as SC has a fast response and high power density but a low energy density.

This chapter focuses on DG slow dynamic compensation by SC for DC microgrid power balancing at DG start-up stage. A cooperative control strategy for SC and DG is proposed to realize the start-up of DG. SC and DG serving as a unity, work together to meet load demand when there is the shortage of RS power or sudden increase of load power. Based on the simulation and experimental results, this section shows that the designed control strategy improves the dynamic characteristics and achieves the maintained power quality. The whole system is given in the Section II.1. The power control strategy is described in section II.2. In Section II.3. and II.4., the simulation results and experimental verifications are presented and analysed. The conclusions of this chapter are given in Section II.5.

II.1. System modelling and description

The DC microgrid system consists of RS energy, batteries storage, SC, and DG. For DC microgrid running in off-grid mode or in standalone mode, DG and storage should work as backup energy equipment. Each of these backup components has a different role for the DC microgrid operation, according to the different power fluctuations that can occur. Storage, which is based on electrochemical batteries, is used for longer fluctuation periods (in the range of minutes/hours). If the storage's state of charge or its stored power reaches their minimum limit, DG has to be turned on and used for supplying the load and even to recharge the storage. However, because of the sluggish response of the DG during the start-up stage, the output power of the generator cannot respond to the rapidly increasing load power, and the voltage of DC bus cannot be maintained constant. The power quality of the system can be enhanced by using SC against the sudden load power surge or the shortage of renewable power. The SC is controlled to compensate the initial slow dynamics of the DG while starting up and keep the DC bus voltage constant. To realize this control, the characteristics of the DG and SC have to be determined: the starting characteristic of DG before reaching its stable output and the SC charging-discharging curve. Based on experimental results as well as technical notices of manufacturer, DG model and SC model are described in the following.

II.1.1. Diesel generator system and modelling

DG sets convert fuel energy (diesel or bio-diesel) into mechanical energy by means of an internal combustion engine, and then into electric energy by means of an electric machine working as generator.

The DG main parts are: internal combustion engine, electric synchronous generator, mechanical coupling, automatic voltage regulation system, speed governor, battery and small motor for dragging the rotor to rated speed in start-up phase, automatic fuel injection and ignition system, fuel tank, command panel. The minimum combined time necessary for the start-up of internal combustion engine, reaching the stabilized regime of the generator is several seconds, or even tens of seconds. When the frequency and voltage have reached their rated value, the switch is closed to connect the generator to DC bus. The DG used in the experiment is SDMO Technic 6500 E AVR. A Kohler diesel engine is mechanically coupled with a single-phase brushless synchronous generator, which has a closed loop automatic voltage regulator that controls and keeps constant the generator output voltage. The speed of engine is constant because of its speed governor system, which ensures the 50Hz frequency of the AC voltage. The DG parameters are listed in Table 2.

Table 2. Parameters of diesel generator.

P_{DG_MAX}	6.5kW	V_{DG_RATED}	230V
P_{DG_RATED}	5.2kW	I_{DG_RATED}	22.6A
Number of Phase	Single	Frequency	50Hz

In order to study the start-up characteristic of DG, no load test of DG has been done and the output voltage has been measured. Figure 4(a) shows the experimental results, namely output voltage curve of DG while starting up and Figure 4(b) presents the details of the changes of the same voltage curve between 4s and 5s. It is noticed that the output voltage increases gradually. At the beginning of this stage, the output power cannot be stable. And if the reference DG power is big while the voltage is not stable, the DG current will be huge which can burn out the generator.

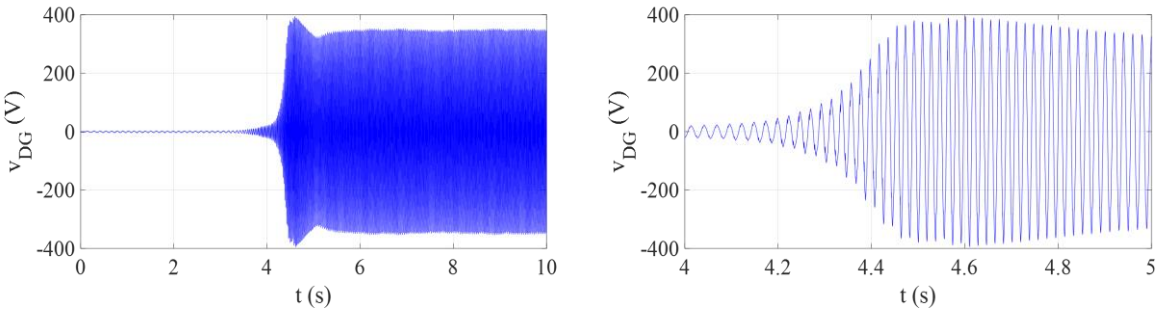

(a) (b)

Figure 4. (a) Start-up voltage curve of DG without load and (b) the voltage curve between 4s and 5s.

Several same tests have been done and the similar results of output voltage curve of DG like in Figure 4, show that this DG needs at least 6 seconds to deliver a stable output power [58].

Since the rotor's speed control system and generator voltage control system are integrated inside the DG as a whole system, this DG can be regarded as an independent voltage source. It is able to maintain the fixed voltage independent of the load resistance or the output current. So, the model of DG is simplified to two main elements: a second order model representing fuel injection and the internal combustion, and a delay time representing the time needed to reach stabilized output. Figure 5 shows the model of the DG by using a controlled voltage source block in Matlab/Simulink SimPowerSystem library.

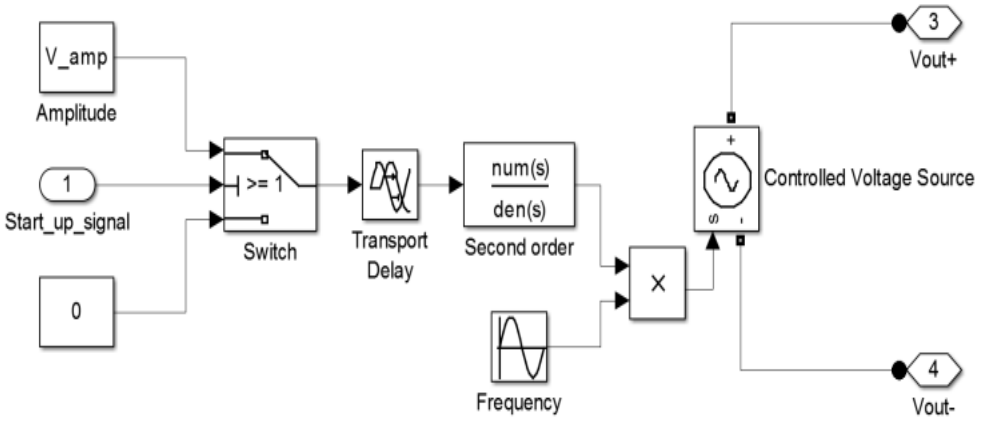

Figure 5. DG model.

By using this model, the DG start-up simulation result is shown in Figure 6 with the blue curve; it is an ideal voltage source ignoring the voltage noises and vibrations. In contrast, the actual voltage curve, which is the red curve in Figure 6, shows the signal image and its noises.

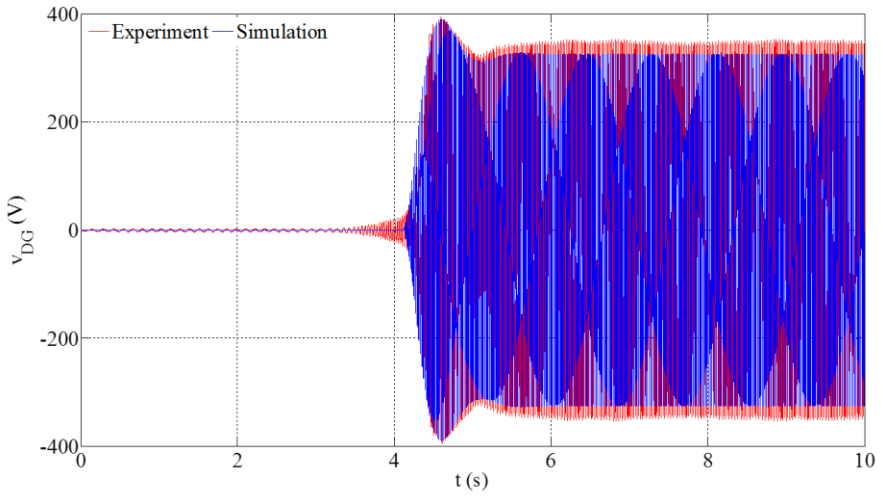

Figure 6. Start-up voltage curve of real DG and of the DG model.

II.1.2. Supercapacitor system and modelling

SC has a high-power density that can be released sharply and rapidly, so that SC can supply a great power in a short term. There are some earlier works which have shown the application of SCs both in AC and DC microgrids. In energy managements mentioned in [39,59–61], SC is effectively used to mitigate high frequency load variations. In addition, hydraulic mining shovels [46], and electric vehicle [62] also use SC to meet and improve the sluggish dynamic performance of diesel engine during load changes. Thus, SC may be integrated in DC microgrid to compensate for dynamic power fluctuations before the steady operation of DG [45].

The general SC model is presented in Figure 7, with C_{SC} capacitor, R_1 equivalent series resistor representing the charging-discharging resistor, and R_2 equivalent parallel resistor as the self-discharging loss.

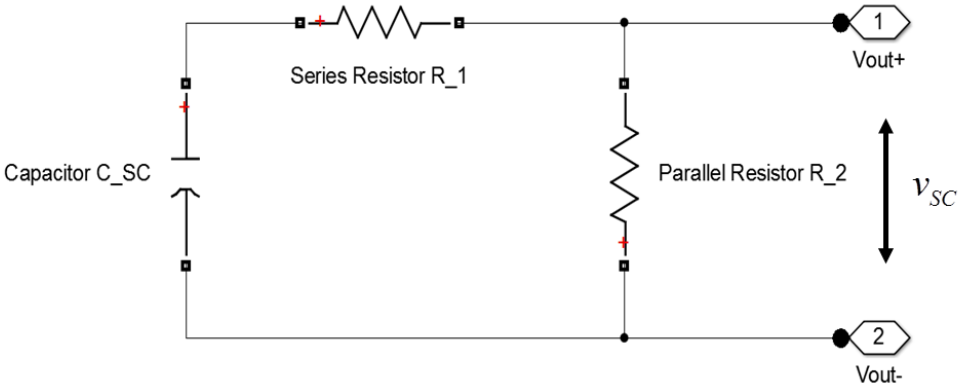

Figure 7. SC model.

Therefore, based on this model, the SC voltage can be calculated by (2.1):

$$v_{SC} = \frac{iR_2 t + C_{SC}(R_2 + R_1)v_{SC\_init} - tv_{SC\_init}}{C_{SC}(R_2 + R_1)} \quad (2.1)$$

where v_{SC_init} represents the initial voltage of SC, v_{SC} the final voltage after charging or discharging, i_{SC} the charging or discharging current, t charging or discharging time.

In the electrical model of SC, each parameter can be calculated according to the data given by the SC manufacturer. This study uses a module from Maxwell Company; its parameters are listed in Table 3 and profiles for constant current discharge curves are shown in Figure 8 [63].

Table 3. Parameters of supercapacitor.

Rated Capacitance	94F	Rated Voltage	75V
Maximum Current	1900A	Maximum Voltage	91V
Leakage Current	50mA	Stored Energy	73Wh
Equl Series Resistor	0.013Ω	Equal Parallel Resistor	1500Ω

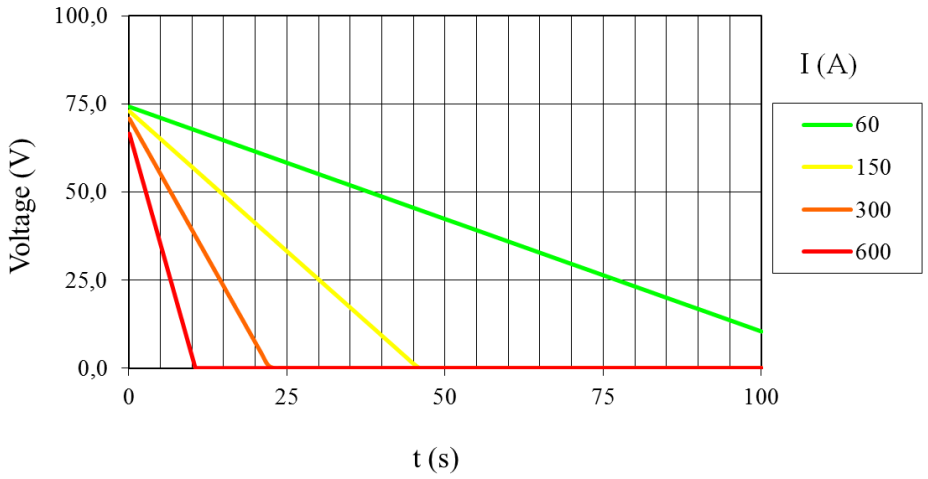

Figure 8. Profiles for different constant current discharge curves.

In order to validate this SC model, the actual discharging-charging experiment has been done. At first, the SC is charged with a recharging current of 25A until reaching its rated voltage value. This process lasts 286.3 seconds. Then, the SC discharges its energy with a discharging current of -25A. The voltage and current curves during SC charging-discharging are measured and presented in Figure 9. With the same recharging and discharging current (±25A), the simulation of this SC mode has been done, the result of which is also draw in Figure 9. The comparisons between them indicate that this simple model can be used.

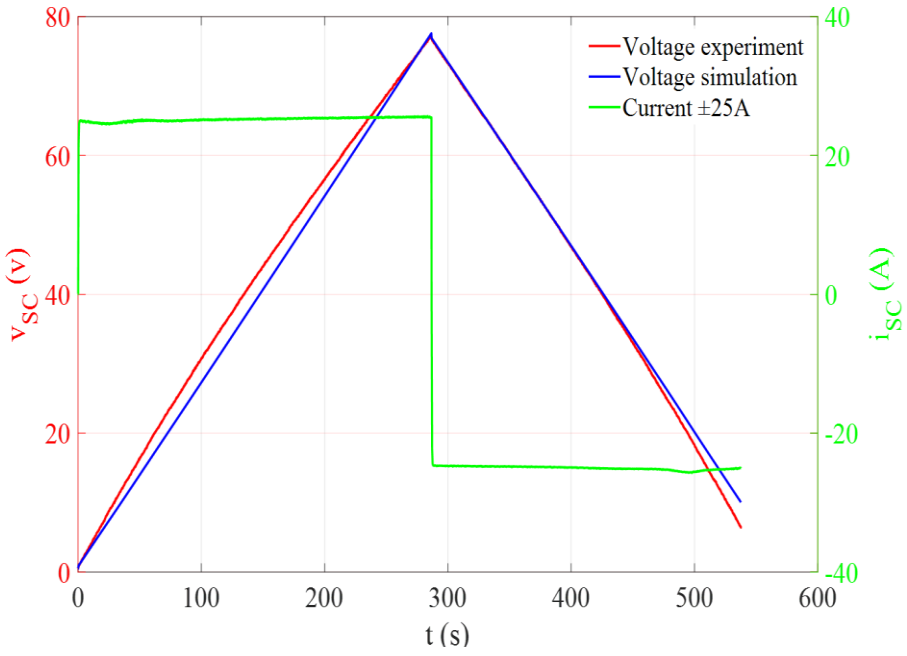

Figure 9. Voltage charging and discharging curve of experiment and simulation.

II.2. Power control strategy

The power control strategy is a self-decision module, whose main function is to generate the switches control signal of SC and DG based on local information, so that to achieve their coordination. The configuration of the power system is shown in Figure 10. Since in this section, the power control strategy concentrates on the coordination of SC and DG, the parts of renewable energies (PV, wind power, etc.) are regarded as a one source, namely RS. RS energy is connected to the DC bus through a DC/DC converter. DG is connected to the common DC bus by an AC/DC rectifier and SC is connected to the DC via a bidirectional DC/DC converter.

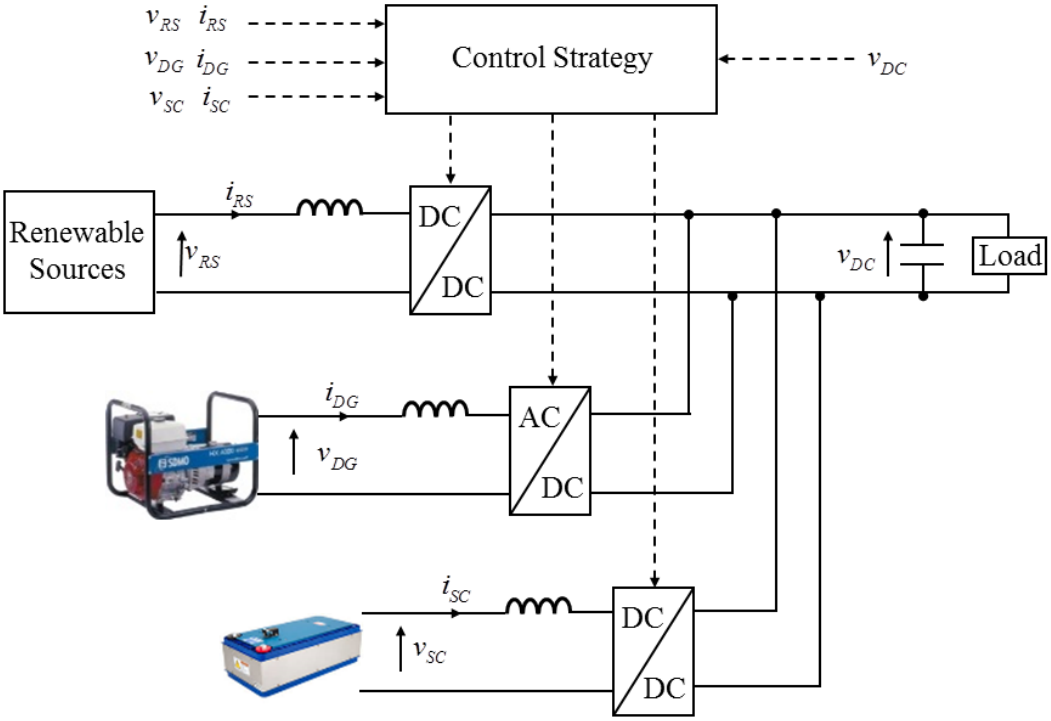

Figure 10. Configuration of the power system.

In Figure 10, the voltages v_{RS}, v_{DG}, and v_{sc} are the measured voltage of RS, DG and SC respectively, while i_{RS}, i_{DG}, and i_{sc} are the measured current of RS, DG and SC respectively. The voltage v_{DC} is the measured DC bus voltage, which is the control object.

In general, if the RS power is enough to meet the load demand, the system operating mode is called RS dominant mode. When microgrid needs to start DG because of shortage of RS power and the power generation of DG is not yet stable, SC outputs power to support the microgrid and to balance the DC bus voltage. This period of time is called SC dominant mode. After completion of DG starting up, DG and SC work together in a specific coordinate strategy to stabilize the DC bus voltage. SC does not discharge anymore, but absorbs power from the microgrid to replenish its lost power in the last period. This period is called as SC/DG cooperative control mode. When SC approaches the depth limit of recharge, in order

to avoid excessive recharge, SC is disconnected, and the power balance is supported by DG. This period is DG dominant mode.

The detailed cooperative control strategy for SC and DG is presented step by step in the following.

Renewable Sources Dominant Mode

Figure 11 presents the RS dominant operating mode. If the RS energy is enough to meet the load demand, the DC bus voltage is mainly stabilized by the RS. Thus, RS controllable logical switch S_1 is positioned at 2 and only the RS energy is participating in the stabilization of DC bus voltage. In addition, DG and SC controllable logical switches S_2 and S_3 are positioned at zero and both SC and DG are not operating.

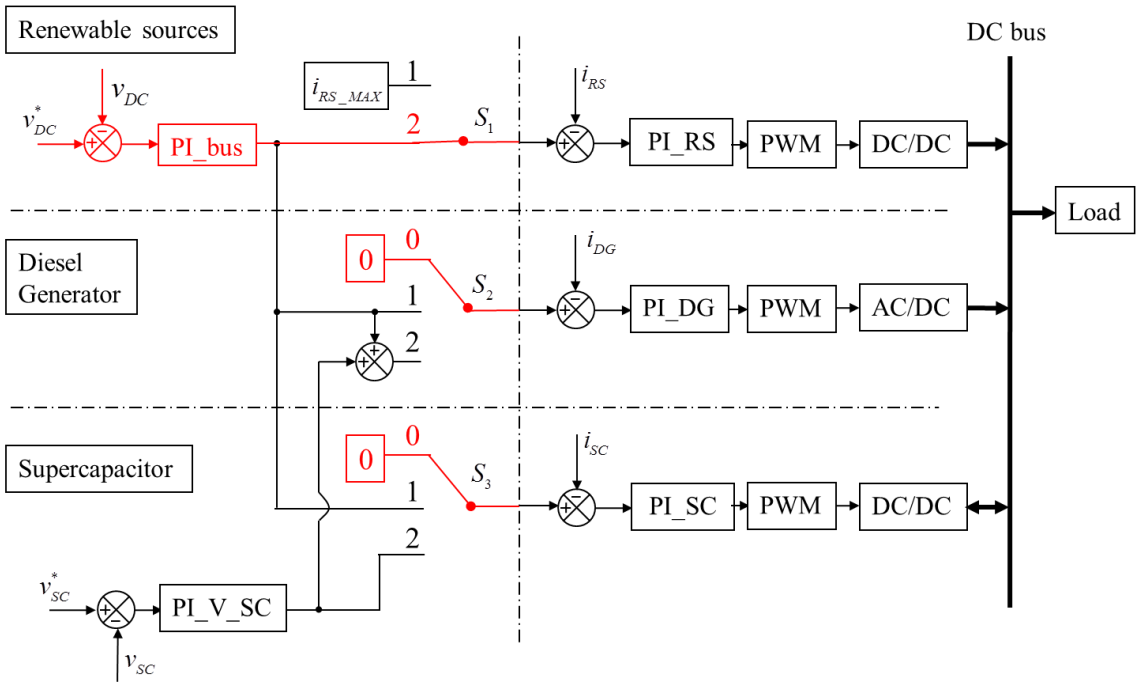

Figure 11. Control block diagram for the renewable source dominant mode.

In Figure 11, DC bus voltage is controlled by a proportional integral (PI) control loop, namely PI_bus, to stabilize the DC bus voltage at the reference v^*_{DC}. The PI controllers PI_RS, PI_DG and PI_SC are utilized to control the current of RS, DG and SC respectively. The PI controller PI_V_SC is used to control the voltage of SC when the SC is needed to recharged to its reference value v^*_{SC}. Pulse width modulation (PWM) is a modulation technique used to allow the control of the electrical power converter.

Supercapacitors Dominant Mode

If the renewable power cannot meet the load power demand, in order to be able to quickly support the DC bus voltage, the SC and DG start-up algorithm is activated. This algorithm has to be based on the specific changes of DC microgrid electrical signals, to determine whether or not it is necessary to start up the DG. When the DC microgrid is stably running, the DC bus voltage is stable in the vicinity of the rated voltage with some slight ripples. But, when the supplied power is not enough, the voltage of DC bus deviates from the allowable range and there is a voltage drop. So, when the DC bus voltage becomes less than lower limiting value, a start-up signal is created to activate the SC and DG. The lower limiting value is chosen according to the voltage fluctuation tolerance range of DC microgrid, generally less than ±5%. When this signal occurs, the SC controller logical switch S_3 is closed to 1, while the DG is in a cold and static standby condition. Before connecting DG to DC bus, the generator's frequency and voltage need to reach the rated values, that is no-load condition. So, the DG logical switch S_2 still stays at 0, as shown in Figure 12. In this period, the role of SC is to stabilize the DC bus voltage and supply the power difference for a short term. Therefore, the RS logical switch is closed to 1, meaning that RS energies are not participating in the DC voltage stabilization but running in the mode of generating power as much as possible. The controller of SC consists of one PI control loop PI_SC, which controls the discharge current inside the DC bus voltage PI controller that controls the DC link voltage.

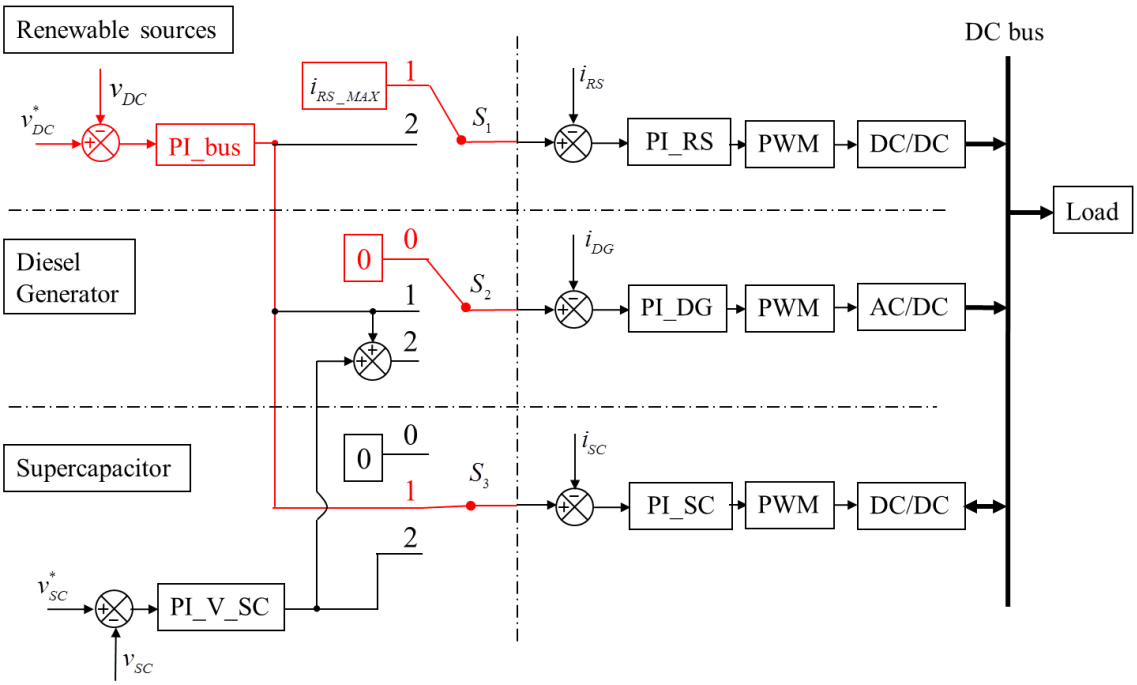

Figure 12. Control block diagram of the supercapacitor dominant mode.

Supercapacitor/Diesel Generator Cooperative Control Mode

Because the SC discharges in the second period, the SC voltage decreases. Since the SC voltage should be recovered after supplying the sudden load power, the SC rated voltage is used as one of the references. So, when the DG reaches the stabilized regime, a charge signal is created. The stable state is given by a program which observes the change of amplitude v_{DG_Peak} and frequency f_{DG} of the DG's output voltage. When these two parameters satisfy (2.2), the DG enters the stable state and the charge signal is excited.

$$\begin{cases} 310\text{V} < V_{DG\_Peak} < 340\text{V} \\ 48\text{Hz} < f_{DG} < 52\text{Hz} \end{cases} \tag{2. 2}$$

This signal is used on one hand as the stimulus of connecting DG, and on the other hand it indicates the SC changing mode from discharging to charging. Therefore, the logical switches S_2 and S_3 are closed to 2, as shown in Figure 13.

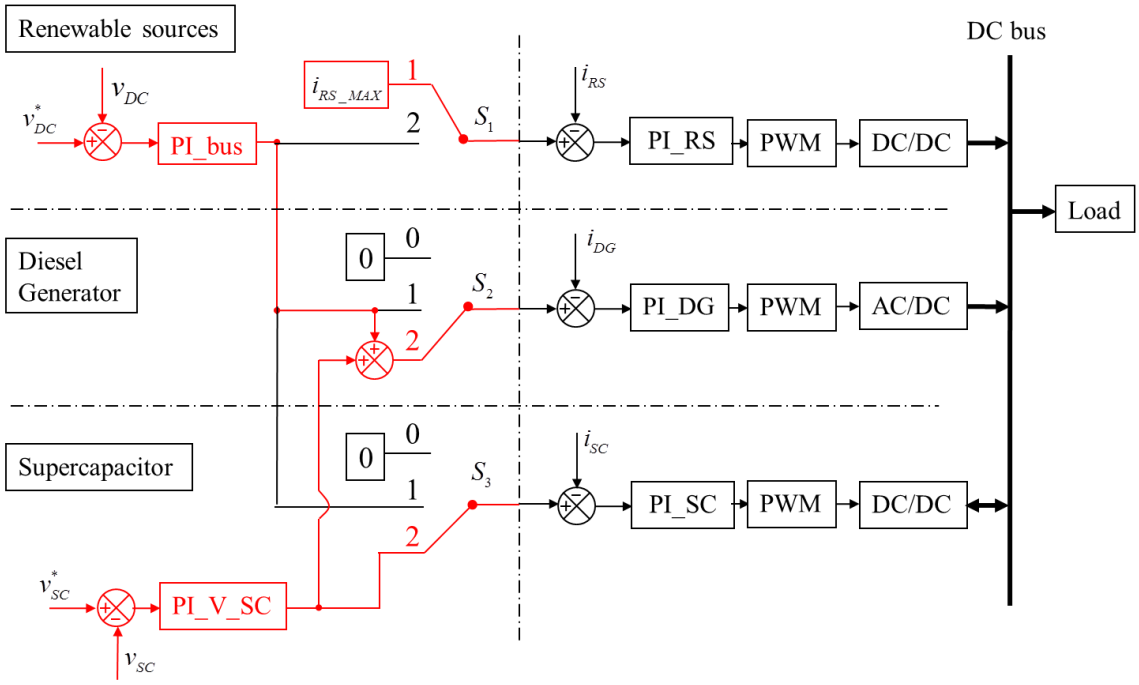

Figure 13. Control block diagram of the SC/DG cooperative control mode.

For DG controller, the SC voltage added with DC bus voltage is regarded as the total reference. The controller of DG includes one PI control loop, which controls the generator current inside another two PI controls that control the DC link voltage and SC voltage. The power is generated according to the load power demand and the required recharge power of SC.

Diesel Generator Dominant Mode.

When the SC voltage reaches the rated voltage, SC off-bus signal is created. The logical switch S_3 is closed to 0, disconnecting SC from the microgrid common bus. At the same time, the logical switch S_2 is changed to 1, as shown in Figure 14. The power balancing is now mainly supported by DG to maintain the DC bus voltage at its rated value.

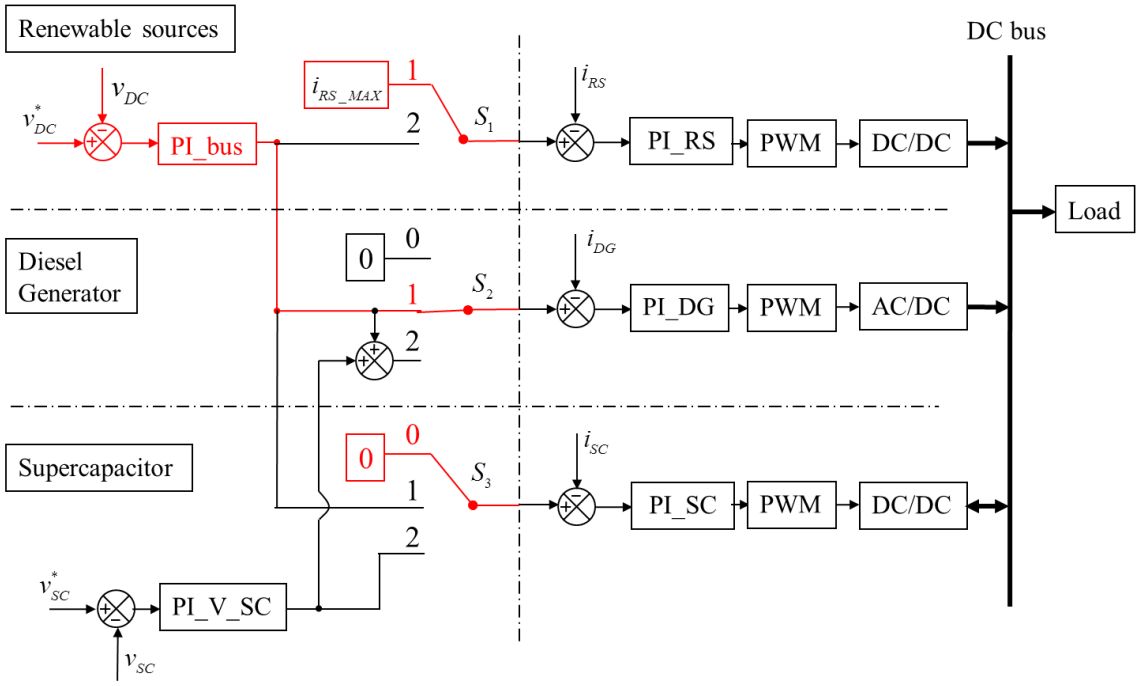

Figure 14. Control block diagram of the DG dominant mode.

Whole process of the control strategy

From RS dominant mode to DG dominant mode, Figure 15 shows the complete conversion process of SC and DG coordination control strategy.

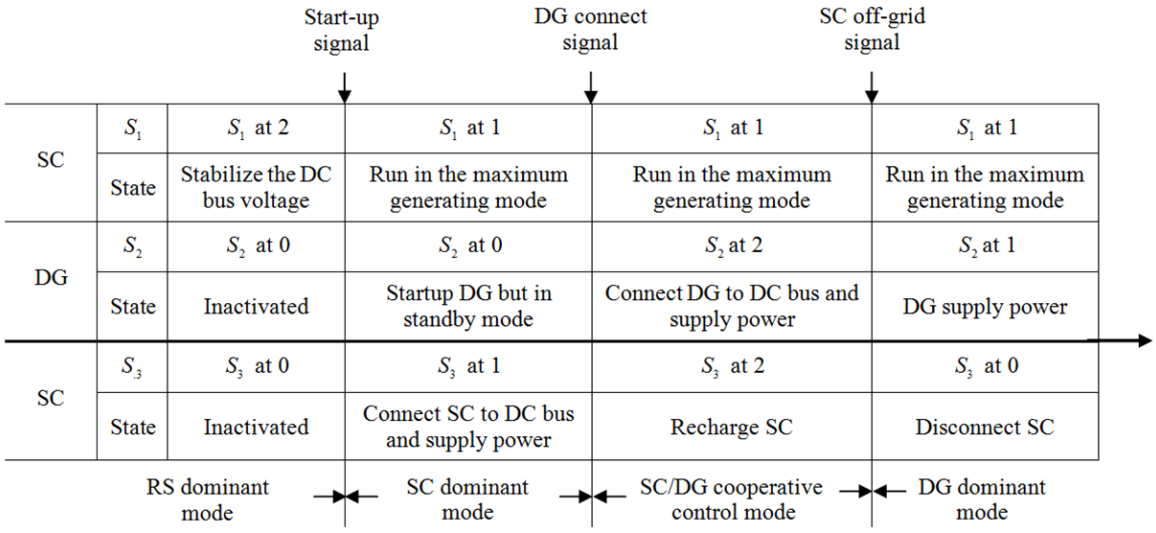

Figure 15. Status of DG and SC in the conversion process.

II.3. Simulation verification

To verify the feasibility of the effective coordination of control strategies, two simulation cases are presented and described by using MATLAB/Simulink software. The relevant structure and system parameters are given in Figure 10. The reference value of DC bus voltage in this thesis is 400V DC [64,65]. One notes that in France the voltage tolerance is within +6%/-10% [66]. Therefore, the lowest limit of DC bus voltage is 360V. In order to further strengthen the stability of the power system and to reduce the influence of voltage fluctuations on the end users' appliances, the lower limiting value to stimulate the start-up signal is set as much smaller, at 390V. Two cases are concerned in the simulation: the load is stable, but the renewable power is insufficient to supply the load (i); the renewable power is operated at maximum power point tracking (MPPT) mode while the load suddenly increases (ii).

II.3.1. Shortage of renewable sources power

Since the simulation is to verify the feasibility of the coordination of SC and DG and the simulation time is short (just several minutes), the load power demand is considered constant in the period of simulation and equals to 1kW. If the renewable power is near zero due to weather conditions and storage is fully discharging, it is necessary to connect the DG to cover the missing power. The simulation results in this case are shown in Figure 16 and zoomed in Figure 17; each stage is explained in detail in the following.

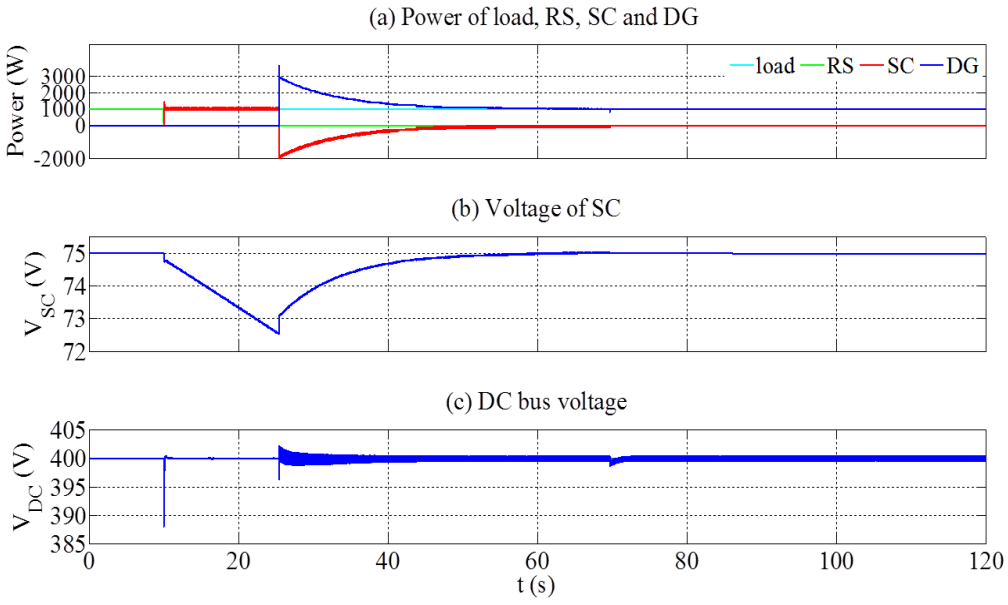

Figure 16. Dynamic response of shortage of renewable power.

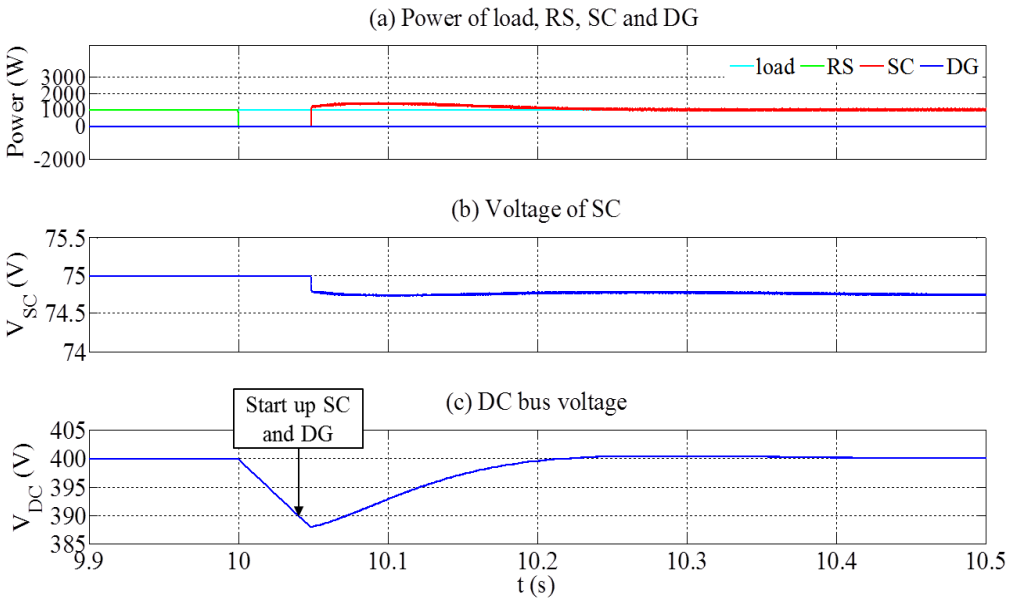

Figure 17. Detailed dynamic response curves of microgrid parameters before and after SC connection in the case of renewable power shortage.

Renewable Sources Dominant Mode. In Figure 16(a), from 0 to 10s, microgrid load is supplied by renewable power. SC and DG are isolated from the DC microgrid through their dedicated switches. The DC bus voltage is 400V.

Supercapacitor Dominant Mode. At time 10s, the renewable power becomes zero and storage is no more available resulting in the drop of the DC voltage (Figure 16(c)). When the lower limiting value (390V) of DC bus voltage is detected at time 10.04s (Figure 16(c)), the SC and DG are activated. SC immediately offers the power needed and at time 10.2s, the bus voltage recovers to the rated value as shown in Figure 16. The detailed dynamic response of connecting SC to the DC bus is also presented in Figure 17, which offers detailed parameters evolution of DC bus voltage getting back to normal. Since DG needs some time to reach the stabilized state, SC supplies the load and maintains the bus voltage at 400V.

Supercapacitor/Diesel Generator Cooperative Control Mode. At time 25.4s, the DG stabilized state is identified. When the DG is connected to common bus, the instantaneous output power jumps to a great value, which leads to a change of the DC bus voltage within an acceptable range. However, due to fast turn on and off of the IGBT (AC/DC converter) and electrical harmonics induced by the PWM, high-frequency electrical noises are injected into DC bus. To replenish the SC power discharged in the first stage, DG not only supplies the load power but also recharges the SC. Figure 16(b) presents the SC voltage gradually recovers and Figure 16(a) shows the DG output power decreases along with it.

Diesel Generator Dominant Mode. When the SC voltage reaches the rated voltage at time 73.7s (Figure 16(b)), SC off-bus signal disconnects the SC from DC bus (Figure 16(a)) and causes a little deviation of DC bus voltage (Figure 16(c)). After that, only DG maintains the power balance.

II.3.2. Sudden increase of load power

If the RS power is in its maximum output status and storage is fully discharging, DG is started up to maintain the power balance for sudden load power increase. The simulation results in this case, for which the load power increases from 1kW to 2kW, are shown in Figure 18 and zoomed in Figure 19; each stage is explained in detail in the following.

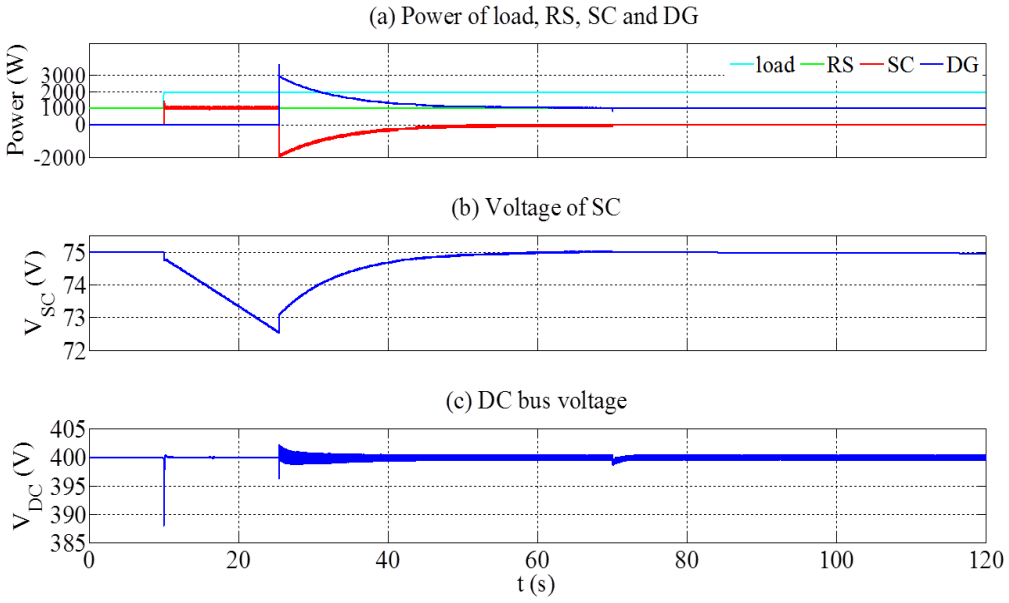

Figure 18. Dynamic response curves of microgrid parameters

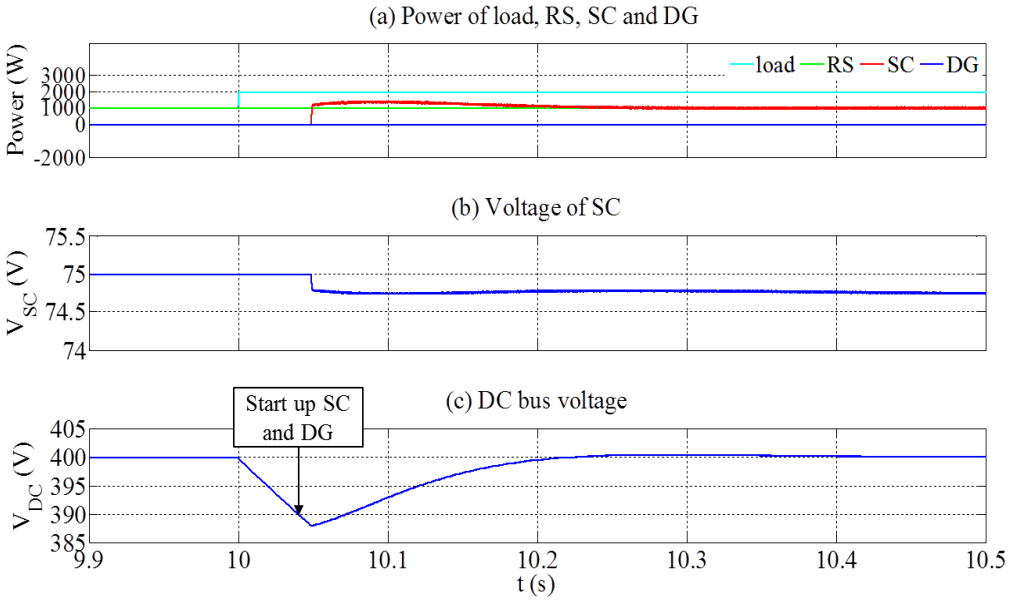

Figure 19. Detailed dynamic response curves of microgrid parameters before and after the SC connection in the case of sudden load power increase.

Renewable Sources Dominant Mode. The renewable power is considered constant and equal to 1kW. In Figure 18(a), from 0 to 10s, the renewable power can meet the load. SC and DG are isolated from the microgrid DC bus through their dedicated switches. The DC bus voltage is 400V (Figure 18(c)).

Supercapacitor Dominant Mode. At time 10s, the load power increases to 2kW (Figure 18(a)), which is higher than the renewable source power, resulting in the drop of the DC voltage (Figure 18(c)). When the lower limiting value (390V) of DC bus voltage is detected at time 10.04s, the SC and DG are activated. SC immediately offers the power needed and at time 10.2s (Figure 18(a) and Figure 18(b)), the bus voltage recovers to the rated value as shown in Figure 18(c). The detailed dynamic response of connecting SC to the DC bus is also presented in Figure 19, which offers detailed parameters evolution of DC bus voltage getting back to normal. Since DG needs some time to reach the stabilized state, both SC and RS supply the load and maintain the bus voltage at 400V.

Supercapacitor/Diesel Generator Cooperative Control Mode. At time 25.4s, the detector finds that the DG reaches the stabilized state. When the DG is connected to the bus, the instantaneous output power jumps to a great value (Figure 18(a)), which leads to a change of the DC bus voltage within an acceptable range (Figure 18(c)). However, due to fast turn on and off of the IGBT (AC/DC converter) and electrical harmonics due to the nature of PWM, high-frequency electrical noises are injected into DC bus. To refill the SC power discharged in the first stage, DG supplies the load power and also recharges the SC. From Figure 18(b), it is observed that the SC voltage gradually recovers and from Figure 18(a) that the DG output power decreases along with it.

Diesel Generator Dominant Mode. When the SC voltage reaches its rated voltage at time 73.7s (Figure 18(b)), SC off-bus signal disconnects the SC from DC bus (Figure 18(a)). There is also a little deviation of DC bus voltage Figure 18(c). After that, DG and renewable source maintain the power balance.

II.4. Experimental verification

To verify the feasibility of the proposed control strategy, an experimental platform is set up. The goal is to operate the two simulation cases in real environment, to verify that the control strategy can be implemented in the real system.

II.4.1. Experimental platform

The experimental platform is composed by SC and the following emulators: a programmable DC electronic load emulates the DC load, a programmable DC source emulates the RS energies, and a programmable AC source emulates the DG. The output voltage of this programmable AC source can be controlled and programmed from the external input through the data cable. The start-up data of the

SDMO Technic 6500 E AVR is firstly recorded in the host computer and then inputted into the programmable AC source through dSPACE controller board. The dSPACE controller board is a processor board, which provides the computing power for the real-time system and also functions as an interface to the I/O boards and the host computer. The sensors are utilised to measure the relevant voltage and current of the experimental platform (v_{DG}, i_{DG}, v_{SC}, etc.), and then transmit the measured values to the host computer through the dSPACE controller board. Recorder is utilised to store the original data for post processing. The host personal computer (PC) is installed with the ControlDesk and Real-time Interface to perform all the necessary tasks and give a human interaction working environment, to compile the programme and then implement it. The details of the experimental platform are shown in Table 4. The picture of the experimental platform is given in Figure 20.

Table 4. Elements detail for experimental test.

Element	**Parameter**	**Device**
Supercapacitor	94F/75V	Maxwell 75V modules: BMOD0094 P075 B02
Renewable source emulator	600V/5.5A	GEN 3.3kW series power supplies: GEN600-5.5
Load emulator	2.6kW	High power DC electronic load: Chroma 63202
DG emulator	3kVA	Programmable AC source Puissance+ PA-3000-B/260V-12A
IGBT converter	600V-100A	SEMIKRON SKM100GB063D
Controller board		dSPACE 1006

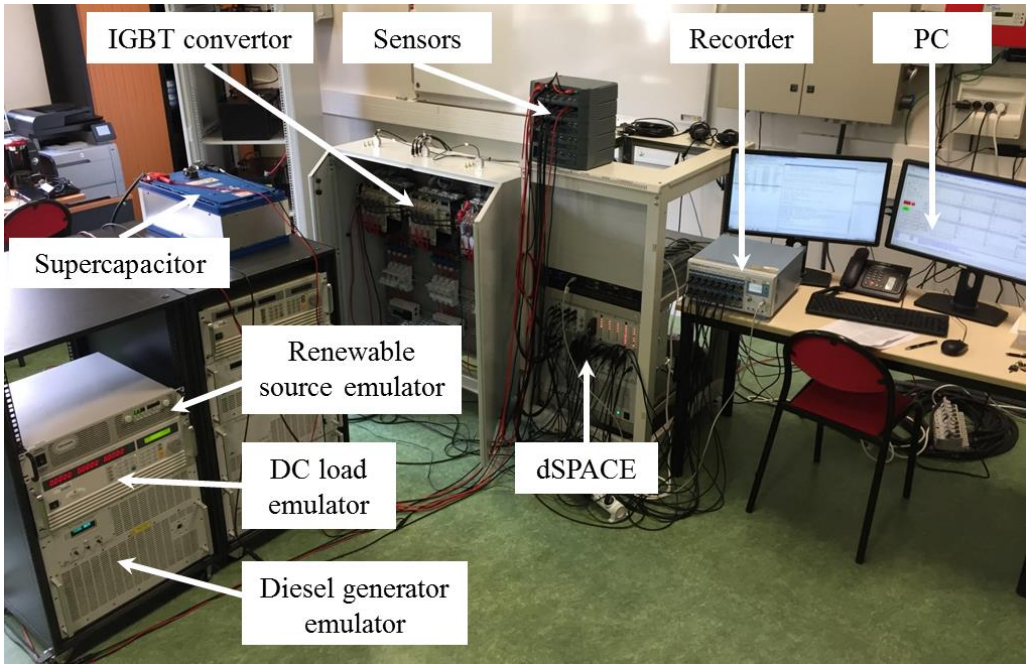

Figure 20. Experimental platform.

II.4.2. Shortage of renewable sources power

The load power in the experimental test is supposed as 1kW at first. This is because the maximum power of load emulator is 2.6kW. On the other hand, as in the next section a sudden increase of load power is required, the load power will be increased to 2kW. Therefore, being subject to the experimental condition, the load power in this test is supposed as 1kW. If the RS is near zero due to weather conditions and storage is fully discharging, it is necessary to connect the DG to cover the missing power. The experimental results in this case are shown in Figure 21 and zoomed in Figure 22; each stage is explained in detail in the following.

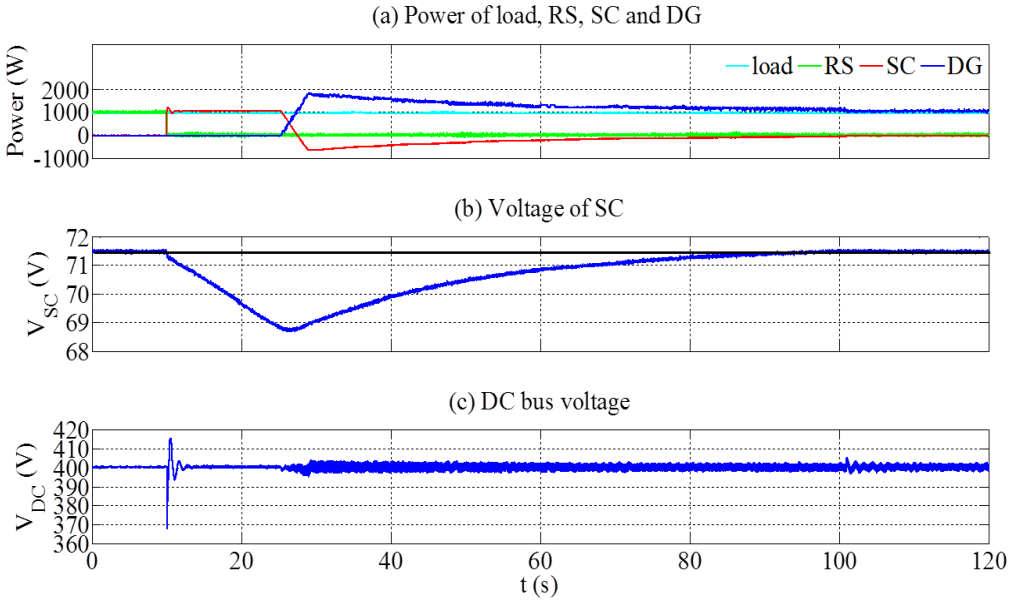

Figure 21. Dynamic response of shortage of renewable power.

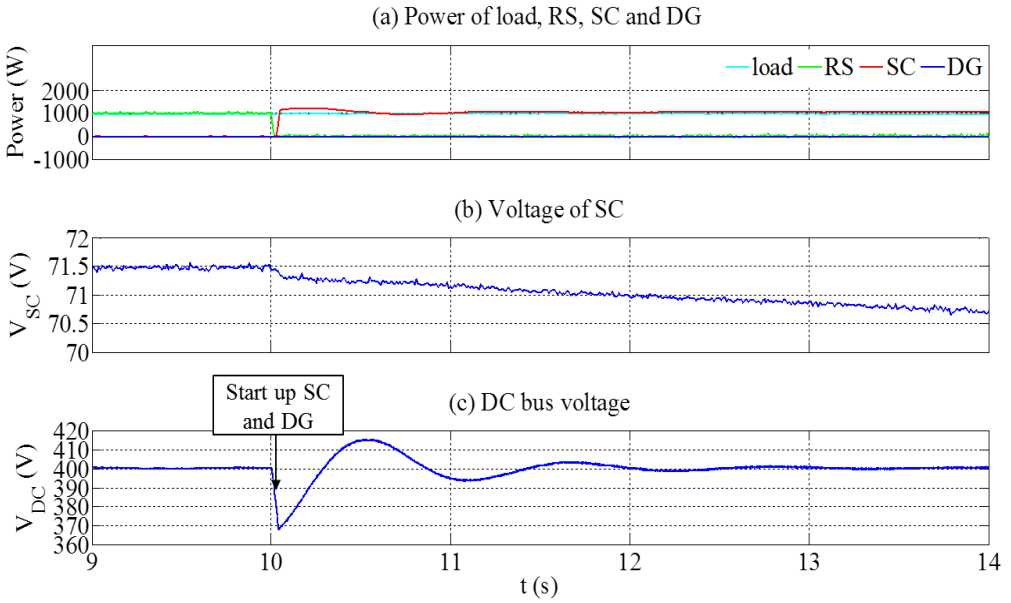

Figure 22. Detailed dynamic response curves of microgrid parameters before and after SC connection in the case of renewable power shortage.

Renewable Sources Dominant Mode. In Figure 21(a) from 0 to 10s, the renewable power is equal to the load demand. SC and DG are isolated from the DC microgrid through their dedicated switches. The DC bus voltage is stable at 400V.

Supercapacitor Dominant Mode. At time 10s, the renewable power becomes zero and the batteries storage is no more available resulting in the drop of the DC voltage (Figure 21 (c)). When the lower limiting value (390V) of DC bus voltage is detected at time 10.02s (Figure 21 (c)), the SC and DG are activated. SC immediately offers the power needed and at time 12s, the bus voltage recovers to the rated value as shown in Figure 22. Compared with the simulation results, the DC bus voltage declines more deeply. This is because that the inertia of experimental system is higher than the simulation. The detailed dynamic response of connecting SC to the DC bus is also presented in Figure 22, which offers detailed parameters evolution of DC bus voltage getting back to normal. Since DG needs some time to reach the stabilized state, SC supplies the load and maintains the bus voltage at 400V.

Supercapacitor/Diesel Generator Cooperative Control Mode. At time 25.4s, the DG stabilized state is identified. When the DG is connected to common bus, there is a rate limiter to limit the instantaneous DG output power, which leads a smooth change of the DC bus voltage within an acceptable range compared with the simulation. However, due to fast turn on and off of the IGBT (AC/DC converter), high-frequency electrical noises are injected into DC bus. To replenish the SC power discharged in the first stage, DG not only supplies the load power but also recharges the SC. Figure 21(b) presents the SC voltage gradually recovers and Figure 21(a) shows the DG output power decreases along with it.

Diesel Generator Dominant Mode. When the SC voltage reaches the rated voltage at time 101.1s (Figure 21(b)), SC off-bus signal disconnects the SC from DC bus (Figure 21(a)) and causes a little deviation of DC bus voltage (Figure 21(c)). After that, only DG maintains the power balance.

II.4.3. Sudden increase of load power

If the RS power is in its maximum output status and storage is fully discharging, DG is started up to maintain the power balance for sudden load power increase. The experimental results in this case, for which the load power increases from 1kW to 2kW, are shown in Figure 23 and zoomed in Figure 24; each stage is explained in detail in the following.

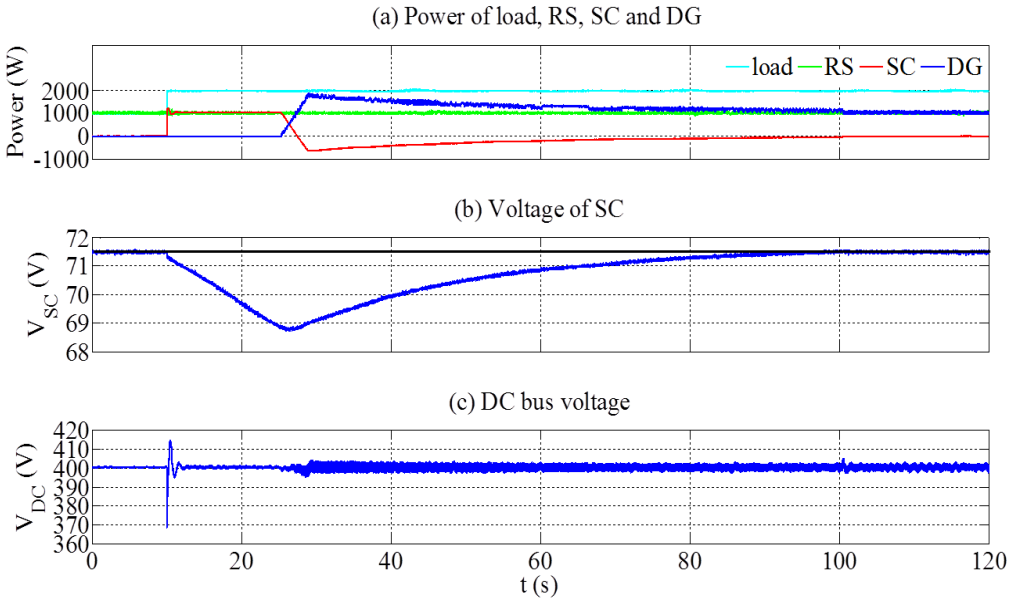

Figure 23. Dynamic response curves of microgrid parameters.

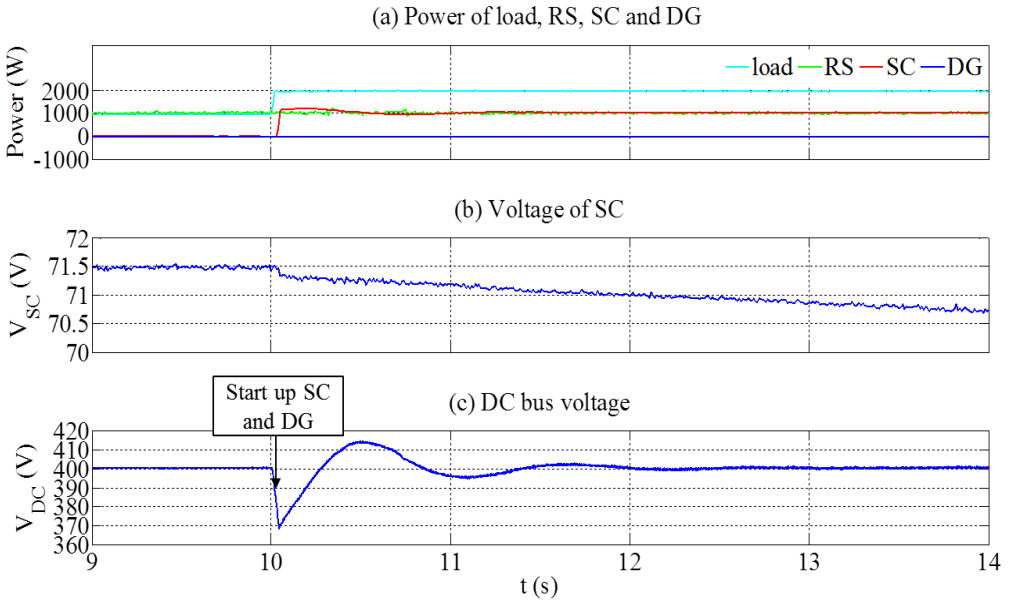

Figure 24. Detailed dynamic response curves of microgrid parameters before and after the SC connection in the case of sudden load power increase.

Renewable Sources Dominant Mode. The renewable power is considered constant and equal to 1kW. In Figure 23(a), from 0 to 10s, the renewable power can meet the load. SC and DG are isolated from the microgrid DC bus through their dedicated switches. The DC bus voltage is 400V (Figure 23(c)).

Supercapacitor Dominant Mode. At time 10s, the load power increases to 2kW (Figure 23(a)), which is higher than the renewable source power, resulting in the drop of the DC voltage (Figure 23(c)). When the lower limiting value (390V) of DC bus voltage is detected at time 10.02s, the SC and DG are activated. SC immediately offers the power needed and at time 12s (Figure 23(a) and Figure 23(b)), the bus voltage recovers to the rated value as shown in Figure 23(c). The detailed dynamic response of

connecting SC to the DC bus is also presented in Figure 24, which offers detailed parameters evolution of DC bus voltage getting back to normal. Since DG needs some time to reach the stabilized state, both SC and RS supply the load and maintain the bus voltage at 400V.

Supercapacitor/Diesel Generator Cooperative Control Mode. At time 25.4s, the detector finds that the DG reaches the stabilized state. When the DG is connected to the bus, there is a rate limiter to limit the instantaneous DG output power so that the DG power increases smoothly (Figure 23(a)). The DC bus voltage is stable within an acceptable range compared with the simulation (Figure 23 (c)). However, due to fast turn on and off of the IGBT (AC/DC converter), high-frequency electrical noises are injected into DC bus, which can be seen through the noises of DC bus voltage. To refill the SC power discharged in the first stage, DG supplies the load power and also recharges the SC. From Figure 23(b), it is observed that the SC voltage gradually recovers and from Figure 23(a) that the DG output power decreases along with it.

Diesel Generator Dominant Mode. When the SC voltage reaches its rated voltage at time 101s (Figure 23(b)), SC off-bus signal disconnects the SC from DC bus (Figure 23(a)). There is also a little deviation of DC bus voltage Figure 23(c). After that, DG and RS maintain the power balance.

Compared with the simulation results, it needs much more time to recharge the SC to its rated voltage in the experimental verification. In addition, the output power of DG at the time of being connected to the DC bus, shows a pulsing increase in the simulation while in the experimental verifications, the output power of DG is much smoother. There are several reasons causing these differences. Firstly, the generator model and the super capacitor model are not very precise. So, there are a lot of inaccuracies. Because this thesis concentrates on the power management for the real time control, the modelling is simple but precise enough to be used for designing the strategy and the controller. Secondly, when experiments are done, there are a lot of factors that can influence the results, for example, the inductor characteristic and the power loss. Thirdly, in order to prevent the DG from increasing its current too rapidly, there is a rate limiter to restrict the rate of rise of DG output power in the experimental tests. This is an artificial factor to further increase the slow dynamics of DG. But with this rate limiter, the DG output power is changed more smoothly.

II.5. Conclusion

In order to overcome the sluggish dynamic behaviour of DG while starting up, SC is used as compensatory energy to resist against the shortage of renewable power or the sudden load power surge. The object of this chapter is to understand the characteristics of DG and SC, to propose a power control strategy of the coordination of starting up DG and SC, and then to verify it.

Firstly, simplified DG and SC models are presented according to experimental results and technical notice data. Then, a power control strategy is proposed to achieve coordination between DG and SC. The individual control schemes are coordinated through the proposed control coordination approach to maintain the DC bus voltage stable and the system's power balance. The simulation results show that the proposed control strategies are able to regulate the DC bus voltage within the acceptable limits and supplying the load during renewable power under generation or load step-increase situations.

An experimental platform is set up, in which several emulators are utilised to simulate the RS energies, DC load and DG. The experimental results show that the proposed control strategies can be used in the real system. It can be implanted into a whole power management strategy, which controls the operation of an off-grid DC microgrid, consisting of PV source, battery storage, SC, DG and DC load. This strategy is a power management of DC microgrid with DG load following mode, which will be introduced and presented in the next chapter.

Chapter III. Power management of DC microgrid with DG load following mode

DG slow dynamic behaviour is compensated by SC, which was investigated in the previous chapter. It presents the coordination control mechanism between the DG and SC. Therefore, this chapter proposes a power management strategy for a hybrid PV-battery-SC-DG power system, which involves the coordination control.

Moreover, concerning the electrochemical storage, used as backup power for an off-grid DC microgrid [67], its charging and discharging power are limited by its maximum charging and discharging current. It cannot provide as much as the required power for DC bus even though its energy capacity is enough to support the electrical power system for operating in a long time. In situation like this, for the power balancing, load shedding strategies are proposed as shown in the several works [67,68]. On the other hand, when the power generation of RS is higher than the demanded load power, the excess power is eliminated by a dedicated limited power control [69,70]. Undeniably, load shedding and limited power control strategies are applicable in these two situations to protect the electrochemical storage from being over-discharged and over-charged. However, with the help of SC, the occurrence number of load shedding and the cut of renewable energy generation can be reduced. For this, the strategy proposed in this power management is that when the power of renewable energy generation and electrochemical storage is not enough, SC can supply the extra power, while conversely, the excess power is absorbed by SC.

This chapter focuses on a power management strategy for a standalone DC microgrid, which consists of PV sources, electrochemical storage combined with DG and SC. The goal is to regulate the DC bus voltage at the required voltage reference and to balance the power in the DC bus. The proposed power management strategy in this section brings the following improvements.

1) DG is compensated by SC during the DG start-up stage. When the microgrid needs to start the DG and the DG output is not yet stable, SC outputs power to support the microgrid bus during this short period.

2) As complementary energy of the electrochemical storage, SC releases or absorbs energy when the power difference between PV and load is greater than the storage maximum charging or discharging power accordingly.

3) An experimental platform, set up in the laboratory, is used for experimental validation, which is lacked in most scientific papers. Twelve possible different cases are shown one by one, and one real day experiment is carried out. Based on the experimental results, this study shows that the designed control strategy improves the DC microgrid dynamic characteristics under these operating conditions.

The organization of this section is summarized as follows. Section III.1. describes each part of the system and respective characteristics. Section III.2. describes the configuration of the proposed hybrid system and details the power management strategy for the real time control, which is verified firstly by simulation in Section III.3. The experimental platform description is given in Section III.4, in which intentionally designed experiments to show the twelve cases of power management are presented together with the one-day experiment. Finally, conclusions and work in progress are given in Section III.5.

III.1. Description of hybrid system and its components

The standalone DC microgrid system consists of PV source, storage formed by electrochemical batteries, DG, SC, and DC load which are shown in Figure 25.

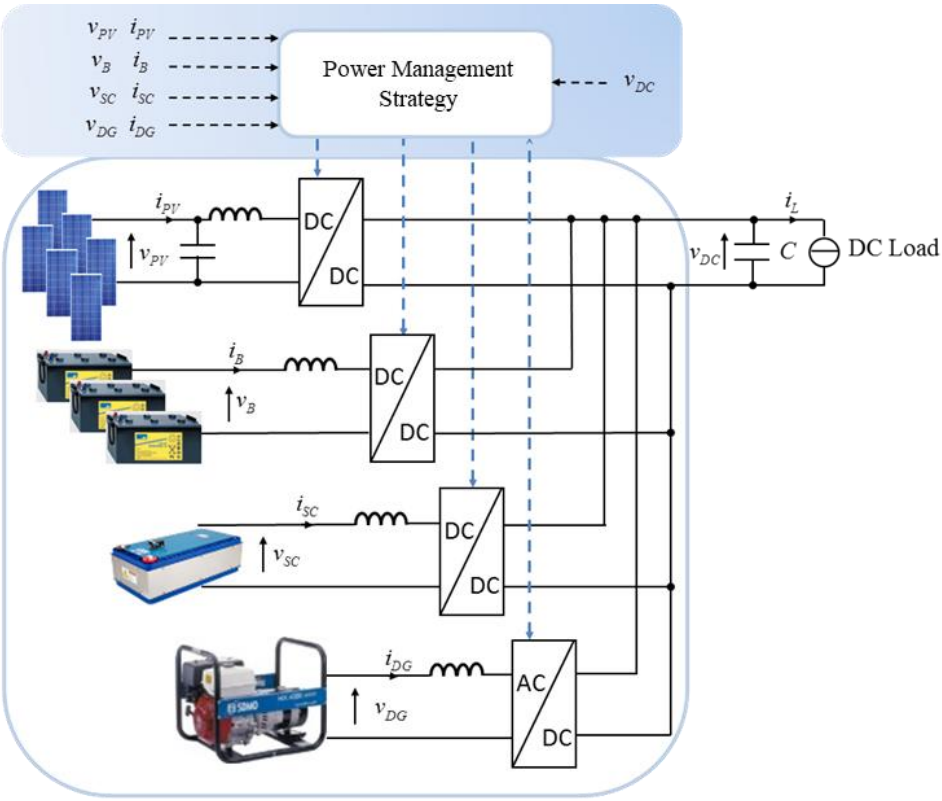

Figure 25. DC microgrid power system configuration [71].

These elements are connected on a common DC bus by their dedicated power converters. Each element is controlled by independent controller, but the power arrangement of each part is managed by power management strategy block. As the main energy source of the system, the PV source is connected on the DC bus through the DC–DC power converter, which is controlled by a MPPT method in most of the cases. However, it can be also operated to output a constrained power [72]. DG, SC and batteries work as backup energy equipment. Each of these three backup components has a different role for the DC microgrid operation, according to the different power fluctuations that can occur. Electrochemical storage is the main backup energy used for longer fluctuation periods (in the range of minutes/hours). If the batteries state of charge SOC_B reaches its minimum limit, DG has to be turned on and used for supplying the load and even to recharge the batteries. However, because of the sluggish response of the DG, the generator cannot immediately respond to power fluctuations, and the DC bus voltage cannot be maintained constant. The power quality of the system can be enhanced by using SC against the power deficit of the DG start-up as shown in the last chapter. Therefore, the SC is controlled to compensate the initial slow dynamics of the DG while starting and keep the DC bus voltage v_{DC} constant. In addition,

SC can be also controlled as complement for batteries charging power, or inversely as buffer for batteries discharging power.

The DC microgrid power flow between the different sources is controlled by a central power management strategy. It provides overall control of the power system and sets the current reference for the different converters that control the power system components according to the energy balance of the system. Moreover, the main controller cooperates with a local DC load controller, which can give the load shedding order. It can reduce a part of the demanded load power when the system is under the deficiency of supplying power.

III.1.1. Photovoltaic array

The generated PV power depends on the solar irradiance, PV cell temperature, array voltage, and the current through the PV array. In order to maximize the produced PV energy, a MPPT method is needed to find and maintain the peak power [73,74]. On the other hand, to prevent electrochemical batteries being overcharged, PV production should be limited via a constrained algorithm [75]. Thus, PV power production p_{PV} is described as:

$$p_{PV}(t) = p_{PV\_MPPT}(t) - p_{PV\_S}(t) \quad (3.1)$$

where p_{PV_MPPT} is the MPPT PV power reference, p_{PV_S} is the PV shed power reference. The calculating result of these two references decides the final PV generation power.

III.1.2. Electrochemical storage

Lead-acid batteries are used as electrochemical storage for this standalone DC microgrid after considering its comparatively low cost and matured technology. In order to protect the batteries from over-recharging and over-discharging, the batteries SOC_B is limited between SOC_{B_MAX} and SOC_{B_MIN} as upper and lower limitation respectively, as shown in (3.2) and computed by (3.3). Moreover, the charge–discharge rate of the batteries is controlled by current regulation and the batteries power can be controlled by giving corresponding current reference. Thus, the discharging and recharging current i_B has to respect the limitations, i_{B_MAX} and i_{B_MIN}, as in (3.4). Since batteries discharging power is positive and recharging power is negative, i_{B_MAX} and i_{B_MIN} are positive and negative separately.

$$SOC_{B\_MIN} \le SOC_B(t) \le SOC_{B\_MAX} \quad (3.2)$$

$$SOC_B(t) = SOC_{B\_init} + \frac{1}{C_B \times 3600 \times v_B}\int_0^t p_B(t)dt = SOC_{B\_init} + \frac{1}{C_B \times 3600 \times v_B}\int_0^t v_B(t) i_B(t)dt \quad (3.3)$$

$$i_{B\_MIN} \le i_B(t) \le i_{B\_MAX} \tag{3. 4}$$

where $p_B(t)$ is the batteries power, SOC_{B_init} is the initial batteries state of charge, v_B is the voltage of batteries bank, and C_B is the total capacity of the batteries bank.

III.1.3. Supercapacitor and diesel generator

SC has a high power density characteristic that can be released suddenly and rapidly, so that the SC can supply a great power during a short time [76]. In general, there is no power constraint and SC power p_{SC} can be positive and negative, which represent discharging power to the DC bus and absorbing power from the DC bus respectively. The SC energy E_{SC}, lies on the SC voltage v_{SC} and the SC capacitance C_{SC}:

$$E_{SC} = \frac{C_{SC} v_{SC}^{\ 2}}{2} \tag{3. 5}$$

Hence, with the change of capacitor voltage, the stored energy will change accordingly and the state charge of SC noted SOC_{SC} can be computed as:

$$SOC_{SC} = \frac{\frac{C_{SC} v_{SC}^{\ 2}}{2}}{\frac{C_{SC} v_{SC\_RATED}^{\ 2}}{2}} \times 100\% = \left(\frac{v_{SC}}{v_{SC\_RATED}} \right)^2 \times 100\% \tag{3. 6}$$

where v_{SC_RATED} is the SC's rated voltage. In addition, it should be noticed that SC has a self-discharging nature. According to the experimental results of self-discharging shown in Figure 26, it is noted that in 40 hours, the SOC_{SC} decreases from 100% to 15%.

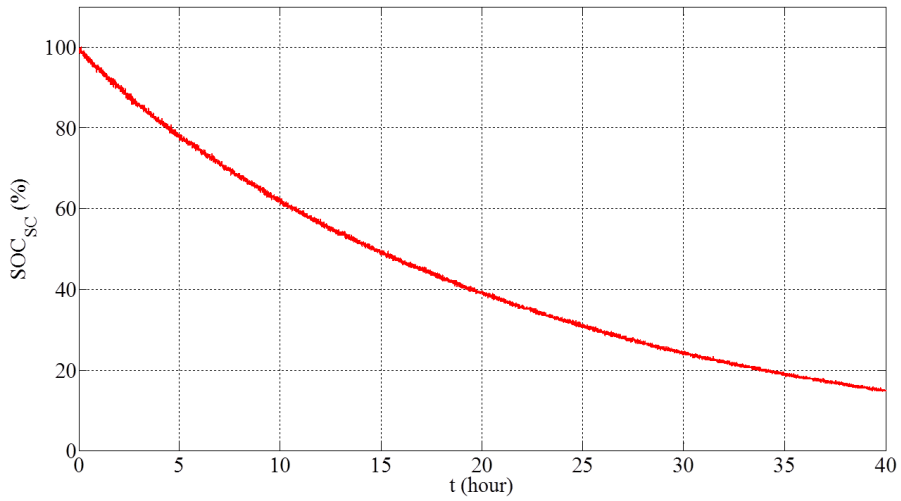

Figure 26. SOC of SC during the self-discharging.

The steady state of DG is described in Section II.2. and the condition to connect DG to the DC microgrid is to satisfy the equation (2.2).

III.2. Power management strategy design

The aim of control strategy is to balance the power in the DC microgrid and therefore to maintain the DC bus voltage, whose configuration is shown in Figure 25. On the other hand, the power system should satisfy the load power demand as much as possible and meanwhile exploit the PV energy to the greatest extent.

In the power system, PV power p_{PV} is uncertain and unreliable, changing with solar irradiance and PV cell temperature. This behavior is also valid for load power p_L, ($p_L = v_{DC} i_L$), varying according to users' demand. But both of them can be limited in case of need; if not, the PV power can be regulated in MPPT mode and the load power can be satisfied. In contrast, batteries power p_B, DG power p_{DG}, and SC power p_{SC} can be controlled, within their physical limits, by giving corresponding current reference, i_B^*, i_{DG}^*, and i_{SC}^*. Neglecting the conversion losses and line power losses, the physical law of power balancing is described as:

$$p_{PV}(t) + p_B(t) + p_{SC}(t) + p_{DG}(t) = p_L(t) + C \times v_{DC} \frac{dv_{DC}(t)}{dt} \quad (3.7)$$

where p_L, p_{PV} and p_{DG} are always positive; p_B and p_{SC} can be positive and negative, which represent discharging power to the system and absorbing power from the system respectively.

At the beginning, with the required measurements and data collecting through the sensors, the PV generated power and the demanded load power are assumed to be known. Secondly, the control management starts by computing the difference of PV generation and load demand, $\Delta p = p_{PV} - p_L$, which causes fluctuations in the DC bus voltage v_{DC}. Steady v_{DC} signifies well balanced power in the power system. Thus, power balance is performed by adjusting other controllable sources for stabilizing the DC bus voltage. The required power is calculated by the error between v_{DC} and its reference v_{DC}^*, with a proportional-integral (PI) controller as in (3.8):

$$p_B(t) + p_{SC}(t) + p_{DG}(t) = K_P(v_{DC}^*(t) - v_{DC}(t)) + K_I \int (v_{DC}^*(t) - v_{DC}(t))dt + p_L(t) - p_{PV}(t) \quad (3.8)$$

where K_P is the proportional gain and K_I is the integral gain. Depending on the priorities of controllable sources, the detailed power management strategy for the DC microgrid is described in the following three subsections according to the constrictive values. Each of the last two subsections offers

six power flow cases according to the possible operating modes of this hybrid system in order to meet the power system restraints.

III.2.1. PV power is equal to the required load power

The first case is when the generated power by the PV array is equal to the power demanded by the users. In this case, the load demand is totally fulfilled by the PV array and there is no power extracted from the batteries. In the long run, the PV power and load power can be regarded as approximately equivalent. But from a short-term period, this case rarely happens since PV power and users' demand are always dynamically changing. Thus, it is not discussed any more in this section.

III.2.2. PV power is less than the required load power

If there is no sufficient power to supply the load demand, the deficient power needs to be complemented by other sources. There are six cases according to the SOC_B as well as to the SOC_{SC}, whose flow chart is shown in Figure 27.

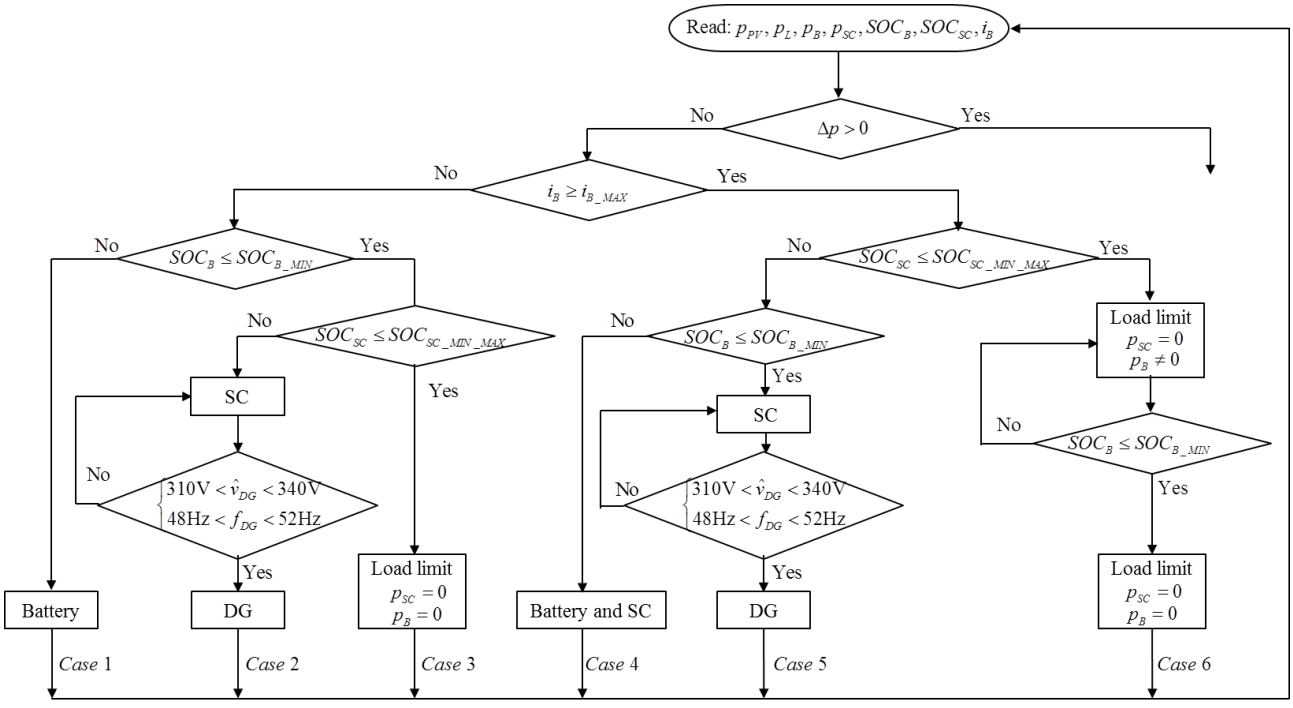

Figure 27. Flow chart of the power management strategy when PV power is less than the required load power.

III.2.2.1. Case 1

This is the case where the PV output power is less than the required load power and the difference between these two powers is calculated to know that the controlling batteries current is lower than the batteries maximum discharging current. The shortage of power is provided only by the batteries.

III.2.2.2. Case 2 and case 3

With the consumption of batteries energy, SOC_B decreases to its minimum value. If SOC_{SC} is higher than $SOC_{SC\_MIN\_MAX}$, DG can be started up. $SOC_{SC\_MIN\_MAX}$ is defined as maximum value of the minimum SOC_{SC} and indicates that the SC energy is enough to launch DG as a last chance to start up DG. Another value of the minimum SOC_{SC} is $SOC_{SC\_MIN\_MIN}$, which is defined as the minimum value of the minimum SOC_{SC} and means that SC already releases its storage energy to the constraint. Before connecting DG to DC bus, the generator's frequency and voltage need to reach the rated values, that is no-load condition. In this period, the role of SC is to stabilize the DC bus voltage and supply the power difference for a short term. When the DG reaches the stabilized output regime, it will be connected to the DC bus and will supply the load together with the PV source. This is the case 2. However, if SOC_{SC} is less than $SOC_{SC\_MIN\_MAX}$, the power system loses its last chance to start up DG. Therefore, the load will be shed partially to prevent the system failure and DC bus voltage drop-down. This is the case 3.

III.2.2.3. Case 4

This case is activated in the condition that power deficit is greater than the maximum power of the batteries which is expressed by the constrained batteries current i_{B_MAX}. The condition is reinforced that SOC_B is higher than SOC_{B_MIN} and SOC_{SC} is also higher than $SOC_{SC\_MIN\_MAX}$, so the batteries can offer the restrictive power while SC supplies the remain of system demanding power.

III.2.2.4. Case 5 and case 6

The cases 5 and 6 are the extensions of case 4. Whether the system turns into case 5 or case 6, it lies on storage if it is completely discharged or not. If the batteries reaches its SOC_{B_MIN} as lower limit, and the SOC_{SC} is higher than $SOC_{SC\_MIN\_MAX}$, SC is able to operate and DG will be launched; this is the case 5. On the other hand, if SC becomes empty earlier than the batteries, load will be limited. Hence, batteries will supply first the restricted power; afterwards, the load will be further shed when the batteries storage is used up. This is the case 6.

III.2.3. PV power is higher than the required load power

This subsection presents the situation when the PV power is higher than the load power. Under this condition, the load demand is fulfilled by the PV source while there is an excess amount of PV energy. For PV power excess, the power management strategy defines six modes of operation, which are represented in the flow chart given in Figure 28.

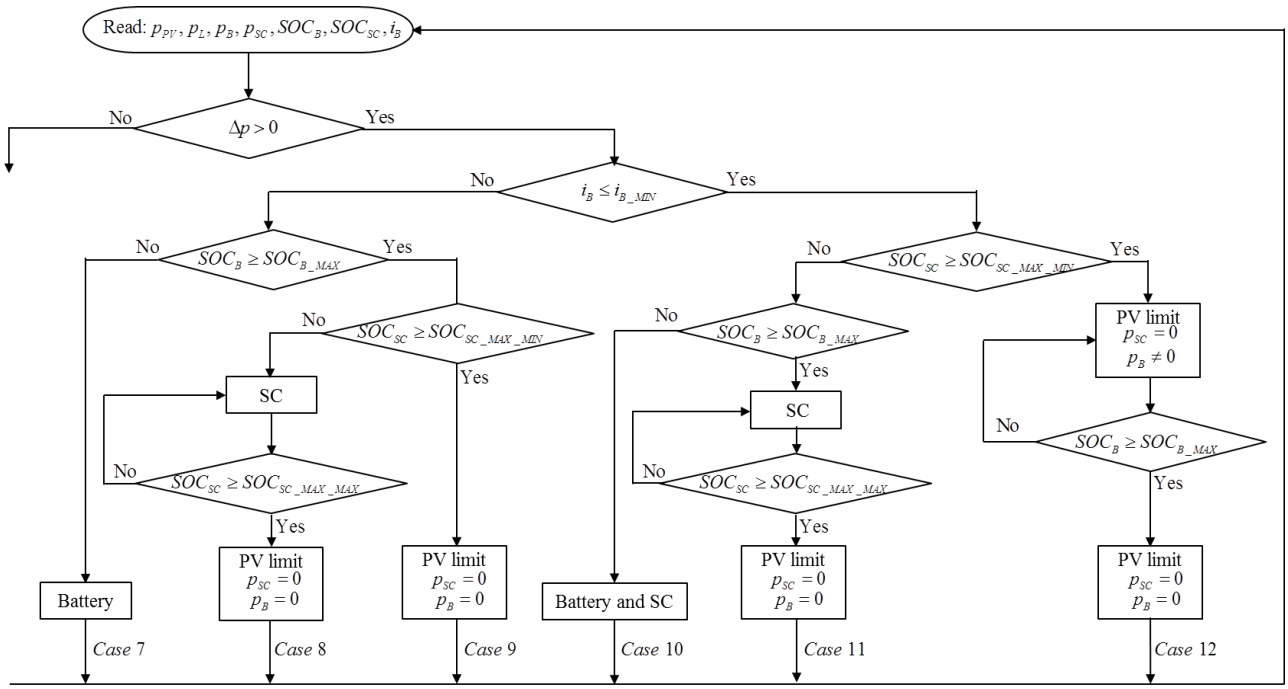

Figure 28. Flow chart of the power management strategy when PV output power is more than the required load power.

III.2.3.1. Case 7

This case is the very common case. After calculating, if the recharged current of batteries is less than the current upper limit, all the surplus power is injected into batteries storage until the SOC_B reaches its maximum limit.

III.2.3.2. Case 8 and case 9

These two cases can be the extensions of case 7. After that the batteries is fully charged, the excess power flows into SC if SOC_{SC} is less than $SOC_{SC\_MAX\_MIN}$ until the SOC_{SC} reaches $SOC_{SC\_MAX\_MAX}$, and then PV source generates energy through the constrained PV power control mode; if not, PV source will operate directly into constrained PV power production mode. These are the cases 8 and 9 respectively. Here, $SOC_{SC\_MAX\_MIN}$ is defined as the minimum value of the maximum SOC_{SC} while $SOC_{SC\_MAX\_MAX}$ is defined as the maximum value of the maximum SOC_{SC}. When SOC_{SC} is in this

range, it means that SC is fully charged. This is because SC has a self-discharging current and after tens of seconds, it can be obviously seen that SOC_{SC} goes down. If the SC's fully charging state is represented by a fixed value, when SOC_{SC} is under this value, SC is recharged to this fixed value but SC will be recharged again after several seconds because SOC_{SC} decreases under this value. So, in order to prevent that SC is frequently recharged, SC saturation state is expressed as a length of range. Therefore, when SC is recharged to $SOC_{SC\_MAX\_MAX}$, the PV power is limited, but after tens of minutes, when SOC_{SC} drops to $SOC_{SC\_MAX\_MIN}$, PV array enters into MPPT mode to recharge again the SC.

III.2.3.3. Case 10

After calculating, if the recharging current of batteries is less than the current lower limit and SOC_B is less than its maximum limit, batteries are recharged by constant recharging current i_{B_MIN} and the remaining surplus power is charged into SC.

III.2.3.4. Case 11 and case 12

Case 11 and case 12 are the extension of case 10. Whether the system turns into case 11 or case 12, depends on if storage is fully recharged or not. If batteries take the lead to be fully recharged, all the excess power will be charged into SC until the SOC_{SC} reaches its maximum maximum value. Then, the PV power will be limited. This is case 11. On the contrary, if SC is recharged entirely, PV power will be limited to supply the load and the batteries recharging; afterwards, the PV power will be damped to only supply the load. This is the case 12.

III.3. Simulation results

The described power system has a hybrid aspect from the higher level, which is centralized power management strategy, to the lower one, which is the dedicated local controller. In order to validate the hybrid power system and the proposed power management strategy from the theory aspect, the hybrid simulation is proposed. Due to the hybrid nature of the power system behaviour, the simulation is carried out under the MATLAB/Simulink software.

The simulation data of PV power generation come from a real PV array during one day MPPT experimental test ($09:00 \le t \le 18:00$ (hour:minute)), which was operated on 16th April 2015, at Compiègne in France. This real PV array, formed by 8 PV panels, has been installed on the university building's roof since 2008. The real solar irradiance and PV cell temperature of this day are illustrated in Figure 29. Under this environment, the MPPT PV power generation, p_{PV_MPPT} is recorded and profiled in Figure 30.

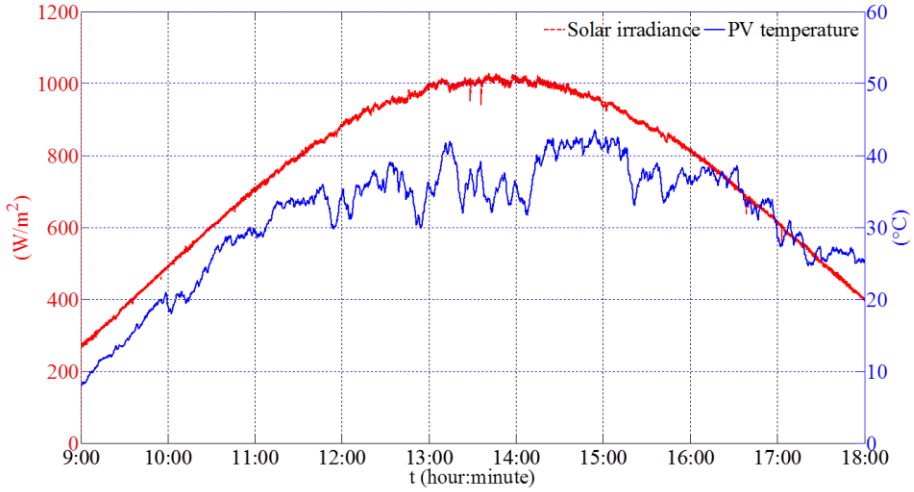

Figure 29. Solar irradiance and PV cell temperature on 16th April 2015.

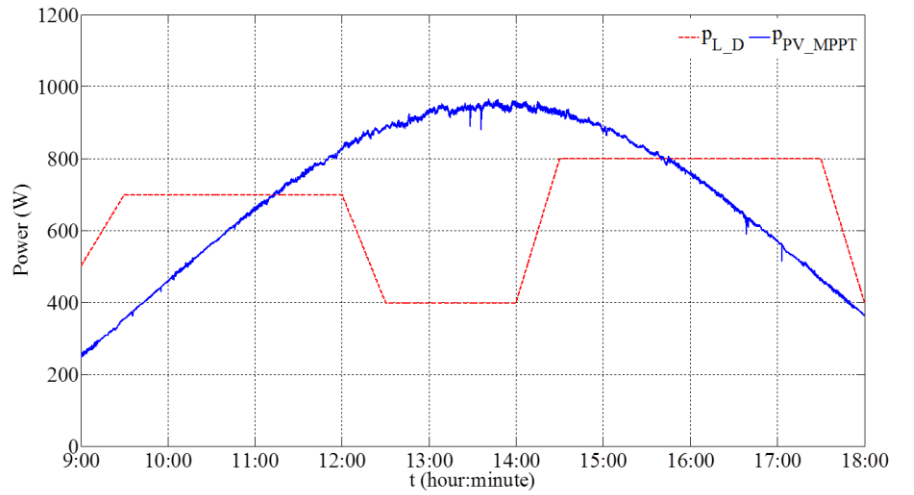

Figure 30. Load power demand and PV MPPT power.

Regarding the load power curve, a simple and arbitrary load power demand evolution is also considered and depicted in Figure 30.

The system constraints and values are also defined and shown in the second column of values in Table 5.

Table 5. Arbitrary values and limits.

Variables	Values	
	Manual	**One-day**
SOC_{B_MAX}	51%	53%
SOC_{B_MIN}	49%	47%
$SOC_{SC\_MAX\_MAX}$	90%	90%
$SOC_{SC\_MAX\_MIN}$	85%	85%
$SOC_{SC\_MIN\_MAX}$	50%	50%
$SOC_{SC\_MIN\_MIN}$	45%	45%
i_{B_MAX}	5A	5A
i_{B_MIN}	-5A	-5A
v_{DC}^{*}	400V	400V

In the first column of values, the word "manual" means that the load power and PV power are changed manually, according to the experimental operators input commands in the twelve experimental verifications (Section III.4.2). On the other hand, the word "one-day" means that the load power and PV power come from the real recorded data, which are not be subject to human interference during the whole process in this simulation and in the one-day experimental test (Section III.4.3). The system constraints and values are set according to the experimental facilities. Regarding the DC microgrid test bench, the batteries bank's capacity is too large for the power level of the test bench. Thus, in order to observe all the twelve cases, SOC_B is limited in a narrow range while the scope of SOC_B in the one-day experimental test is slightly larger. Similarly, the batteries bank's current limit is limited at the same power level of experimental bench. Moreover, the SC current is not limited, but the same amount of power can cause great current in the case of the low SC voltage, which can be harmful to the experimental facility. Thus, SOC_{SC} is limited to a minimum of 45% since it is quadratically proportional to the SC voltage.

Figure 31 shows the power evolutions performance of the simulation results. During the first interval ($09:00 \le t < 10:23$), the load is firstly supplied by the batteries (case 1). During the second interval ($10:24 \le t < 11:14$), around $10:24$, SOC_B reaches its lower limit value and then SC supplies the load before the DG starting up to generate power. With the increasing of PV power, DG power gradually decreases until PV power is higher than the load power demand. This is the case 2.

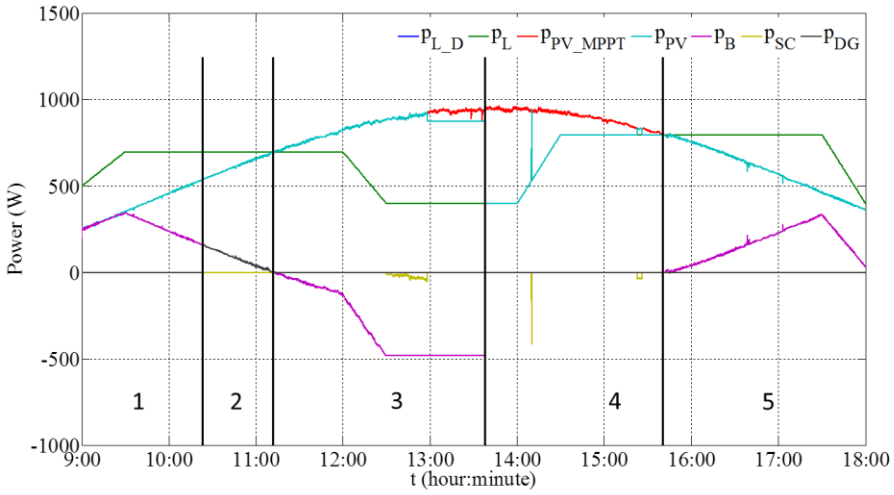

Figure 31. Power evolution.

Thereafter, during the third interval ($11:14 \le t < 13:38$), the DG is out-of-service and the excess PV generation is used to charge the batteries. This is the case 7. However, from $12:30$ to $12:58$, the excess PV power surpasses the maximum recharging power of batteries. Hence, the excessive PV power is absorbed by SC. This is case 8. And when the SC is fully recharged, there is PV power shedding and the batteries absorb the PV power in its maximum recharging power, which is case 12. In the fourth interval ($13:38 \le t < 15:40$), since the batteries are already fully charged and the SC is also in maximum state, PV power shedding is operated to only supply the load. But SC is recharged again up to $SOC_{SC\_MAX\_MAX}$ when SOC_{SC} reaches the value $SOC_{SC\_MAX\_MIN}$ at the time $14:11$ and $15:23$. And then, PV power is shed once more until PV power is less than load demand. This is the case 8. After this moment, load power demand is only provided by batteries during the fifth interval ($15:40 \le t < 18:00$).

SOC_B and SOC_{SC} evolutions in Figure 32 and Figure 33, show that storage capacities are entirely respected. Battery and SC work well for both providing energy and absorbing energy. The DC bus voltage evolution shown in Figure 34, remains almost constant even though there are small variations (less than 1% of the rated DC bus voltage), signifying that the proposed control strategy is able to regulate the DC bus voltage within the acceptable limits. The simulation results show the correctness of the logic of the proposed power management.

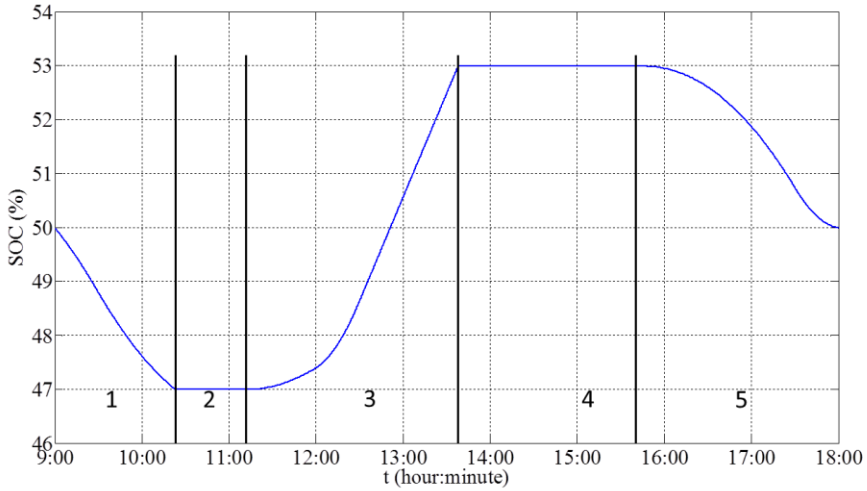

Figure 32. *SOC* evolution of batteries.

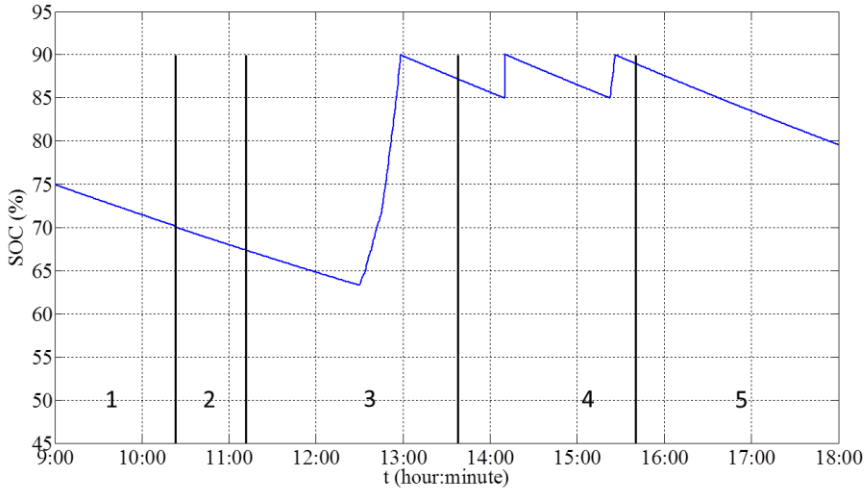

Figure 33. *SOC* evolution of supercapacitor.

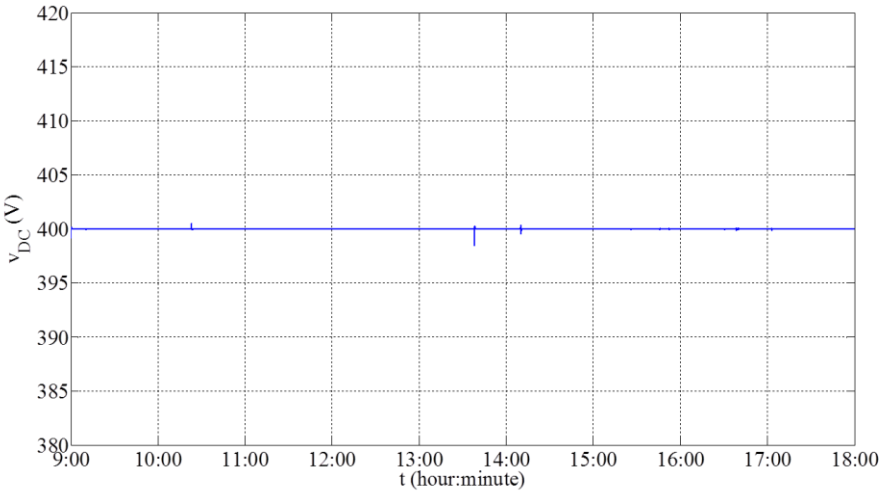

Figure 34. Evolution of DC bus voltage.

III.4. Experimental verification

To verify the feasibility of the proposed power management strategy, an experimental platform is implemented with the purpose of checking the strategy in the real environment so that it can be put into use in the industrial field. The goal is to operate the twelve possible cases, one by one as controllable experiments, and also to operate a continuous test of one-day period (9 hours) for the proposed DC microgrid.

III.4.1. Experimental platform

The experimental platform is composed by electrochemical storage, SC, and the following emulators: a programmable DC electronic load emulates the DC load, a programmable DC source emulates the PV source, and a programmable AC source emulates the DG following the start-up data of the SDMO Technic 6500 E AVR recorded and then implemented. All these elements are connected on the same DC bus through their dedicated power converters. In addition, a set of inductors and capacitors is added in order to ensure compatibility between the different elements.

The DC load is powered directly by the DC bus. The PV power is outputted by the PV array emulator. The batteries, SC, and DG are controlled by hysteresis controller following current references given by the power management strategy algorithm, which is compiled into dSPACE. The fundamental calculating sample time is 50µs. The DC bus voltage reference value in this test is 400V DC. Aiming a building integrated DC microgrid, the choosing of the value of 400V DC takes into account the energy efficiency and the use of the already existing cable infrastructure (400/230 V AC) [64,65]. Concerning the SC, the rated capacitance C_{SC} is 94F, the rated voltage v_{SC_RATED} is 75V, and therefore the rated stored energy is equal to 73Wh. The other main parameters of the experimental platform are given in Table 5 and Table 6 and the image is presented in Figure 35.

Table 6. Elements detail for experimental test.

Element	**Parameter**	**Device**
Bateries (serial 8 units)	96V/130Ah	Sonnenschein Solar: S12/130A
Supercapacitor	94F/75V	Maxwell 75V modules: BMOD0094 P075 B02
PV emulator	600V/5.5A	GEN 3.3kW series power supplies: GEN600-5.5
Load emulator	2.6kW	High power DC electronic load: Chroma 63202
DG emulator	3kVA	Programmable AC source Puissance+ PA-3000-B/260V-12A
IGBT	600V-100A	SEMIKRON SKM100GB063D
Controller board		dSPACE 1103

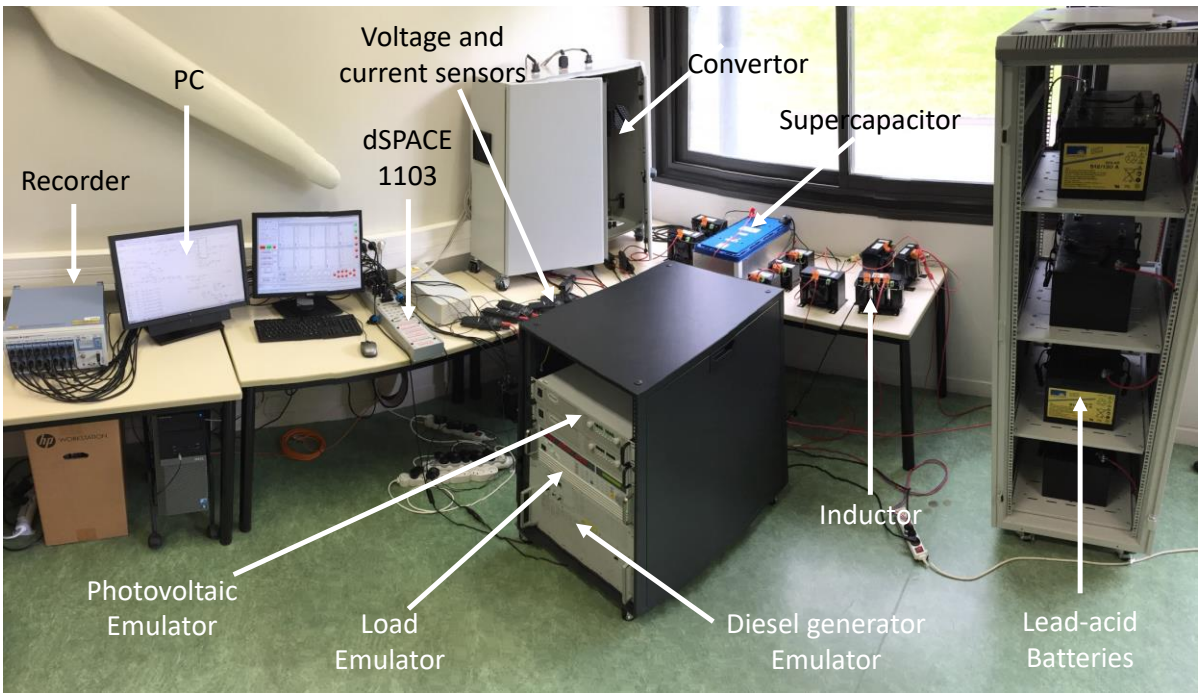

Figure 35. Image of experimental platform

III.4.2. Twelve experimental cases

In these twelve experimental cases, both the load power and PV power are changed manually. The experiments are divided into two parts depending on the cases which are expected to be shown. Before carrying out the experiments, system constraints and values are defined and shown in the first column of values in Table 5.

III.4.2.1. PV power is less than the required load power

This experiment mainly discusses the cases where PV power is less than the load demand. The entire sequence is divided into six intervals according to the described cases. Figure 36 shows the power evolution of the proposed microgrid during different operating cases. The SOC_B and SOC_{SC} evolutions are shown in Figure 37 and Figure 38 respectively.

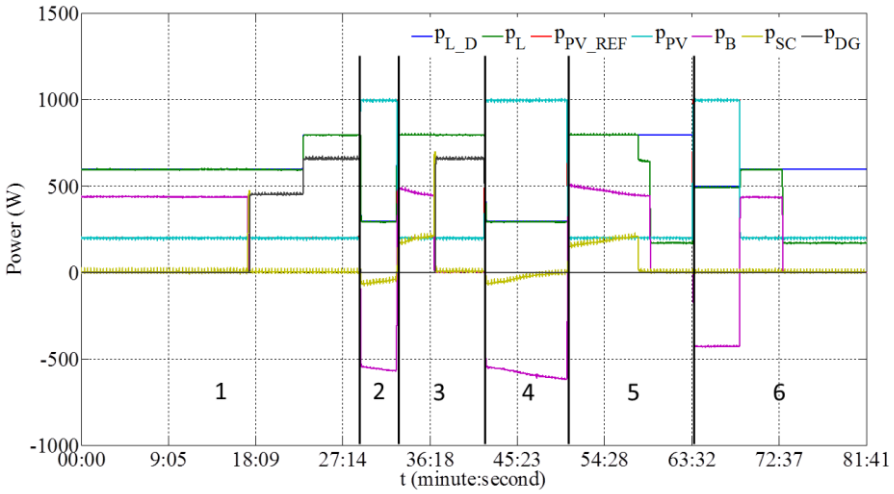

Figure 36. Power evolutions.

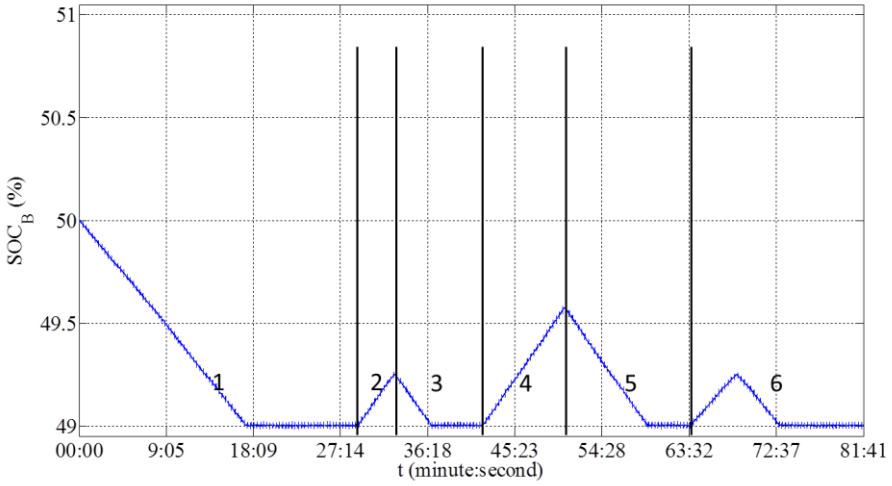

Figure 37. *SOC* evolution of batteries.

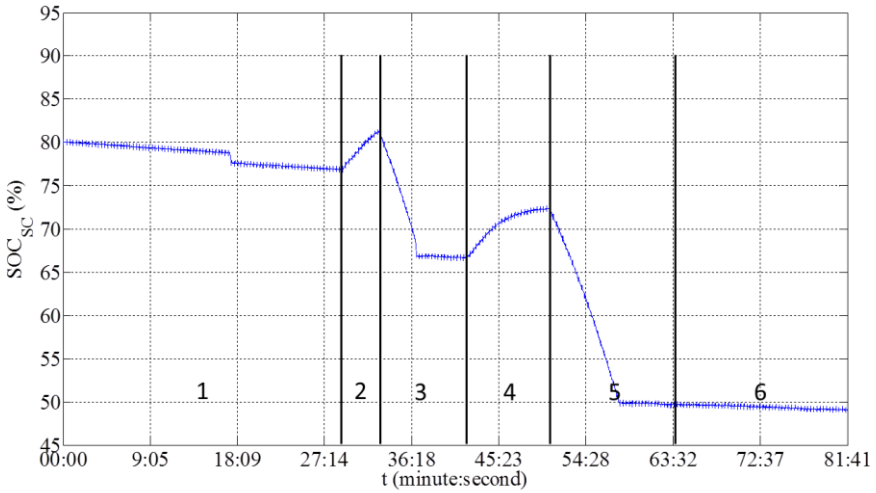

Figure 38. *SOC* evolution of supercapacitor.

During the first interval ($00:00 \le t < 29:00$ (minute:second)), the input PV power reference p_{PV_REF} is set to be 200W and the load power demand p_{L_D} is 600W; the deficient power is only supplied by the batteries (case 1). At $t = 17:23$, SOC_B reaches its minimum value and since SOC_{SC} is still greater than its minimum maximum value, DG can be started. Hence, before connecting DG on the DC bus, SC supplies power; and after being connected to the DC bus, DG provides the power. When the load power changes to 800W, the DG power also changes correspondingly. This is the case 2.

For the second interval ($29:00 \le t < 33:00$), the following powers are chosen: $p_{PV\_REF} = 1000W$ and $p_{L\_D} = 300\text{W}$. This experiment is to charge the batteries and SC because the energy in the batteries is used up in the first interval. Thus, it has to recharge the batteries to continue observe the other cases. The charging operations of both batteries and SC are shown in Figure 37 and Figure 38 respectively. This is also the display of case 10.

During the third interval ($33:00 \le t < 42:00$), $p_{PV\_REF} = 200W$ and load demand $p_{L\_D} = 800\text{W}$; after calculating, the needed batteries discharging current is higher than its constrained limit i_{B_MAX}. Therefore, SC has to offer the complementary power, which is the case 4. When the SOC_B reaches the minimum value, because the SOC_{SC} is still higher than the minimum maximum value, the DG can be started. Before connecting the DG on the DC bus, SC supplies power. When the DG meets the connection requirements, DG is jointed into the system and provides the deficient power. This is the case 4.

For the fourth interval ($42:00 \le t < 50:30$), the following powers are chosen: $p_{PV\_REF} = 1000W$ and $p_{L\_D} = 300\text{W}$. This experiment is to charge the batteries and SC because the energy in the battery is used up in the third interval. Thus, it has to recharge the batteries to continue observe the other cases. The charging operations of both batteries and SC are shown in shown in Figure 37 and Figure 38 respectively. This is again the display of case 10.

During the fifth interval ($50:30 \le t < 63:35$), the case 6 can be seen. At the beginning of this interval, both the batteries and SC are operating to provide the power to the load. But SOC_{SC} reaches its lower limit faster than SOC_B. So, at $t = 57:57$, SC stops to supply the system and at the same time, the load is shed that only the batteries supply the restricted power. But after one minute sixteen seconds (at $t = 59:13$), the batteries are also completely used up. However, the SOC_{SC} is lower than the minimum maximum value so that DG cannot be started up. Without any doubt, load has no choice but to be shed again and only the PV source supplies the partial load.

During the last interval ($63:35 \le t \le 81:41$), the chosen powers at the beginning are $p_{PV\_REF} = 1000W$ and $p_{L\_D} = 500W$. In this case, the batteries are recharged firstly while the SC is not recharged to make sure that SOC_{SC} is lower than its minimum maximum value. At $t = 68:30$, the PV power decreases from 1000W to 200W while the load power demand increases from 500W to 600W. Under these conditions, the batteries can provide sufficient power to the system within its current limit. After a few minutes, the batteries are completely consumed. As the SOC_{SC} is still below the minimum maximum value, the DG cannot be activated. So, the load power is directly shed to 200W even though the load power demand is 600W. This is the case 3.

The whole DC bus voltage evaluation in this experiment is presented in Figure 39. It can be noted that the DC bus voltage remains almost constant with some negligible fluctuations.

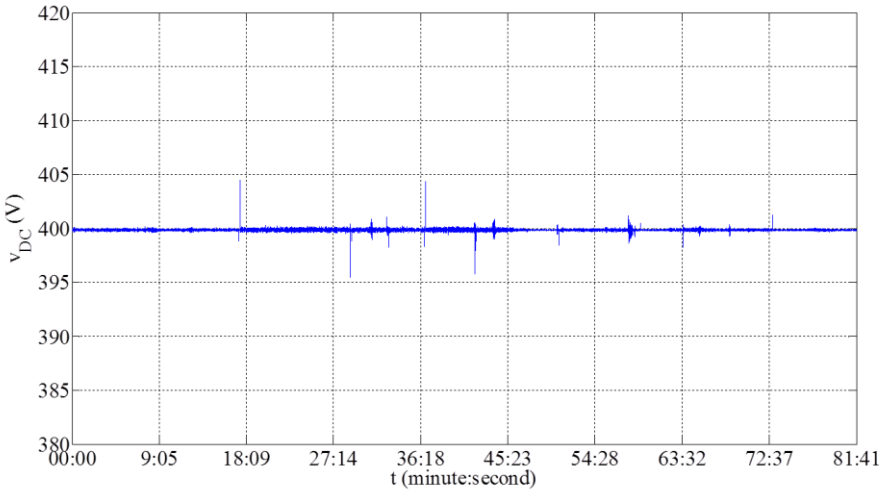

Figure 39. Evolution of DC bus voltage.

III.4.2.2. PV power is more than the required load power

This experiment mainly discusses these cases that PV power is higher than the load power demand. The entire sequence is divided into six intervals according to the cases described. Figure 40 shows the power evolutions performance of the proposed microgrid during different operating cases. The SOC_B and SOC_{SC} evolutions are shown in Figure 41 and Figure 42 respectively.

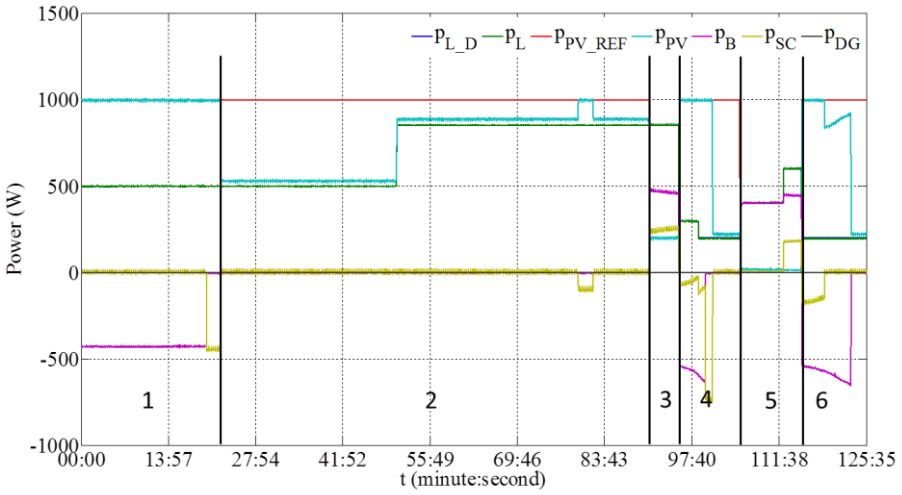

Figure 40. Power evolutions.

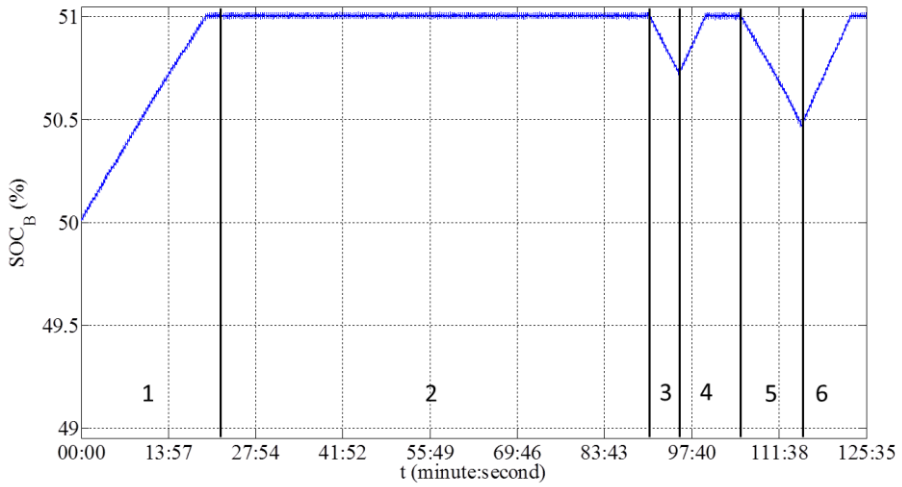

Figure 41. *SOC* evolution of battery.

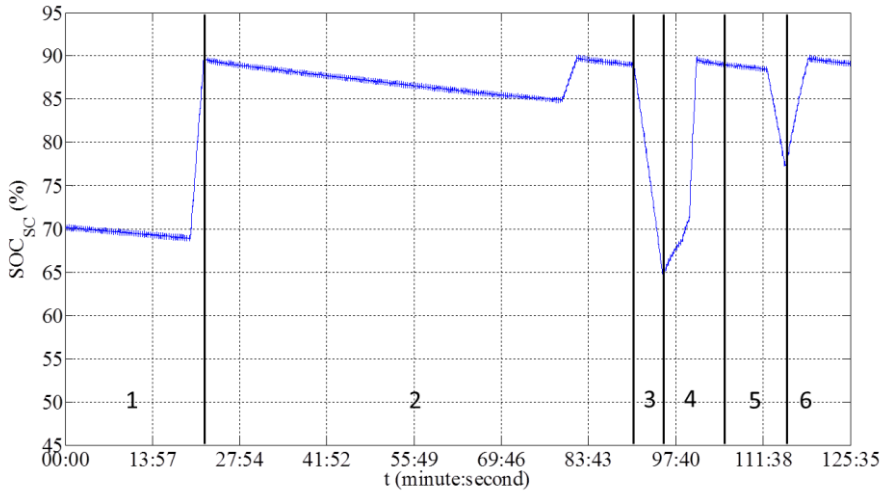

Figure 42. *SOC* evolution of SC.

During the first interval ($00:00 \le t < 22:15$), the PV power (1000W) is greater than the load power demand (500W). Thus, the excess power recharges firstly the batteries (Case 7). Then, at $t = 17:23$, the SOC_B reaches its maximum value. Because SOC_{SC} is less than its maximum minimum value, the excess power recharges now the SC until reaching SC fully charging state ($SOC_{SC\_MAX\_MAX}$). This is the case 8. The charging operations of both batteries and SC are shown in Figure 41 and Figure 42 respectively.

During the second interval ($22:15 \le t < 91:00$), when batteries and SC are completely recharged, the PV power is limited to only supply the load and to balance the power system. When the load power increases from 500W to 800W, the limited power of PV source also changes correspondingly. This is the case 9. Within this interval, the SOC_{SC} goes down gradually and slowly because of the self-discharge nature of SC as shown in Figure 42. After 57 minutes and 14 seconds (at $t = 79:29$), SOC_{SC} reaches the $SOC_{SC\_MAX\_MIN}$ and then the SC is recharged again up to $SOC_{SC\_MAX\_MAX}$.

For the third interval ($91:00 \le t < 95:40$), the following powers are chosen: $p_{PV\_REF} = 200W$, $p_{L\_D} = 800W$. As both of storages are already fully recharged, this part is to release the energy of the batteries and SC, in order to continue to observe the other cases later. This is also the display of case 4.

During the fourth interval ($95:40 \le t < 105:24$), $p_{PV\_REF} = 1000W$ and $p_{L\_D} = 300W$; after calculating, the batteries recharging current is lower than its constrained limit i_{B_MIN}. Meanwhile, SOC_{SC} is lower than $SOC_{SC\_MAX\_MIN}$. Therefore, SC also has to absorb the surplus power, which is the case 10. When the load demand power drops from 300W to 200W at $t = 98:40$, SC absorbs more extra surplus power. At $t = 99:51$, the SOC_B reaches its maximum value. So after this time, only SC absorbs the surplus power until reaching its maximum state. When both of the storages are fully recharged, the PV power is limited by the dedicated control. This describes the case 11.

During the fifth interval ($105:24 \le t < 115:17$), with $p_{PV\_REF} = 0W$, the load power demand p_{L_D} is firstly set to be $400W$ and then goes up to 600W; this part is to release the energy of the battery and SC to continue observe the case 12 afterwards.

During the sixth interval ($115:17 \le t < 125:35$), the following powers are chosen at the beginning: $p_{PV\_REF} = 1000W$ and $p_{L\_D} = 200W$. Both storages are recharged but SOC_{SC} reaches its higher limit faster than SOC_B. Therefore, at $t = 118:52$, SC stops to absorb power from the system and at the same time, PV power is limited that only the batteries absorb the restricted power. At $t = 123:08$, the batteries are also completely recharged. Therefore, PV power is limited again and only supplies the load.

The whole DC bus voltage evaluation in this experiment is presented in Figure 43; the DC bus voltage remains almost constant with some negligible fluctuations.

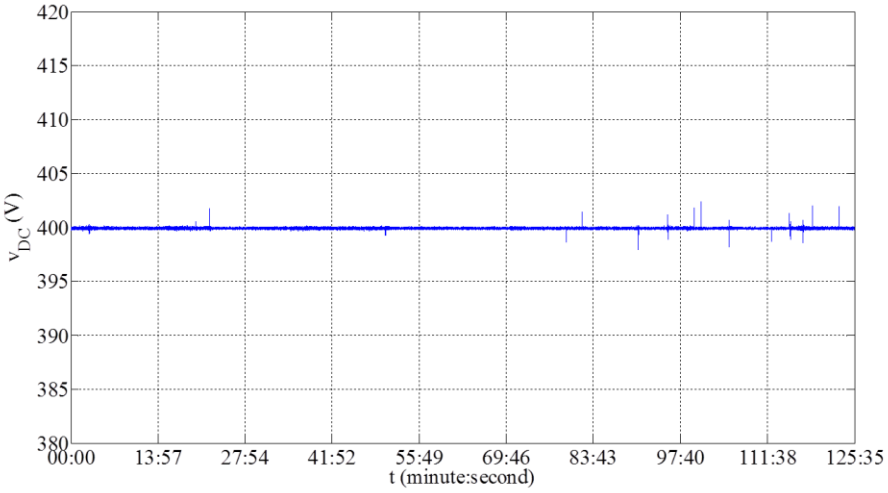

Figure 43. Evolution of DC bus voltage.

III.4.3. One-day experimental test

Unlike the previous two tests which are to show the twelve possible cases, the aim of one-day experiment is to illustrate and prove the effectiveness and application of the whole system strategy in a genuine and natural circumstance. So, this test is without human interference during the whole process. It is to verify that under the control of the proposed strategy, the hybrid PV/DG/battery/SC power system can work well with the real PV power and load profile.

During the one-day test ($09:00 \le t \le 18:00$ (hour:minute)), the real solar irradiance and PV cell temperature of this day are illustrated in Figure 29. The MPPT PV power generation and the load power curve are the same as the data of simulation, which are profiled in Figure 30. For this one-day experimental test, the recorded PV power data are implemented into the PV emulator which simulates the real 8 PV panels' MPPT power production. The system constraints and values are also defined and shown in the second column of values in Table 5.

Figure 44 shows the power evolutions performance of the proposed DC microgrid during 9 hours. During the first interval ($09:00 \le t < 10:24$), the load is firstly supplied by the batteries (case 1). During the second interval ($10:24 \le t < 11:14$), around $10:24$, SOC_B reaches its lower limit value and then SC supplies the load before the DG starting up to generate power. With the increasing of PV power, DG power gradually decreases until PV power is higher than the load power demand. This is the case 2.

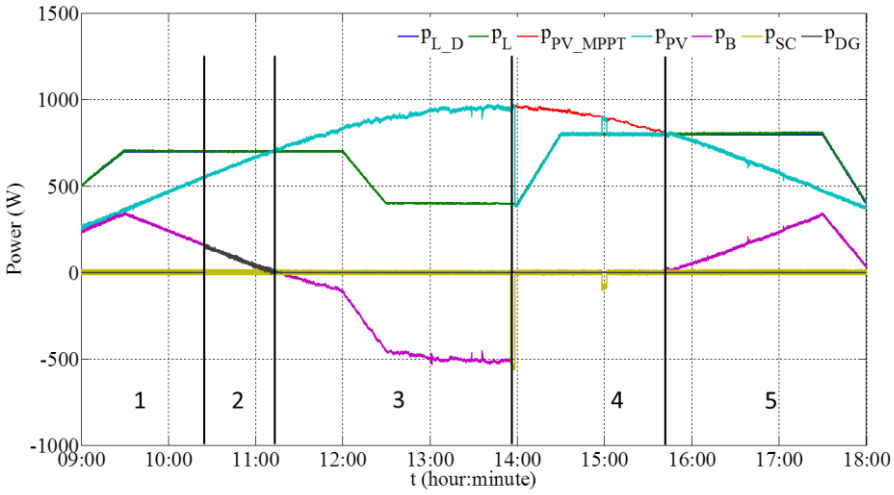

Figure 44. Power evolutions.

Thereafter, during the third interval ($11{:}14 \le t < 13{:}55$), the DG is out-of-service and the excess PV generation is used to charge the batteries. This is the case 7. At the beginning of the fourth interval ($13{:}55 \le t < 15{:}40$), since the batteries are already fully charged, the excess PV power flows into SC. After about three minutes, around $13{:}58$, SC also reaches its maximum state. Therefore, PV power shedding is operated to only supply the load. But SC is recharged again up to $SOC_{SC\_MAX\_MAX}$ when SOC_{SC} reaches the value $SOC_{SC\_MAX\_MIN}$ and then, PV power is shed once more until PV power is less than load demand. This is the case 8. After this moment, load power demand is only provided by batteries during the fifth interval ($15{:}40 \le t < 18{:}00$).

SOC_B and SOC_{SC} evolutions in Figure 45 and Figure 46, show that storage capacities are entirely respected. Battery and SC work well for both providing energy and absorbing energy. The DC bus voltage evolution shown in Figure 47, remains almost constant even though there are small variations (less than 1.5% of the rated DC bus voltage), signifying that the proposed control strategy is able to regulate the DC bus voltage within the acceptable limits. Taking into account that the goal of this one-day test is to further verify the feasibility of the proposed control strategy in a real environment, the experiment results display that the power is well balanced in the proposed microgrid system. What is more, the feasibility of this strategy shows that it can be put into use in an off-grid community or an islanded remote village with the hybrid PV/DG/battery/SC power system.

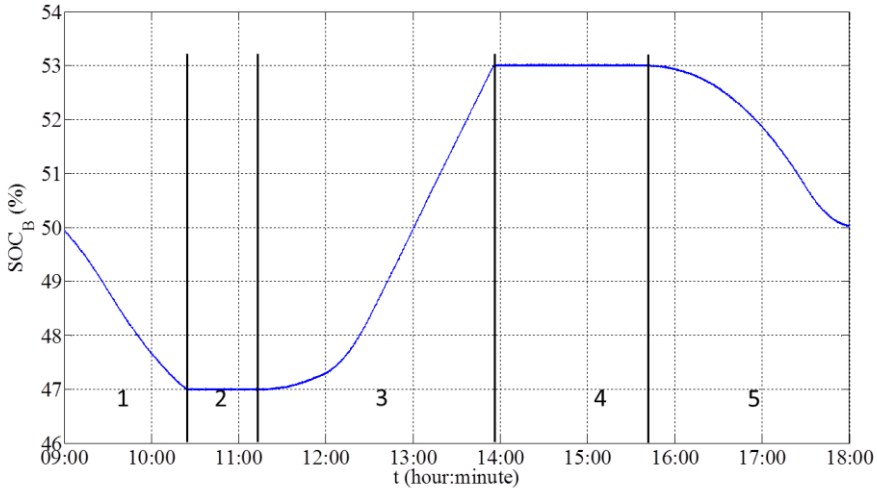

Figure 45. *SOC* evolution of batteries.

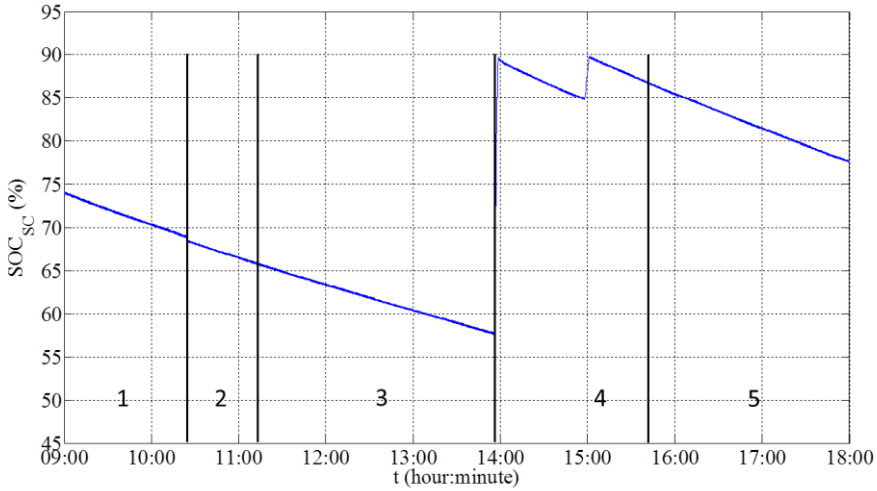

Figure 46. *SOC* evolution of supercapacitor.

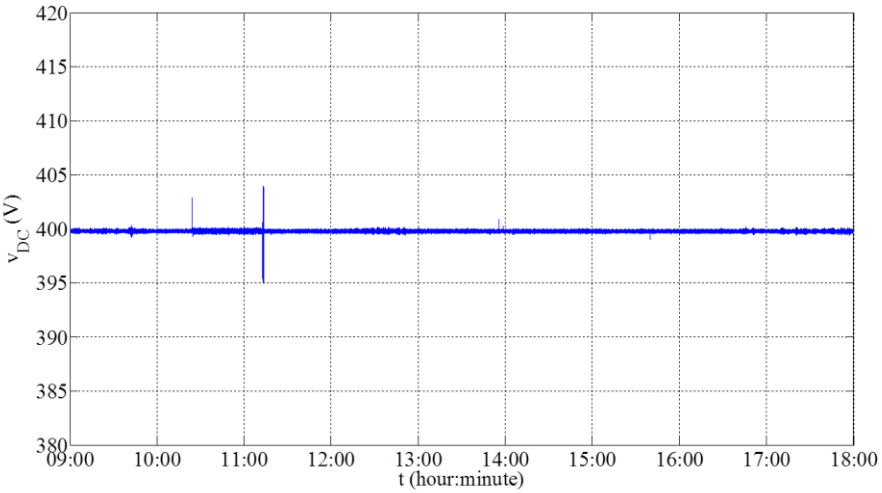

Figure 47. Evolution of DC bus voltage.

III.5. Conclusion

DG can be a good choice in off-grid and isolated microgrid as a backup power when electrochemical storage is used up. But it cannot be launched immediately and needs several seconds to produce stable power. In order to overcome this sluggish dynamic behavior of DG while starting up, SC is used as compensatory energy source to resist against the shortage of PV array power and batteries. The second function of using SC is to supply/absorb power when the needed batteries power is out of the range of its discharging/recharging power. Thus, this chapter firstly presents the hybrid system including PV, batteries, SC and DG. Then, a power management strategy is proposed to achieve coordination between these sources. The individual control schemes are coordinated through the proposed control coordination, approaching to maintain the DC bus voltage stable and the system's power balance. According to the different constraint conditions, twelve cases are likely to appear in a true situation, which are illustrated in detail.

In order to validate the hybrid power system and the proposed power management strategy from the theory aspect, the hybrid simulation is proposed, which is carried out under the MATLAB/Simulink software. The simulation results show the correctness of the logic of the proposed power management.

In order to further verify all the twelve possible cases, controllable experimental cases are operated. In order to verify the feasibility of implementing the power management algorithm in a real environment, based on real weather data, a one-day experiment is operated in the real-time. The experimental results show that the proposed control strategy is able to regulate the DC bus voltage within the acceptable limits, balance the power, and supply the DC load. Fairly good performance of one-day experimental test proves that the power management strategy can be employed in a real hybrid PV/DG/battery/SC power system. Furthermore, the strategy can be programmed into Digital Signal Processor or Field Programmable Gate Array to replace the real-time simulation system (dSPACE), so that it can have application in industrial field.

A power management strategy for a PV-battery-SC-DG based DC microgrid system is proposed in this section, which is verified by test bed. The experiment results show that it can correctly balance the DC bus power and stabilize the DC bus voltage. However, there are cases that the DG outputs low power and there is no consideration about the fuel cost and fuel consumption of the DG. The efficiency and energy consumption of DG need to be considered in this power management strategy, which means to search the optimal rate between power production and diesel fuel consumption. In the beginning of the next chapter, the economic criteria of DG operating modes will be done to understand its energy cost and fuel consumption.

Chapter IV. Power management of DC microgrid with DG economical mode

In the Chapter III, a power management strategy for a PV-battery-SC-DG based DC microgrid system. The simulation and experiment results show that it can well balance the DC bus power and maintain the DC bus voltage. However, there are cases that DG is operated in the low load situation and there is no consideration about the fuel cost and fuel consumption of DG. What's more, the priority of batteries storage is higher than SC in this power management strategy, so that it is possible that the energy stored in SC will be empty because of the self-discharging. Under this case, the DG cannot be started up and the stability of the hybrid power system is reduced. The DG runs in load-following strategy to only supply the load, so that there is no fuel cost comparison with the duty cycle mode in which DG also recharges the battery.

Therefore, in order to advance the research work of the fuel cost and fuel consumption of the hybrid PV-battery-DG-SC power system, this section is the further research on the basis of Chapter III. Furthermore, facing to the power management strategy proposed in Chapter III, a new power management strategy consisting of nine cases for the real time control is presented to balance the power and regulate DC bus voltage, which is verified by the experiments and simulation. The results show that the new strategy can save more fuel cost than the previous one (DG load following mode).

The rest arrangement of this chapter is depicted as follows. Firstly, fuel consumption and cost analysis through experiments is presented in Section IV.1. Then, the DC microgrid system and its components are described in Section IV.2. The power management strategy is introduced and analyzed in Section IV.3 while the simulation verification and experimental verification are given in Section IV.4 and Section IV.5. Finally, Section IV.6 gives the conclusions.

IV.1. Fuel consumption and cost analysis through experiment

Even though the handbook of manufacturers gives the basic information about DG, such as the rated power and the root-mean-square value of output voltage, the situation of fuel consumption is not clearly addressed especially in low power generating situation. Different researchers and research teams use different fuel consumption functions to express the fuel consumption of DG.

In the papers [31] [77], a linear function (4.1), is used for fuel consumption calculation, based on its rated power P_{DG_RATED} and the actual output power p_{DG} supplied by the DG.

$$F(p_{DG}) = b_{DG\_1} P_{DG\_RATED} + a_{DG\_1} p_{DG} \tag{4. 1}$$

where $F(p_{DG})$ is the fuel consumption (L/h), b_{DG_1} and a_{DG_1} are the coefficients of fuel consumption function.

In the papers [78] [79] [52], the fuel consumption noted F (L/kWh) is formulated as a quadratic function of the corresponding generated power p_{DG}.

$$F(p_{DG}) = c_{DG\_2} p_{DG}^2 + b_{DG\_2} p_{DG} + a_{DG\_2} \tag{4. 2}$$

where c_{DG_2}, b_{DG_2}, and a_{DG_2} are the coefficients of fuel consumption function and can be found by curve fitting by the Approximate Diesel Fuel Consumption Chart given by different manufacture [53]. In the research work [54], a similar third order polynomial fuel consumption cost function is also obtained by being fitted to this fuel consumption chart. However, this chart shows an estimate of the fuel consumption of a DG based on the size of the generator and the load at which the generator is operating. It is not an exact figure as various factors can alter the amount of fuel consumed. This is based on consumption per hour. Therefore, the exact fuel consumption should be known by experiments.

IV.1.1. Electrical scheme and experimental platform

In order to measure the actual fuel consumption rate, an experimental platform has been set as show in Figure 48, and the detail parameters of the experimental devices are listed in Table 7.

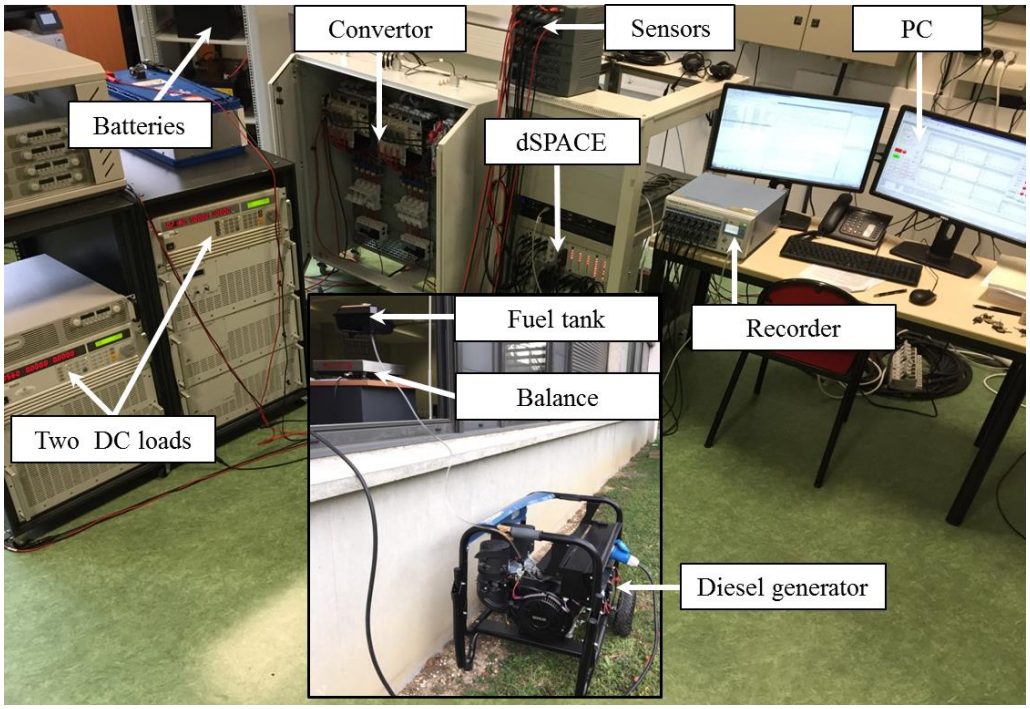

Figure 48. The figure of experimental platform.

Table 7. Elements detail for experimental test.

Element	**Parameter**	**Device**
DC Load	2×2.6kW	High power DC electronic load: Chroma 63202
Bateries (serial 8 units)	96V/130Ah	Sonnenschein Solar: S12/130A
Diesel generator	5.2kW	SDMO Technic 6500E
IGBT converter	600V-100A	SEMIKRON SKM100GB063D
Controller board		dSPACE 1006
Weight balance		Ohaus Defender D15HR
Measuring device		Scaime CPJ Analog signal conditioner

Even though the maximum rated power of DC electronic load is 2.6kW and two loads can theoretically consume the DG maximum output power (5.2kW), the DC electronic load cannot absorb 2.6 kW in reality. Therefore, there are two DC electronic loads in addition with batteries storage, which can be used to absorb a certain power. The two DC loads are connected directly into the DC bus while the batteries storage is connected vie DC-DC converter. The DG is connected to the DC bus through the AC-DC rectifier. Hence, the physical law of power balancing must be completely respected according to the following equation at any time:

$$p_{DG}(t) = p_{DC}(t) + p_B(t) + C \cdot v_{DC}(t) \frac{dv_{DC}(t)}{dt} \quad (4.\ 3)$$

where p_{DC} is the DC load, C is the DC bus capacitor and v_{DC} is the DC bus voltage. The batteries storage is utilized on one hand to absorb partial power and on the other hand to regulate the DC bus voltage.

IV.1.2. Diesel consumption and cost optimization analysis

In this section, aiming at analysing the fuel consumption of DG, several experiments has been done to study the temperature influence on the DG and diesel fuel consumption rate under different output power value. DG operation and maintenance cost is also gotten according to the instruction manual of manufacture.

IV.1.2.1. Temperature influence

The total cost of power production from the DGs includes fuel, start-up, and shut down costs. The start-up cost is largely dependent on the temperature of the diesel turbine and ambient atmospheric conditions [80]. The fuel consumption during the cold start-up is higher than the start-up if the diesel turbine is warm, especially the large capacity generator unit. But for a small capacity DG, like less than 10kW, the influence of temperature is not studied yet. So, the temperature influence of SDMO DG is firstly researched. Three experiments have been done in January, Compiègne, France, where the environmental temperature is about 1~3 °C and each test lasts 12 minutes. The interval of the test is one day so that to ensure the diesel turbine is enough cold. All the three tests are under no load so that to show the diesel consumption condition during the start-up. The fuel consumption curves are shown in Figure 49, in which the blue lines are the measured weight of diesel fuel and the blue lines are the curve-fitting.

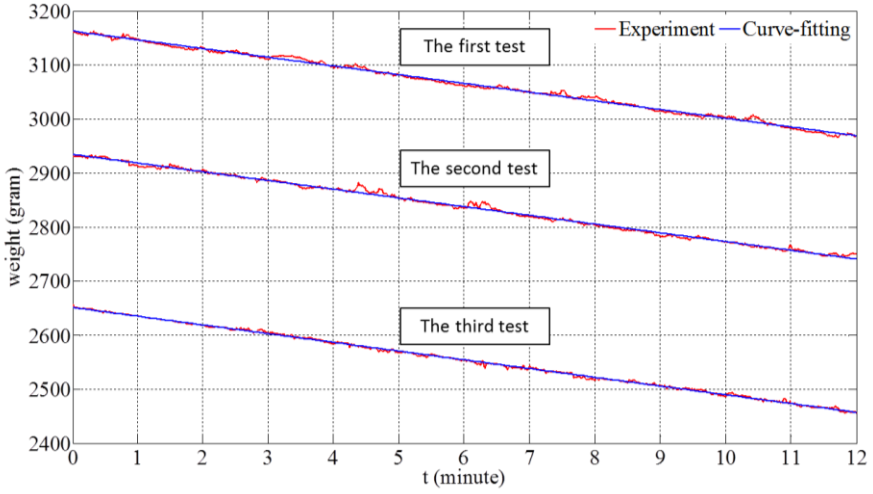

Figure 49. Three tests of declining curve of weight of fuel in 12 minutes experiment.

From the three experimental curves, it can be seen that there is no evident decline of diesel consumption during the cold start-up. So, the temperature has little influence on this type of DG. After calculating according to the curve-fitting of linear function, the absolute values of slope are the diesel consumption rates, which are 0.2688g/s, 0.2691g/s and 0.2695g/s separately. Therefore, the no load diesel fuel consumption rate can be got as mean value 0.2691g/s.

IV.1.2.2. Diesel fuel consumption rate under different output power value

In order to get the diesel fuel consumption rates, the experiments have been done under different output power values ($p_{DG} = v_{DG} \cdot i_{DG}$). For example, the output power of DG is set as 250W and when DG operates during 12 minutes, the situation of diesel fuel weight is observed and measured. The experimental results are drawn partially in Figure 50. The diesel consumption rates are listed in Table 8 and drew in Figure 51.

Table 8. The diesel consumption rates.

Power (W)	**Rate(g/s)**	**Power (W)**	**Rate(g/s)**
0	0.2691	2500	0.4611
250	0.2929	3000	0.5060
500	0.2852	3500	0.5607
750	0.3105	4000	0.6009
1000	0.3281	4500	0.6366
1500	0.3780	5000	0.6880
2000	0.4183	5200	0.7184

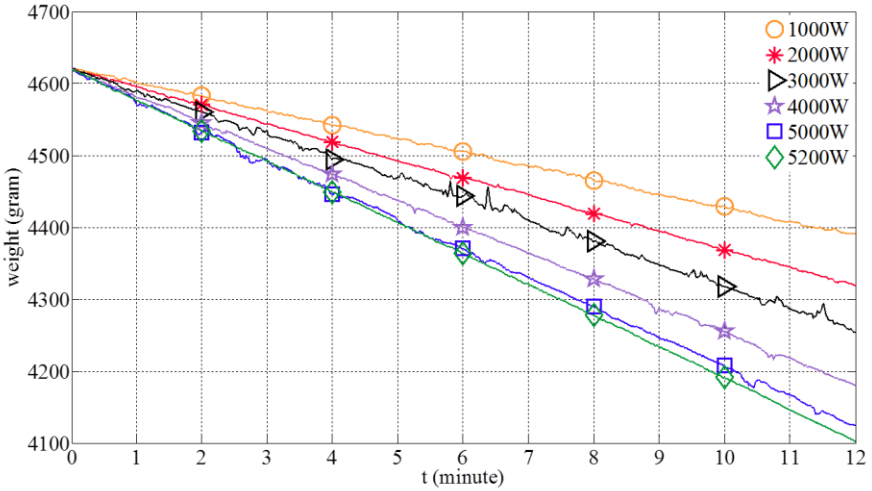

Figure 50. Declining curve of weight of fuel of different output power.

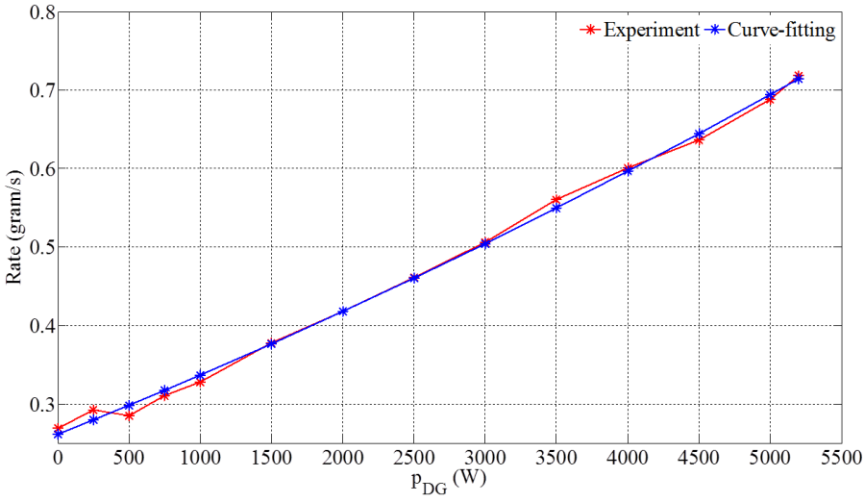

Figure 51. The diesel consumption rate along with the output power.

Just like the fuel cost function (4.2), the diesel consumption rate (*Rate*: gram/s) can be also fitted as a quadratic equation according to the data given in Figure 51. This function is shown in the following:

$$Rate(p_{DG}) = 2.7615\times10^{-9}\times p_{DG}^2 + 7.2729\times10^{-5}\times p_{DG} + 0.2615 \qquad (4.4)$$

According to this function, even though the diesel consumption rate at different output power value is still calculated roughly, it is much more precise than the calculated results from function (4.2). According to the data given in [26], the fuel price in France currently is 1.24 euro/liter, which is updated dynamically every week, and according to the data given in [81], the diesel density is about 0.835 kg/liter. Thus, the DG production tariff under different output power value is shown in Figure 52.

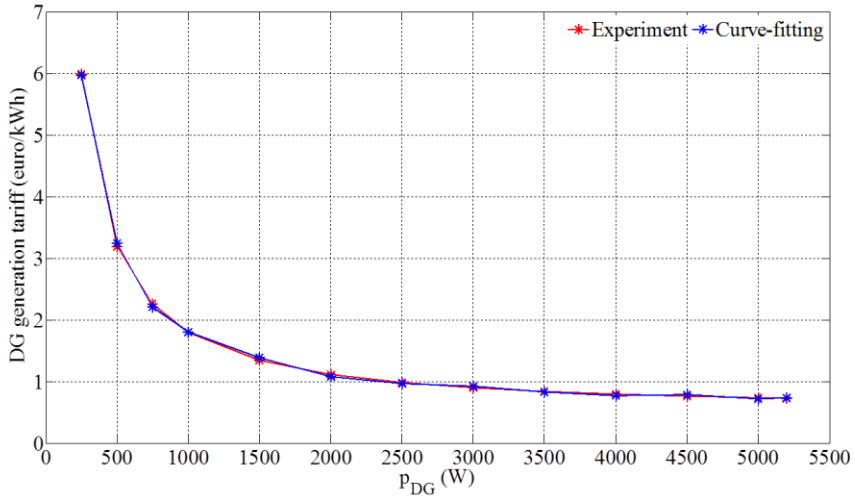

Figure 52. DG generation tariff along with the output power.

From this figure, it is observed that once the DG is started up, the minimum efficient generating power of DG would be better more than 2 kW. Furthermore, the DG power production cost can be fitted as a polynomial equation of degree 8.

$$c_{DG}(p_{DG}) = c_8 \times p_{DG}^8 + c_7 \times p_{DG}^7 + c_6 \times p_{DG}^6 + ... + c_1 \times p_{DG}^1 + c_0 \quad (4.5)$$

in which c_{DG} is the DG power production tariff, $c_8 = 5.9231 \times 10^{-27}$, $c_7 = -1.4176 \times 10^{-22}$, $c_6 = 1.4239 \times 10^{-18}$, $c_5 = -7.7990 \times 10^{-15}$, $c_4 = 2.5345 \times 10^{-11}$, $c_3 = -4.9859 \times 10^{-8}$, $c_2 = 5.8162 \times 10^{-5}$, $c_1 = -0.0378$, $c_0 = 12.4759$.

IV.1.3. DG operation and maintenance cost

DG operation and maintenance (O&M) cost $C_{DG\_O\&M}$ is defined as follows. According to the instruction manual of manufacture, DG O&M costs include oil change and the replacement of Quad-Clean precleaner at a cost of 15€ every 50 hours, the replacement of air cleaner element at a cost of 25€ every 200 hours, the replacement of low-profile air cleaner element and the replacement of fuel filter at a cost of 35€ every 300 hours, and the replacement of spark plug at a cost of 45€ every 500 hours. So, the average O&M cost per hour is 0.63 euro/h and the DG O&M cost is described in (4.6).

$$C_{DG\_O\&M} = T_{DG\_run} \cdot c_{DG\_O\&M} \quad (4.6)$$

where $c_{DG\_O\&M}$ is the average O&M cost per hour, and T_{DG_run} (h) is the running time of DG.

In this part, the fuel cost function is found according to the experimental results. Thus, the lower limit generating power is confirmed so that the generation tariff of the DG is kept in a low status. Firstly, it studies the temperature influence on the start-up stage of DG, resulting that these is little influence of temperature on the research DG object in this thesis. And then, several experiments have been done to get fuel consuming rate at different DG output power. Based on the real time fuel price which is updated every week, the curve of the generation tariff of the DG is got. At last, the DG operation and maintenance cost is calculated according to the user manual. The outcomes of this section about the energy tariff of DG will be applied into the proposed power management in the following parties, to further decline the power system whole cost.

IV.2. Power management strategy design

The core of the hybrid power system is related to the power management design, which concerns the power balancing, load shedding, PV power limiting and imposed limits by the system itself characteristic, like the maximum recharging power of batteries. To obtain a real time control, power system elements must be ranged in specified sequence and an algorithm could be obtained. Hence, the continuous dynamics of the system are operated through an implemented algorithm that calculates power system references with respect to imposed limitations and gives the load shedding level. This

algorithm focuses on the power system control strategy. The system configuration will be firstly described and then the energy tariff of each element will be defined.

IV.2.1. System configuration

The configuration of a typical PV-based off-grid DC microgrid is shown in Figure 53. In order to well adapt to the existing cable infrastructure in a building or a community, the rated DC bus voltage is chosen as 400 V [64,65]. This off-grid electrical power system consists of PV source, electrochemical batteries, DG, SC and DC load. All components of the system are connected through power electronic converters to a common DC bus. The PV source is connected to the DC bus through a DC-DC converter, which can be controlled by a MPPT method to exploit the PV energy as much as possible. The DG is connected through an AC-DC rectifier. The electrochemical batteries are installed in series as a pack and then connected via a bidirectional DC-DC converter. The SC is also connected by a bidirectional DC-DC converter. The DC load can be connected directly to the DC bus if its rated voltage is equal to that of the DC bus. However, in most cases, the voltages are different so that a DC-DC buck or boost converter may be involved. In addition, the AC load requires DC-AC power inverter to change the current form. Taking into account that this study focuses on power control and power management strategy, both the AC load and DC load are regarded as the DC power demanded on the DC bus.

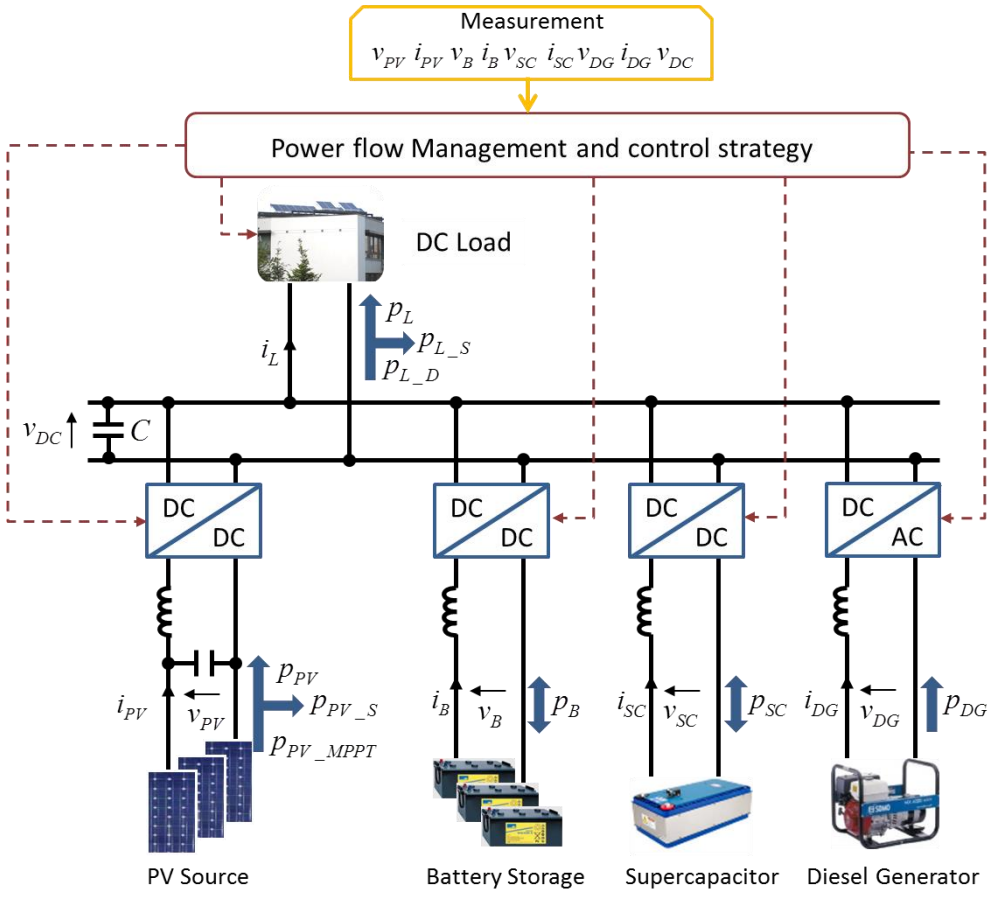

Figure 53. Topology of proposed off-grid DC microgrid system.

A central power management strategy is proposed to control the power flow between the different sources while each element is controlled by their respective controller. The centralized power management gives the current reference of each element according to their respective restrictive condition and the power balance of the system. Each independent controller receives the reference command and controls the respective power source. Although this study supposes to avoid the occurrence of load shedding, some objective circumstances will lead to power supply shortage, such as short-circuit of distribution lines due to adverse weather and the accidental fault of distributed energy sources. Therefore, there is also a local load controller which can reduce partly the power demand when receiving the load shedding order from the central power management block or fault detection program. But this is the fault recognition and protection research area [82], which is important but not emphasized in this study. However, in this section, the load shedding percentage is supposed to be equal or less 20% of the total power demand; when the shortage of power supply from batteries and PV source is more than this value, the DG will be started up.

IV.2.2. Definition of energy tariff of each element

In order to compare the merits and demerits between the DG load following mode and DG duty cycle mode, the energy cost of the whole system is a good index. On the other hand, concerning PV shedding, load shedding and storage aging cost, their energy tariffs calculation is quite complex and depends on the chosen technology. This is why energy tariffs used in this study are somewhat arbitrary; however, numerical values of energy tariffs given here below are chosen according to the manufacture's handbook, which is as approximate as possible to the actual values.

Diesel generator

The DG power production tariff c_{DG} is calculated and given in the equation (4.5). Therefore, the DG fuel consumption cost C_{DG_Fuel} for a given time period, from initial instant t_0 to final instant t_F, is calculated as:

$$C_{DG\_Fuel} = \frac{1}{3.6\times10^6}\sum_{i=t_0}^{t_F} c_{DG}(p_{DG}(i))\cdot p_{DG}(i)\cdot\Delta t \qquad (4.7)$$

The DG operation and maintenance (O&M) cost $C_{DG\_O\&M}$ is defined and given in the equation (4.6).

Supercapacitor

The expected life of SC (held continuously at rated voltage at 25°C) is fifteen years [83]. However, SC cannot be always under rated voltage so that its expected life is supposed as ten years and the SC ageing cost is calculated in (4.8).

$$C_{SC\_Ageing} = \frac{1}{3.6\times10^{6}} \sum_{i=t_0}^{t_F} c_{SC\_Ageing} \cdot \left| p_{SC}(i) \right| \cdot \Delta t \tag{4. 8}$$

where c_{SC_Ageing} is the SC energy tariff.

Electrochemical batteries bank

Like the ageing of SC, battery aging should also be considered. The battery used in this thesis is the Sonnenschein Solar Block of Exide Technologies, which has five years as expected life [84]. Its cost is calculated in the following (4.9).

$$C_{B\_Ageing} = \frac{1}{3.6\times10^{6}} \sum_{i=t_0}^{t_F} c_{B\_Ageing} \cdot \left| p_{B}(i) \right| \cdot \Delta t \tag{4. 9}$$

where c_{B_Ageing} is the batteries energy tariff.

PV shedding

Once the PV panels have been installed, the power generation does not need extra fee. However, the occurrence of PV shedding means that the assets are not used efficiently. Therefore, the PV shedding is penalized and its cost is defined as in (4.10).

$$C_{PV\_S} = \frac{1}{3.6\times10^{6}} \sum_{i=t_0}^{t_F} c_{PV\_S} \cdot p_{PV\_S}(i) \cdot \Delta t \tag{4. 10}$$

where c_{PV_S} is the PV shedding energy tariff.

Load shedding

The main objective of the electrical power system is to guarantee the users' power supply. However, the load shedding case is possible to occur when the power demand is shortly superior to the power supply. Thus, the electric appliances of a building which do not have priority, can be shortly shut down and be restarted later. Hence, the load power p_L is described as:

$$p_L(t) = p_{L\_D}(t) - p_{L\_S}(t) \tag{4. 11}$$

where p_{L_D} is the load power demand, p_{L_S} is the load shed power reference.

It is supposed that the unimportant appliances account for at most 20% of the total power demand and when the shortage of power supply from batteries and PV source is more than this value, the DG will be started up. But the load shedding truly leads to the inconvenience for the end-users. Therefore, the load shedding is penalized and its cost is defined as in (4.12).

$$C_{L\_S} = \frac{1}{3.6\times10^{6}} \sum_{i=t_0}^{t_F} c_{L\_S} \cdot p_{L\_S}(i) \cdot \Delta t \tag{4. 12}$$

where c_{L_S} is the load shedding tariff.

Finally, the total energy cost of this DC microgrid is calculated as following.

$$C_{Total} = C_{DG\_Fuel} + C_{DG\_O\&M} + C_{SC\_Ageing} + C_{PV\_S} + C_{B\_Ageing} + C_{L\_S} \quad (4.\ 13)$$

Concerning the energy tariff, arbitrary values are taken into account but with respect to:

$$c_{L\_S} > c_{PV\_S} > c_{SC\_Ageing} > c_{B\_Ageing} \quad (4.\ 14)$$

IV.2.3. Power management strategy

In the power system, both PV power p_{PV} and load power p_L are randomly variable, but PV power can be limited and load power can be shed if needed. On the contrary, batteries power p_B, DG power p_{DG}, and SC power p_{SC} are the controllable elements. Hence, the physical law of power balancing must be completely respected at any time according to the equation (3.7):

To get a real-time power control, an algorithm should be designed to arrange the power system elements in a specified sequence. Therefore, this algorithm should assign the power references to each source and give the power shedding references for the PV source and the load. This algorithm must comply with the power balance equation, the predefined priority order of the components to operate in the DC microgrid and the imposed limitations. The PV source has the first priority to supply the load. Accordingly, the batteries are essential to ensure stable operation of the whole system due to the intermittence of the PV generation. Otherwise, when SOC_B decreases to its constraint, the DG operates to supply the load and also to recharge storages, the electrochemical one and the electrostatic one. Nevertheless, the DG needs some time to start up and cannot immediately offer the needed power. Therefore, the SC is used to compensate the power deficiency during the DG start-up, *i.e.* the SC and the DG are unified together as a backup source to supply the DC bus. The SC must always have enough energy to supply the whole DC microgrid during the start-up phase of the DG. Because of this, the priority of the SC is higher than that of the batteries in recharging sequence, so the excess power is preferentially injected into the SC. In order to describe the overall power management strategy, Figure 54 presents the power system control algorithm flowchart and the nine possible power flow cases are described in detail in the following.

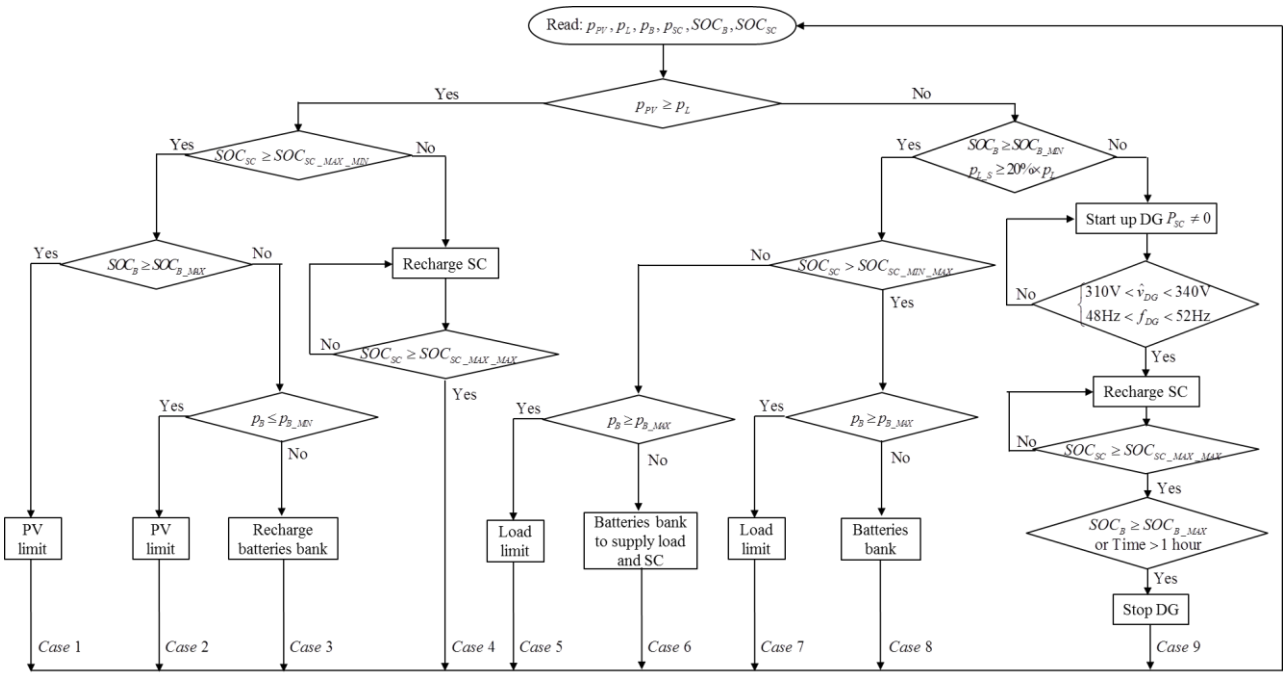

Figure 54. Flow chart of the power management strategy.

From this figure, it can be noted that there are four definitions on the constraints of SC's state of charge: $SOC_{SC\_MAX\_MAX}$, $SOC_{SC\_MAX\_MIN}$, $SOC_{SC\_MIN\_MAX}$, and $SOC_{SC\_MIN\_MIN}$. This is because of the SC self-discharging nature and they are explained one by one in the following.

1) $SOC_{SC\_MAX\_MAX}$ is described as the maximum value of the maximum SOC_{SC} while $SOC_{SC\_MAX\_MIN}$ is described as minimum value of maximum SOC_{SC}. Because of its self-discharging current, SOC_{SC} observably goes down after tens of seconds even though there is no command. If the SC's fully charged state is described as a fixed value, when SOC_{SC} drops below this value, SC is recharged but SC will be recharged again after several seconds once SOC_{SC} drops below this value. Under this case, SC is discharged and recharged again and again which is harmful to SC and its converter. Thus, SC's fully charged state is designated as a range.

2) Symmetrically, $SOC_{SC\_MIN\_MAX}$ and $SOC_{SC\_MIN\_MIN}$ define a range in which the SC is considered to be empty. While $SOC_{SC\_MIN\_MIN}$ is the lower limit of SOC_{SC}, $SOC_{SC\_MIN\_MAX}$ indicates that the SC has still enough energy to support the whole system alone during the start-up of DG. Hence, the SC must be recharged if SOC_{SC} falls to $SOC_{SC\_MIN\_MAX}$ due to the self-discharging and in such case, the recharging power can be so weak that the self-charging is merely compensated.

Hence, SC should always have enough energy to stat up DG when there is no stored energy in electrochemical batteries, which means that it is prohibited that SOC_{SC} is smaller than $SOC_{SC\_MIN\_MAX}$. Thus, when the SOC_{SC} reaches this value, the SC will be recharged like a load; the recharging power is little and equal to the self-discharging power so that the SC's stored energy is maintained to wait for starting up DG. According to the self-discharging curve, the average self-discharging current is calculated about 0.03A.

IV.2.3.1. Cases 1, 2, 3, 4

When PV power is greater than users' demand, there exists the excess PV power after fully supplying the load. If both the SC and the batteries are fully recharged, the PV power is limited to supply only the load and stabilize the DC bus. This is case 1. If the batteries are not full, the excess PV power is injected into the batteries bank. But if the excess PV power is more than the batteries' maximal recharging power, the PV power is limited to supply only the load and the batteries' maximal recharging power. This is case 2. Otherwise, the PV power is not limited. This is case 3. On the other hand, if the SC is not in its saturation state, *i.e.* $SOC_{SC} \le SOC_{SC\_MAX\_MIN}$, the excess power will be firstly injected into SC until SOC_{SC} reaches $SOC_{SC\_MAX\_MAX}$. This is the case 4.

IV.2.3.2. Cases 5, 6, 7, 8, 9

If there is not enough PV power to meet the load demand, other sources are required to complement the deficient power. The batteries are set to provide the energy in the first place. At the same time, the energy in the SC decreases on account of self-discharging as the time goes by. It is possible that the SC becomes empty before the batteries energy is depleted. As the SC is essential to start up the DG, the drain of the SC energy should be avoided. Hence, when SOC_{SC} reaches $SOC_{SC\_MIN\_MAX}$, the batteries should provide an additional amount of power to compensate the self-discharging power of SC, so that the start-up of the DG can always be supported by the SC power. The role of batteries is not only to supply the load but also to recharge the SC. But it is possible that the demanded power is more than the maximal batteries discharging power, so the load power is limited and this is the case 5. Otherwise, the batteries power is enough and this is the case 6. On the other hand, if SOC_{SC} does not reach $SOC_{SC\_MIN\_MAX}$, the batteries bank only supplies the load demand. There are also two branches depending on whether the batteries power is insufficient or not; these are the case 7 and the case 8 respectively.

There are two conditions to start up the DG. Either of them is met, the DG will be started up. The first condition is that the load power shedding demand is more than 20% of total load power demand. The second is that SOC_B reaches its lower limit. During the period of DG start-up, the SC is used to stabilize the DC bus voltage and balance the DC bus power for a short term. When the DG reaches its stabilized output state, it will be connected to the DC bus and operates not only to replenish the shortage of PV power, but also to recharge up the two storages. In this case, the power reference of the DG is set to be greater than or equal to 2kW, in order to have a reasonably low cost energy for the DG power as aforementioned. According to the recharging priority, the SC is firstly recharged to $SOC_{SC\_MAX\_MAX}$, and then, all the excess power will be injected into the batteries. The DG will then be stopped if one of the two conditions is met: (i) the batteries are fully recharged and (ii) the DG has run for more than one hour. The maximal running time limitation is for economical purpose. A short limit can save fuel but it risks to lead to the frequent start-up of the DG since the batteries are not fully recharged, which can reduce the DG lifespan. The one hour duty cycle is proposed as a good trade-off between the fuel consumption and the start-up frequency. The case 9 is the only case in which the DG is started and stopped.

IV.3. Simulation results

The power management is simulated firstly with numerical values based on the experimental DC microgrid platform. In this section, simulation results are given. In order to compare the fuel cost and fuel consumption with the other power management strategy presented in Chapter III, in which the DG cost is not taken into account, the operating strategy of the DG in the case 9 in Figure 54 is changed to load-following mode, producing the same amount of power as the load demand but freeing of recharging the batteries and the SC. This modified strategy is also carried out through the experimental platform in the next section.

For simulation validation, the PV generation real profiles are recorded under MPPT control, recorded at Compiègne in France by our research team AVENUES. In addition, a simple and arbitrary load power demand evolution is considered. In order to show all the possible 9 cases, three simulations of the proposed power management are carried out over three given days considering the constraints and values given in Table 9, which is based on the experimental platform.

Table 9. Arbitrary values, tariffs, and constraints.

Parameter	Value	Parameter	Value
SOC_{B_MAX}	60%	v_{DC}^{*}	400V
SOC_{B_MIN}	40%	$c_{DG\_O\&M}$	0.63€/h
$SOC_{SC\_MAX\_MAX}$	90%	c_{SC_Ageing}	0.3€/kWh
$SOC_{SC\_MAX\_MIN}$	85%	c_{PV_S}	0.7€/kWh
$SOC_{SC\_MIN\_MAX}$	50%	c_{B_Aging}	0.07€/kWh
$SOC_{SC\_MIN\_MIN}$	45%	c_{L_S}	1€/kWh
p_{B_MAX}	1kW	p_{B_MIN}	-1kW

According to the density of lead-acid batteries compared to the power level of the test bench, and in order to observe all the cases, the SOC_B is chosen in a narrow range [85]. Similarly, the batteries bank's power limit is limited at the same power level of the PV power. Concerning the SC, its power is not limited, but the same amount of power can cause great current in the case of the low SC voltage, which can be harmful to the experimental facility. Thus, SOC_{SC} is limited to a minimum of 45% since it is quadratically proportional to the SC voltage.

Depending on the meteorological day profile, the three chosen days represent three types of solar irradiance: mixed high-low solar irradiance with some fluctuations and low solar irradiance almost without fluctuations (Test 1, the 8th July 2016), high solar irradiance with strong fluctuations (Test 2, the 9th July 2016), and high solar irradiance without fluctuations (Test 3, the 10th July 2016). The simulation results are explained in the following.

IV.3.1. Simulation 1

The solar irradiance and the PV temperature of the first test are profiled in Figure 55. As can be seen from this figure, it is an overcast weather, in most of the time the irradiance is under 400W/m^2. So, the PV power is far less than the load power demand, which can be seen from Figure 56. Under this weather circumstance and load profile, two simulations are done according to the operating mode of DG: duty-cycle model and load-following mode.

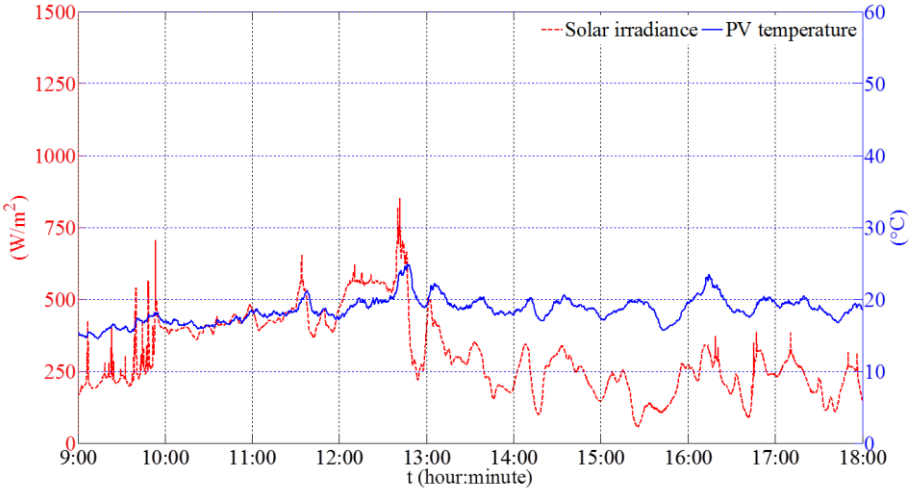

Figure 55. Solar irradiance and PV cell temperature.

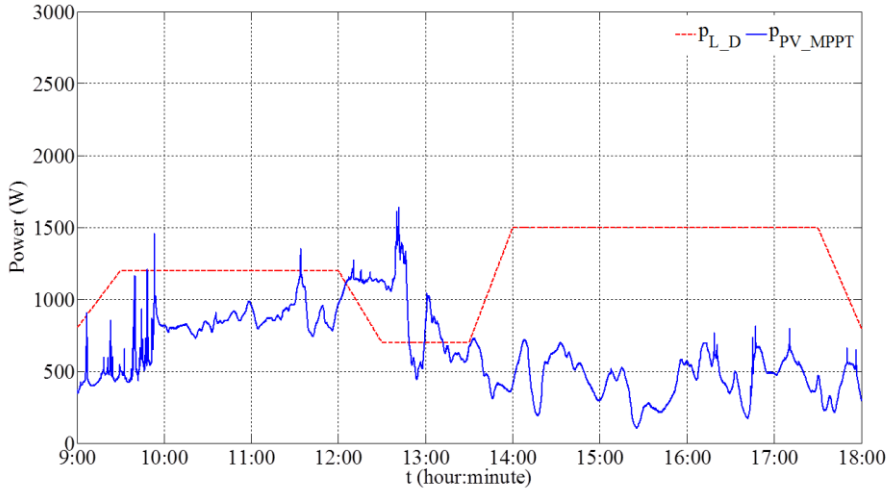

Figure 56. Load power demand and PV MPPT power.

IV.3.1.1. DG duty cycle mode

Taking into account the generation tariff of DG, the DG power is cheaper with a minimal generation of 2kW. However, due to the power constraints of the batteries (±1kW) in the experimental environment and the power balance in the microgrid, the DG output power cannot be set to be always equal to or more than 2kW. For the sake of reducing the DG power cost, the DG power is set to be the sum of the maximal batteries recharging power and the difference between the PV power and the load power at the moment when the DG is started.

Figure 57 shows the DC microgrid power evolutions during the nine hours. During the first interval ($9:00 \le t < 11:06$), the batteries and PV are the main suppliers (case 8). With the time going on, the energy stored in the SC is self-discharging until reaching the constraint. So, during the second interval ($11:06 \le t < 12:05$), the batteries bank not only supplies the load demand, but also gives some power to

the SC to maintain the energy stored in the SC. This is case 6. Then, in the third interval ($12:05 \le t < 13:57$), there is an excess PV power, which is preferentially recharged into the SC. This is case 4. Around $12:18$, the energy in the SC is full. In the next interval ($13:57 \le t < 14:57$), around $13:57$, the energy in the batteries is used up. SOC_B reaches its lower limit value and then SC supplies the load before the DG start-up. After DG can offer stable power, the excess power firstly recharges the SC. Afterwards, batteries begin to absorb power when the SC reaches its maximum state. When the DG runs for one hour, it stops. This is the case 9. In the fifth interval ($14:57 \le t < 15:22$), there is load shedding. In the sixth interval ($15:22 \le t < 17:40$), around $15:22$, the DG is started up for one hour because the load shedding demand is more than 20% of the total power demand. Around $16:40$, the DG is started up again for one hour because the load shedding demand is once again more than 20% of the total power demand. This is case 9. In the last interval ($17:40 \le t < 18:00$), the batteries bank supplies the deficient power. These are case 8.

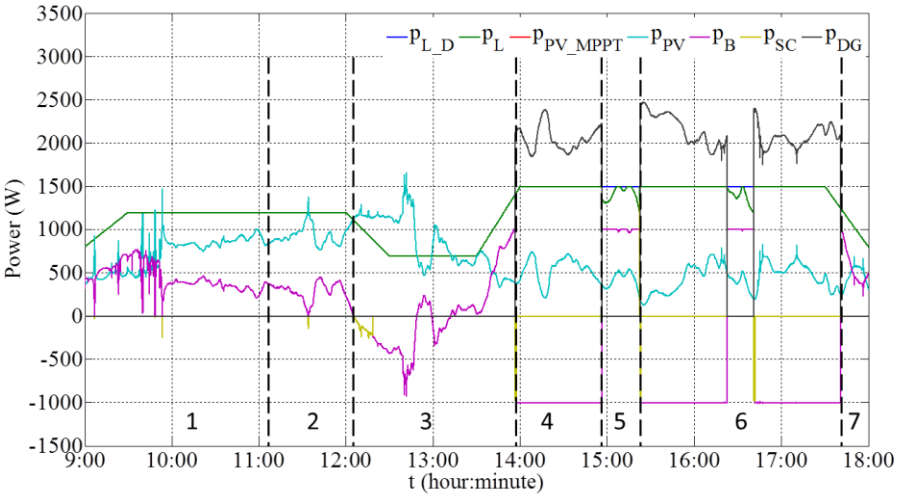

Figure 57. DC microgrid power evolutions.

Figure 58 and Figure 59 show SOC_B and SOC_{SC} evolutions, reflecting that the batteries and the SC run well for providing and absorbing energy within their respective restrictions. Considering that the goal of this nine hours simulation is to verify the feasibility of the proposed power management strategy in a real PV power profile, the simulation results display that the power is well balanced and the DC bus voltage is stable with acceptable fluctuations (the maximum fluctuation error is less than 2.5% of the rated DC bus voltage), shown in Figure 60.

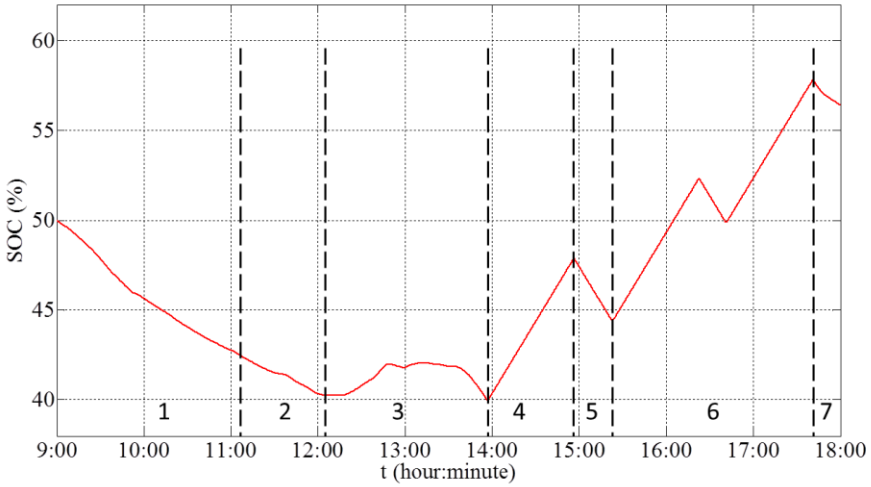

Figure 58. *SOC* evolution of electrochemical batteries.

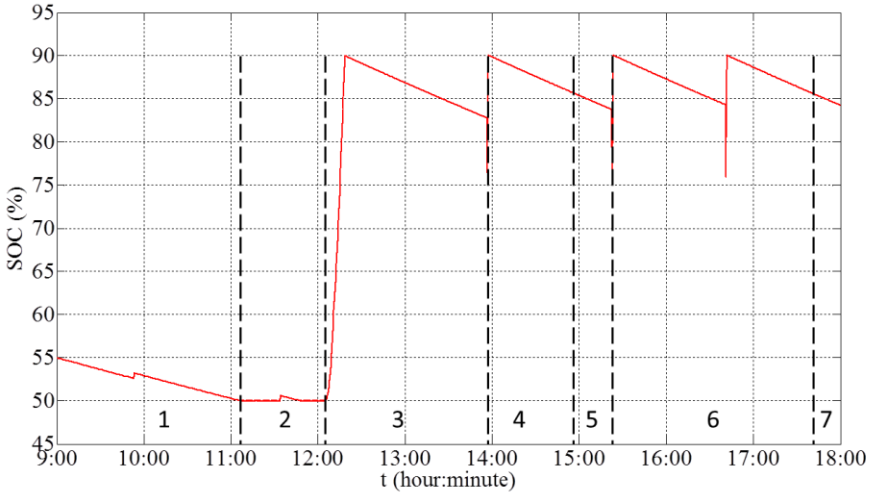

Figure 59. *SOC* evolution of supercapacitor.

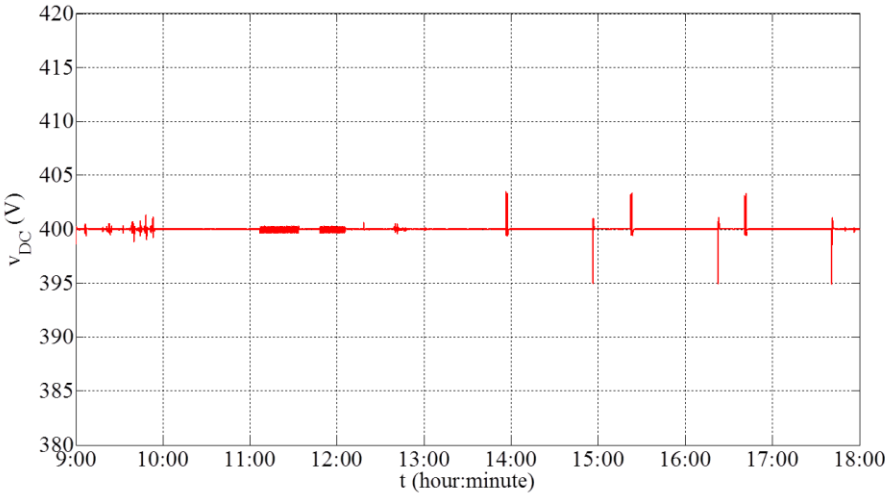

Figure 60. DC bus voltage.

IV.3.1.2. DG load following mode

In the case 9 in Figure 54, after DG is started up, the reference of DG generating power is given as the deficient PV power, which is only used to supply the load demand. There is no consideration for minimum efficient generating power of DG and there is no excessive power to recharge SC and batteries. The simulation results are analyzed in the following.

Figure 61 shows the DC microgrid power evolutions during the nine hours. Before the diesel generator being started up, the power evolutions are the same as these in Figure 57. In the fourth interval ($13:55 \le t < 18:00$), after the instant when the DG can generate stable power into the system, its output power is equal to the load demand and there is no longer the situation of load shedding.

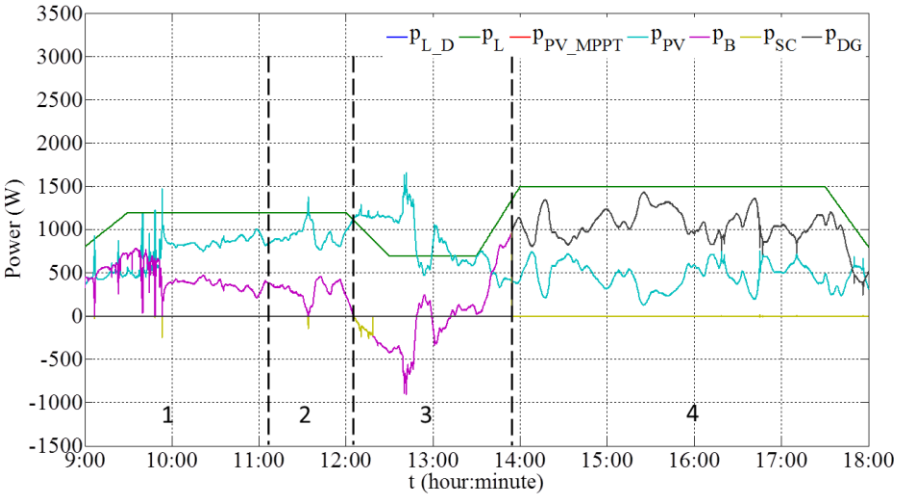

Figure 61. DC microgrid power evolutions.

Figure 62 and Figure 63 show SOC_B and SOC_{SC} evolutions, reflecting that the batteries and the SC run well for providing and absorbing energy within their respective restrictions. Since there is no power to recharge SC and batteries after DG being stated up, the SOC_B shows that the batteries continue to be in the empty state and the SOC_{SC} shows that the SC is in a continued momentum of decline. The DC bus voltage is stable with acceptable fluctuations (the maximum fluctuation error is less than 2.5% of the rated DC bus voltage), shown in Figure 64.

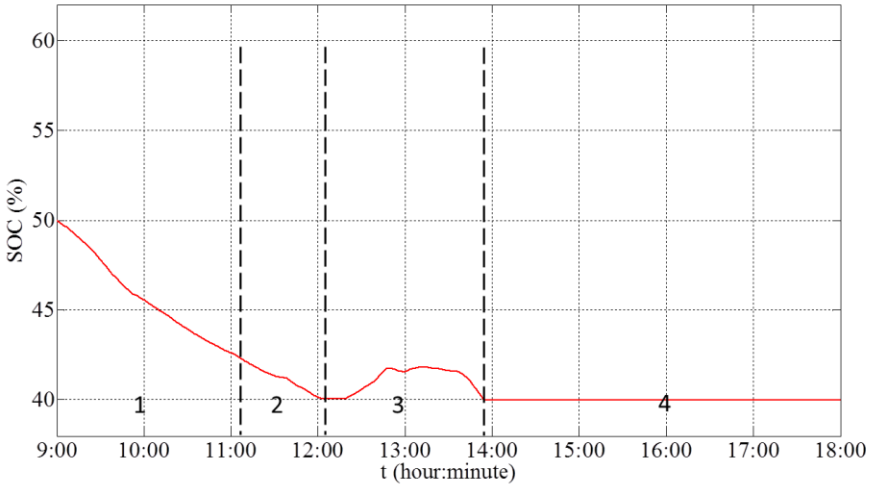

Figure 62. *SOC* evolution of electrochemical batteries.

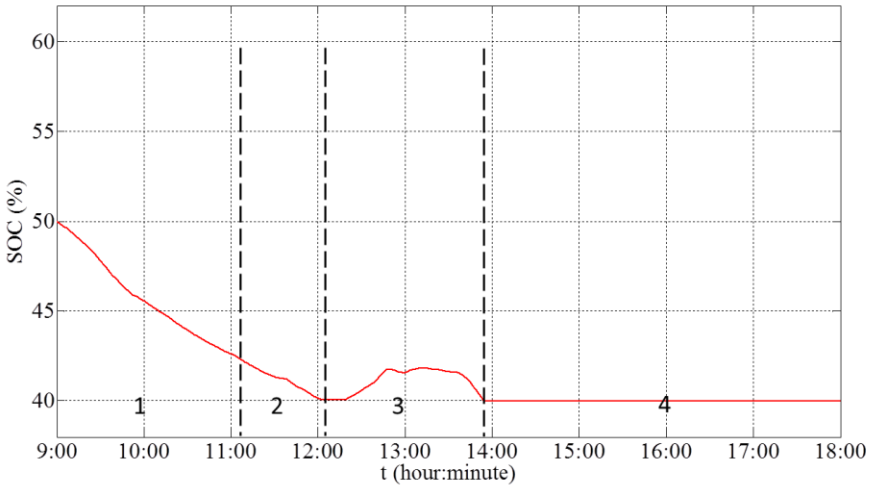

Figure 63. *SOC* evolution of supercapacitor.

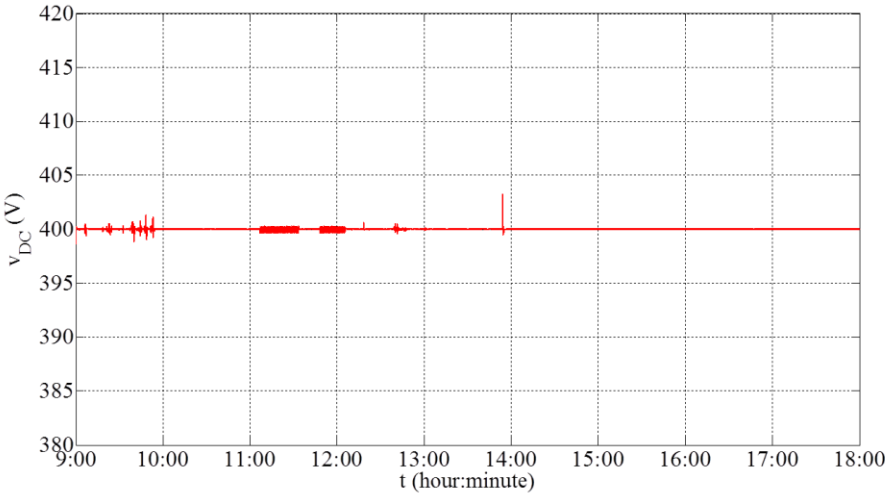

Figure 64. DC bus voltage.

IV.3.2. Simulation 2

The solar irradiance and PV temperature is profiled in Figure 65. The weather is cloudy. It can be seen from this figure that the solar irradiation fluctuates very violently, causing the solar power also has strong fluctuations in Figure 66.

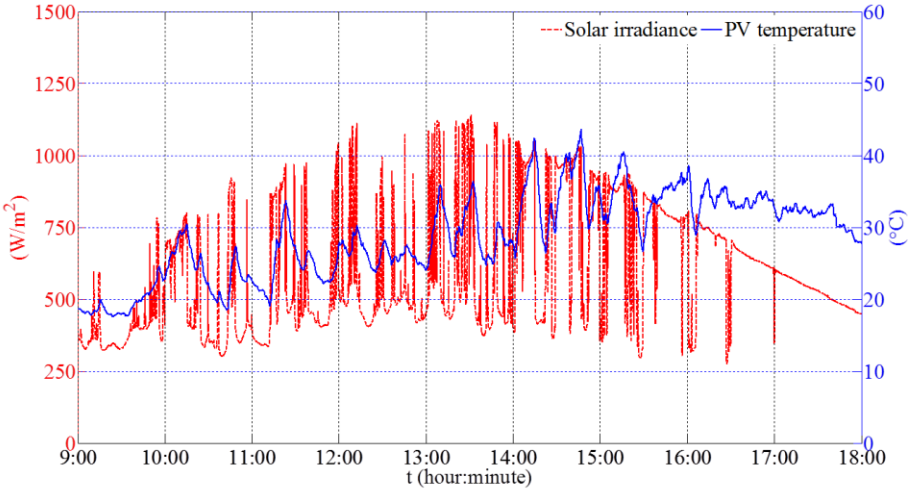

Figure 65. Solar irradiance and PV cell temperature.

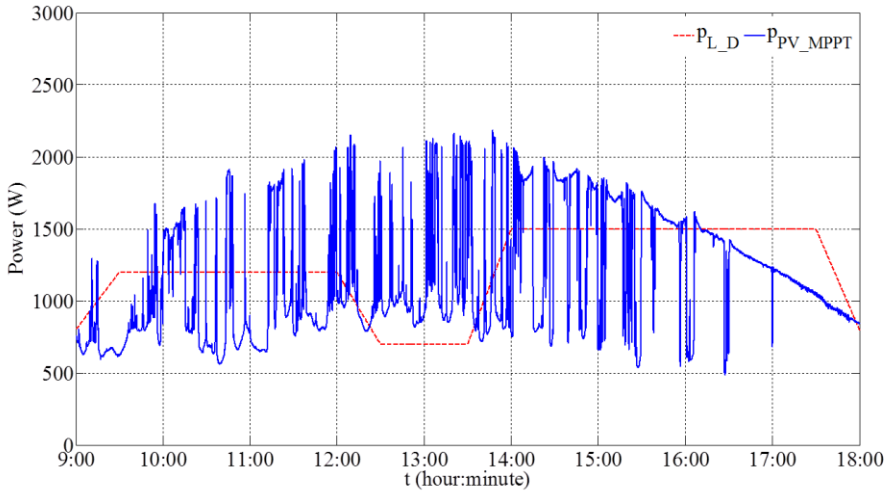

Figure 66. Load power demand and PV MPPT power.

Figure 67 shows the power evolutions during the nine hours. At noon, since the excess PV power goes beyond the batteries absorbing limit, the PV power is restrained now and then. In the afternoon, the deficient PV power surpasses the batteries supplying limit so that load power is restrained now and then by load shedding actions.

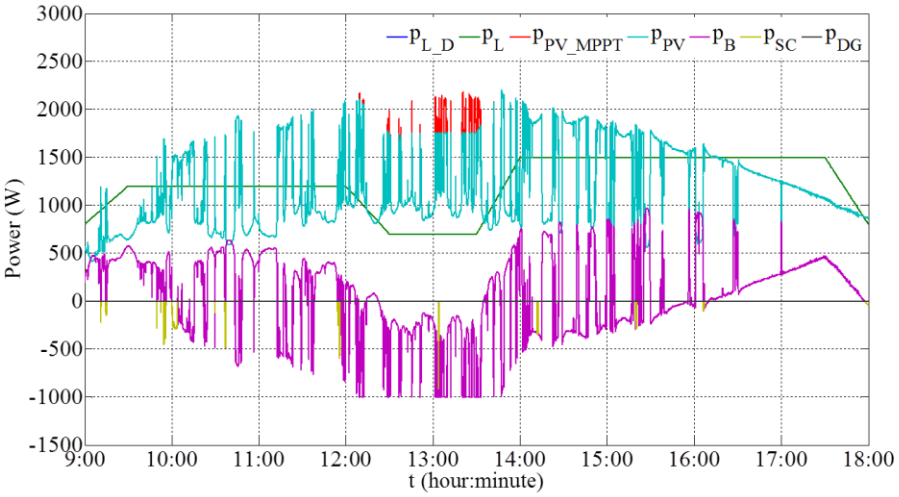

Figure 67. DC microgrid power evolutions.

Figure 68 and Figure 69 show SOC_B and SOC_{SC} evolutions, reflecting that the batteries and the SC run well for providing and absorbing energy within their respective restrictions. In the reason that PV power fluctuates seriously, the DC bus voltage fluctuates up and down with acceptable range (the maximum fluctuation error is less than 1.5% of the rated DC bus voltage), shown Figure 70. Since there is no situation to start up DG, the other simulation with DG load following is not necessary to be done.

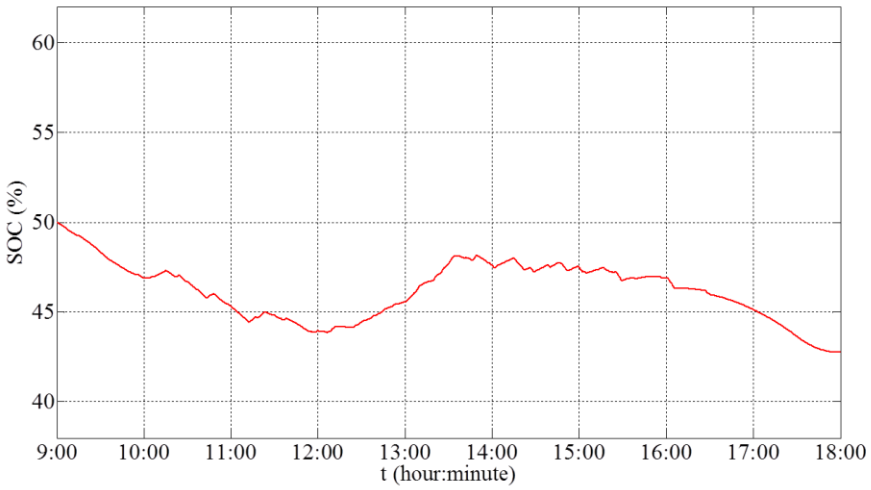

Figure 68. *SOC* evolution of electrochemical batteries.

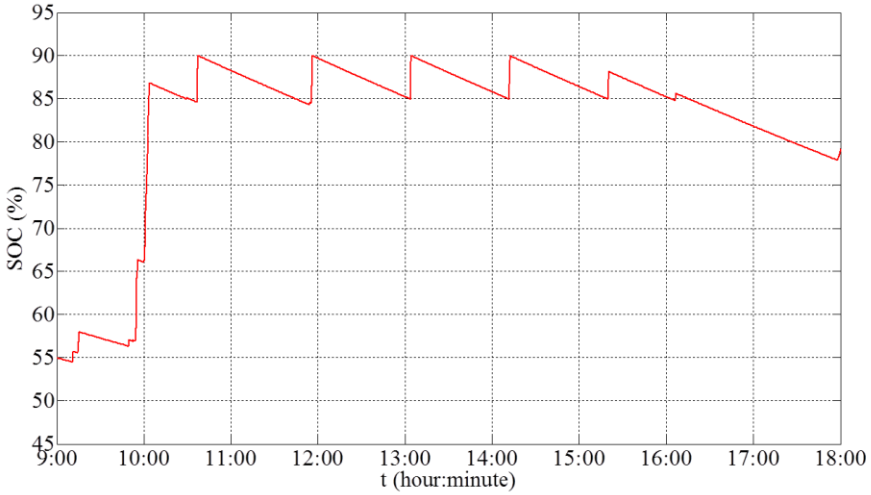

Figure 69. *SOC* evolution of supercapacitor.

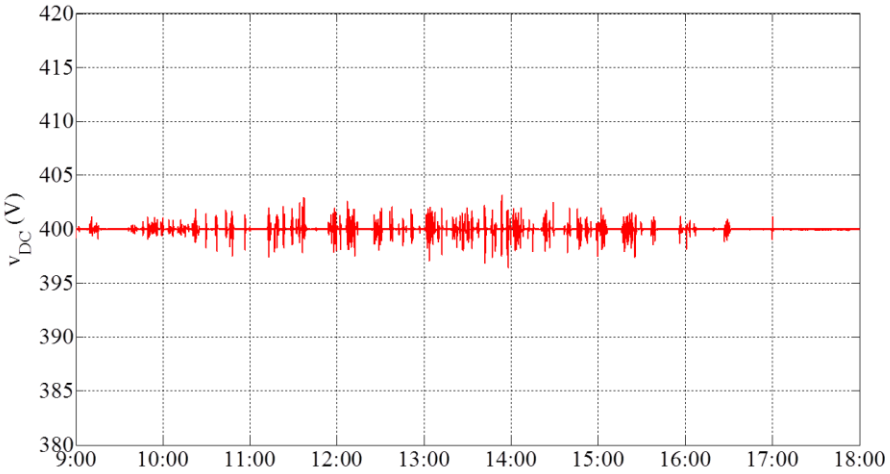

Figure 70. DC bus voltage.

IV.3.3. Simulation 3

The solar irradiance and the PV temperature of first test are profiled in Figure 71. As can be seen from this figure, it is a perfect sunny day without any fluctuations, in most of the time the irradiance is higher than 700W/m^2. So, the PV power is more than the load demand in most of the time, which can be seen from Figure 72.

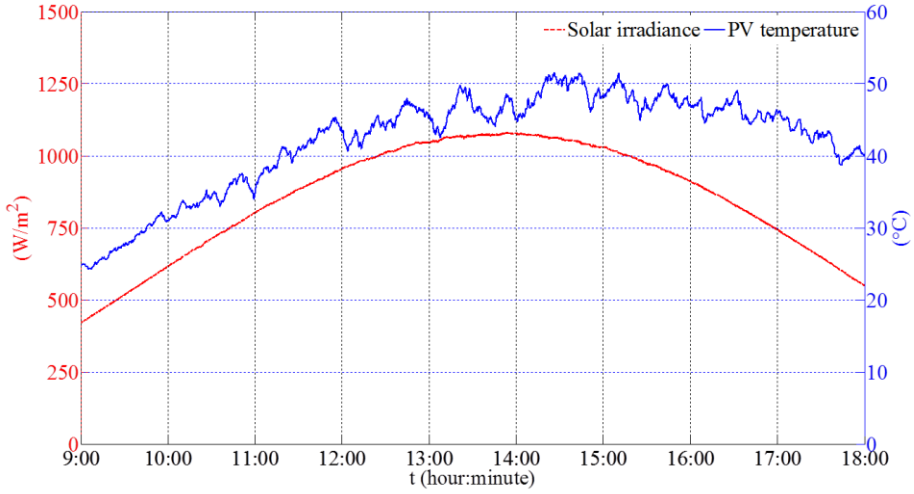

Figure 71. Solar irradiance and PV cell temperature.

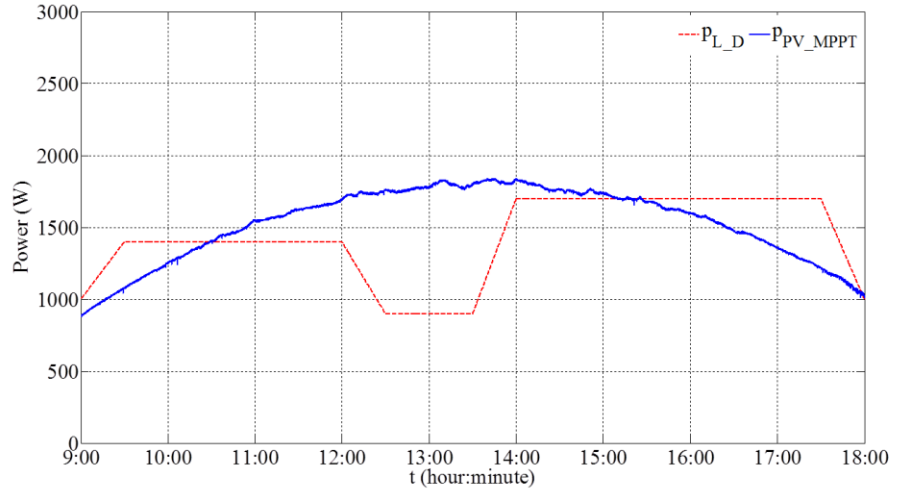

Figure 72. Load power demand and PV MPPT power.

Figure 73 shows the power evolutions during the nine hours. During the first interval ($9{:}00 \le t < 10{:}21$), the batteries and PV are the main suppliers (case 8). During the second interval ($10{:}21 \le t < 10{:}55$), there are excess PV power, which is preferentially recharged into the SC. This is case 4. Around $10{:}55$, the energy in the SC is full. Afterwards in the third interval ($10{:}55 \le t < 13{:}36$), batteries begin to absorb power. This is case 3. During this interval, around the time $12{:}02$ and $13{:}10$, SC is recharged again when SOC_{SC} is under the value $SOC_{SC\_MAX\_MIN}$ and when there is excess PV

power. This is case 4. In the next interval ($13:36 \le t < 15:40$), after the battery is fully charged, PV power shedding is operated to only supply the load. In the last interval ($15:40 \le t \le 18:00$), the batteries bank supplies the deficient power. These are case 8.

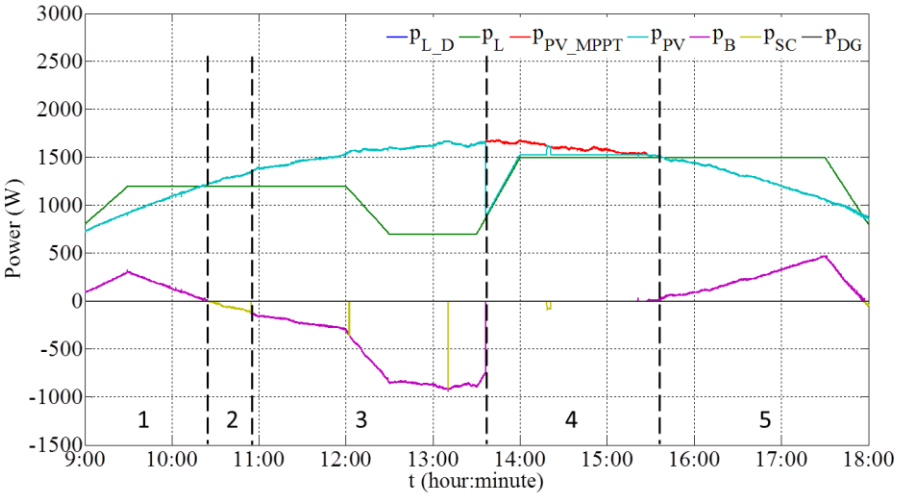

Figure 73. DC microgrid power evolutions.

Figure 74 and Figure 75 show SOC_B and SOC_{SC} evolutions, reflecting that the batteries and the SC run well for providing and absorbing energy within their respective restrictions. Since the solar irradiation is approximatively perfect without any big fluctuations, the DC bus voltage is stable (the maximum fluctuation error is less than 1.5% of the rated DC bus voltage), shown in Figure 76. Since there is no situation to start up DG, the other simulation with DG load following is not necessary to be done here.

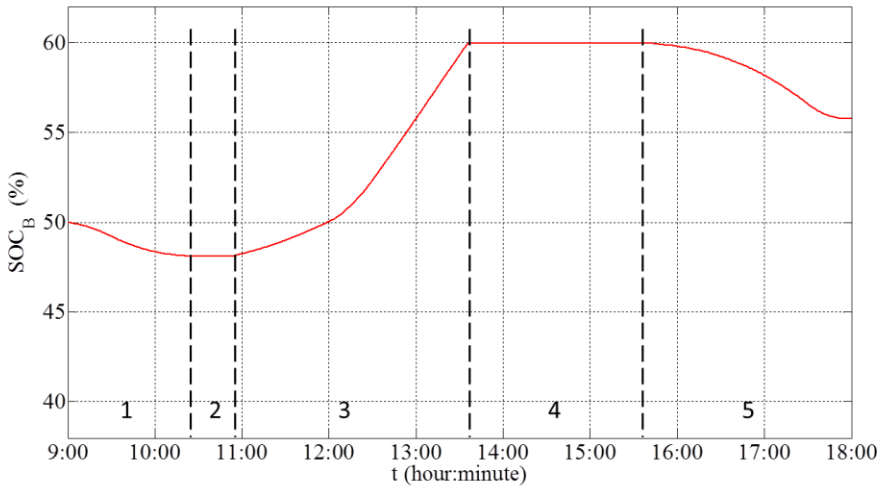

Figure 74. *SOC* evolution of electrochemical batteries.

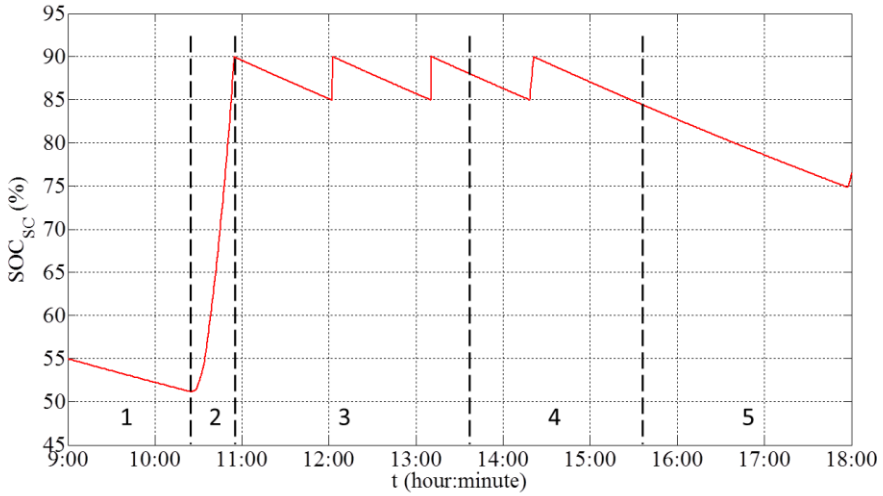

Figure 75. *SOC* evolution of supercapacitor.

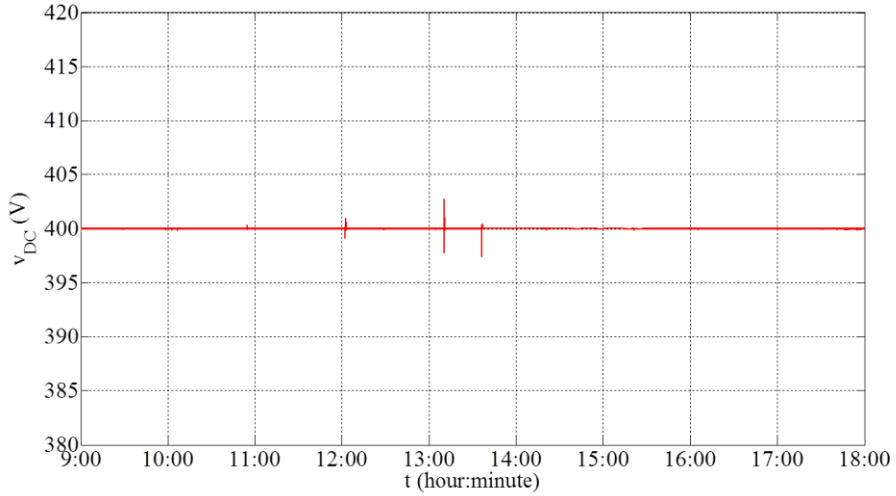

Figure 76. DC bus voltage.

IV.4. Experimental verification

Through the simulation test in the last section, it theoretically validated the effectives of the power management strategy. It shows the correctness of logic of the strategy. The power flow abides by the rule based strategy and the DC bus is stable in the acceptable limit. In this section, the proposed power management strategy is verified through experimental tests with the purpose of identifying and illustrating the merits and disadvantages in real operating conditions.

An experimental platform, whose image is given in Figure 77, is set up. To simplify the comparison, a PV emulator is installed instead of real PV panels. In order to compare the difference with the simulation tests, this PV emulator follows the PV generation real profiles, which are shown in the last simulation section and the load emulator also follows the same load profile.

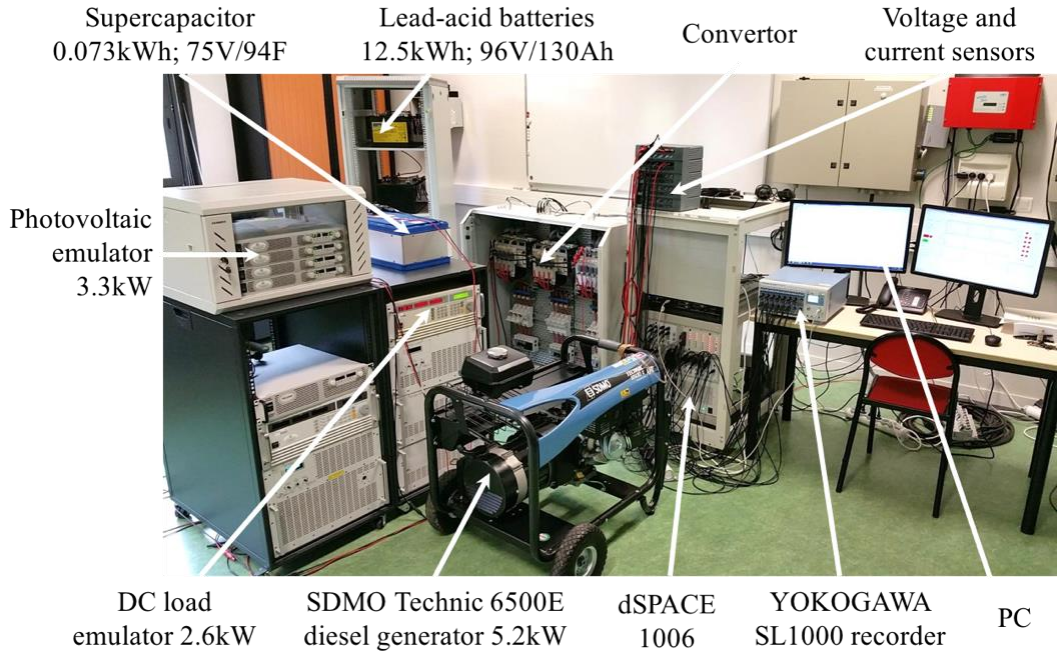

Figure 77. Off-grid DC microgrid experimental platform.

The parameters of the DC microgrid components are listed in Table 10 and the arbitrary values, tariffs, and constraints are as same as in the simulation tests, listed in Table 9.

Table 10. Elements detail for experimental test.

Element	Parameter	Device
Bateries (serial 8 units)	96V/130Ah	Sonnenschein Solar: S12/130A
Supercapacitor	94F/75V	Maxwell 75V modules: BMOD0094 P075 B02
PV emulator	600V/5.5A	GEN 3.3kW series power supplies: GEN600-5.5
Load emulator	2.6kW	High power DC electronic load: Chroma 63202
Diesel generator	5.2kW	SDMO Technic 6500E AVR
IGBT	600V-100A	SEMIKRON SKM100GB063D
Controller board		dSPACE 1006

IV.4.1. Test 1

Under the weather circumstance and load profile shown in Section IV.3.1, two experiments are done according to the operating mode of DG: duty-cycle model and load-following mode.

IV.4.1.1. DG duty cycle mode

Figure 78 shows the DC microgrid power evolutions during the nine hours. During the first interval ($9:00 \le t < 11:01$), the batteries and the PV sources are the main suppliers (case 8). With the time going on, the energy stored in the SC is decreasing by self-discharging until reaching the constraint. So, during the second interval ($11:01 \le t < 12:05$), the batteries bank not only supplies the load, but also gives some power to the SC to maintain the energy level stored in the SC. This is case 6. Then, in the third interval ($12:05 \le t < 13:52$), there is an excess PV power, which is preferentially recharged into the SC. This is case 4. Around $12:22$, the SC is full. In the next interval ($13:52 \le t < 14:52$), the energy of the batteries is firstly used up. SOC_B reaches its lower limit and then the SC supplies the load during the DG start-up. After the DG can offer stable power, the excess power firstly recharges the SC. Afterwards, batteries begin to absorb power when the SC is fully recharged. Then, the DG is stopped after one hour. This is the case 9. In the fifth interval ($14:52 \le t < 15:21$), the deficient power is more than the batteries maximal discharging power so that the load shedding takes place. This is case 7. In the sixth interval ($15:21 \le t < 17:38$), around $15:21$ and $16:38$, the DG is started up twice because the load shedding demand is more than 20% of the total power demand. This is case 9. In the last interval ($17:38 \le t < 18:00$), the batteries bank supplies the deficient power. This is case 8.

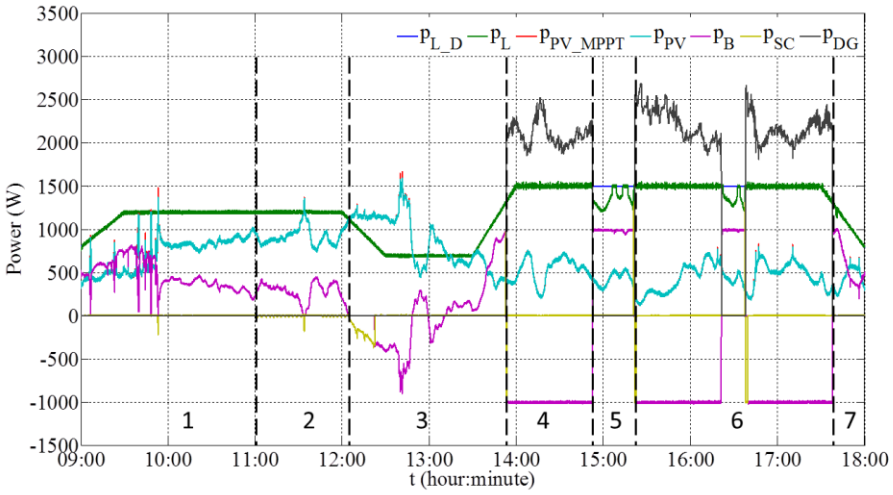

Figure 78. DC microgrid power evolutions.

Figure 79 and Figure 80 show SOC_B and SOC_{SC} evolutions, reflecting that the batteries and the SC run well for providing and absorbing energy within their respective restrictions. Considering that the goal of this nine hours experiment is to verify the feasibility of the proposed strategy with a real PV power profile, the experimental results display that the power is well balanced and the DC bus voltage is stable with acceptable fluctuations (the maximum fluctuation error is less than 1.5% of the rated DC bus voltage), as shown in Figure 81.

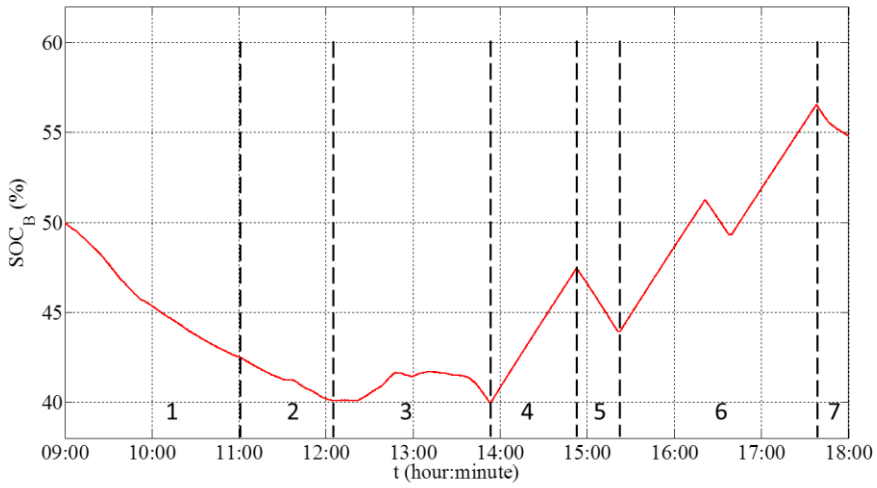

Figure 79. *SOC* evolution of electrochemical batteries.

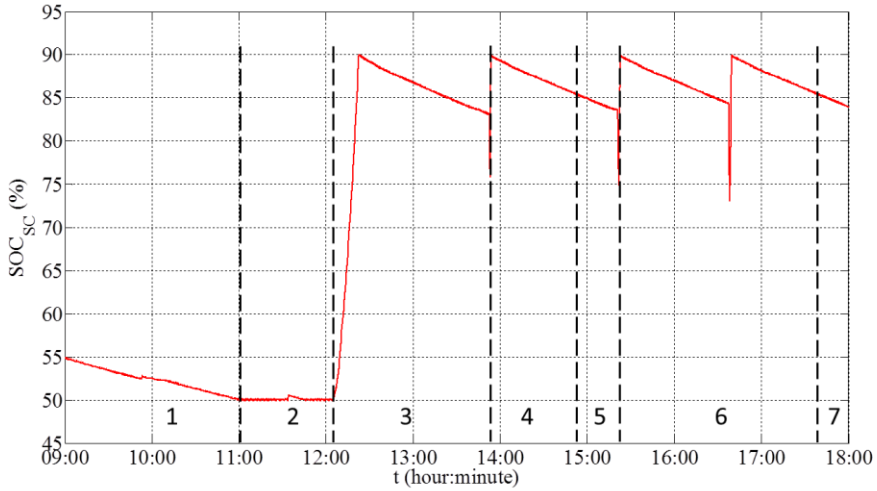

Figure 80. *SOC* evolution of supercapacitor.

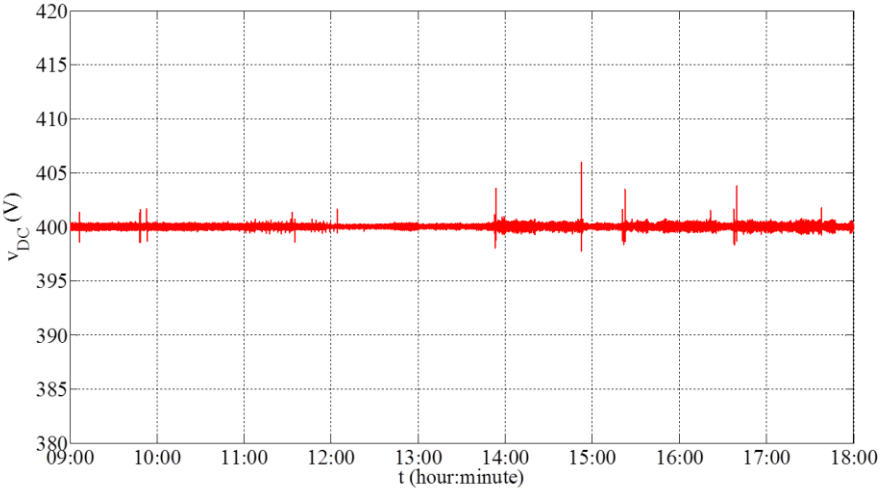

Figure 81. DC bus voltage.

IV.4.1.2. DG load following mode

In the load following mode, the reference of the DG generating power is given as the deficient power, meaning that it only satisfies the load demand. There is no consideration for the DG power cost and there is no excessive power to recharge SC and batteries. The experimental test of this mode is carried out and the results are analyzed in the following.

Figure 82 shows the DC microgrid power evolutions during the nine hours. Before the DG being started up, the power evolution of each component is similar to that given in Figure 78. In the fourth interval ($13:52 \le t < 18:00$), the DG output power is equal to the load demand so that there is no longer load shedding, but there is also no excessive power to recharge SC and batteries.

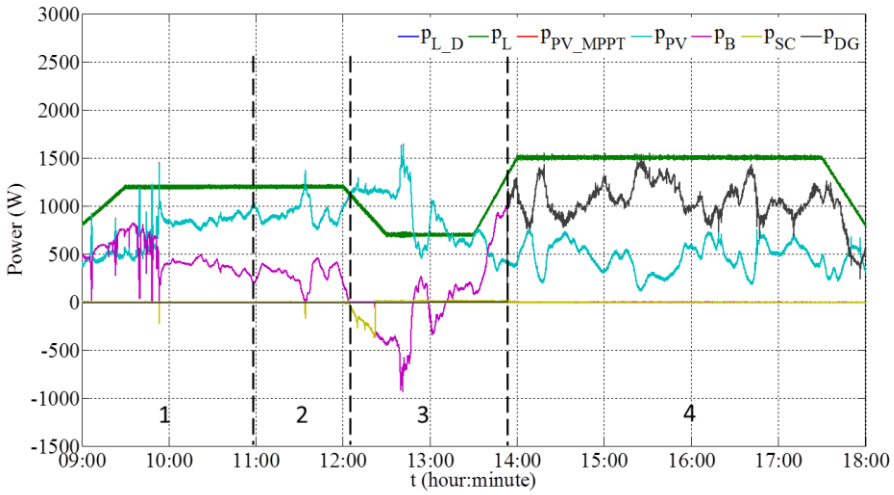

Figure 82. DC microgrid power evolutions.

Figure 83 and Figure 84 show SOC_B and SOC_{SC} evolutions, reflecting that the batteries and the SC run well for providing and absorbing energy within their respective restrictions. Since there is no power to recharge SC and batteries after DG being stated up, the SOC_B evolution shows that the batteries continue to be in the empty state and the SOC_{SC} evolution shows that the SC is in a continuous decline. The DC bus voltage is stable with acceptable fluctuations (the maximum fluctuation error is less than 1.5% of the rated DC bus voltage), shown in Figure 85.

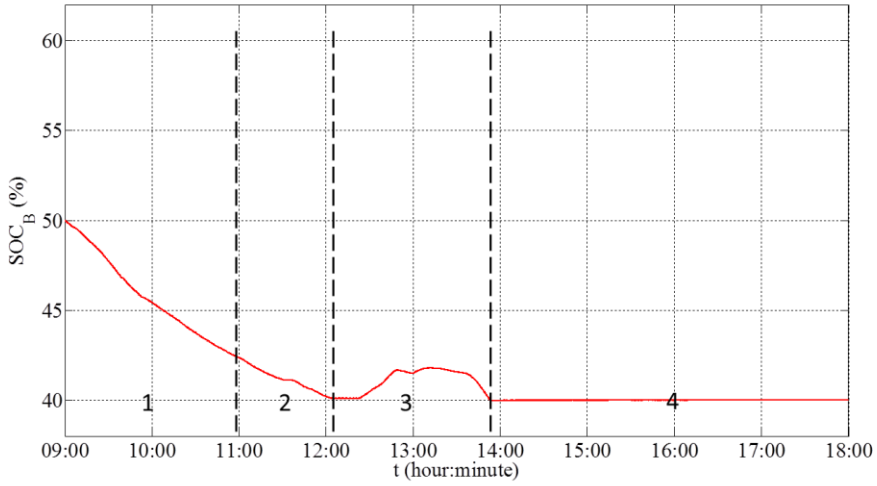

Figure 83. *SOC* evolution of electrochemical batteries.

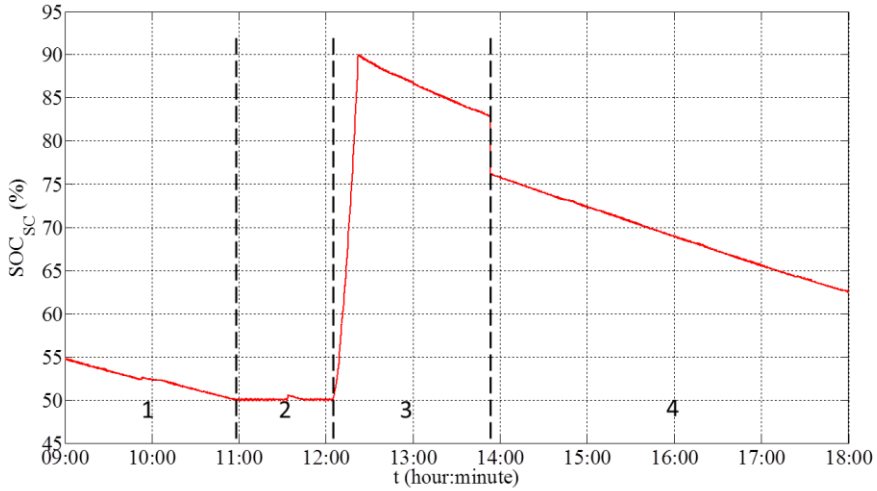

Figure 84. *SOC* evolution of supercapacitor.

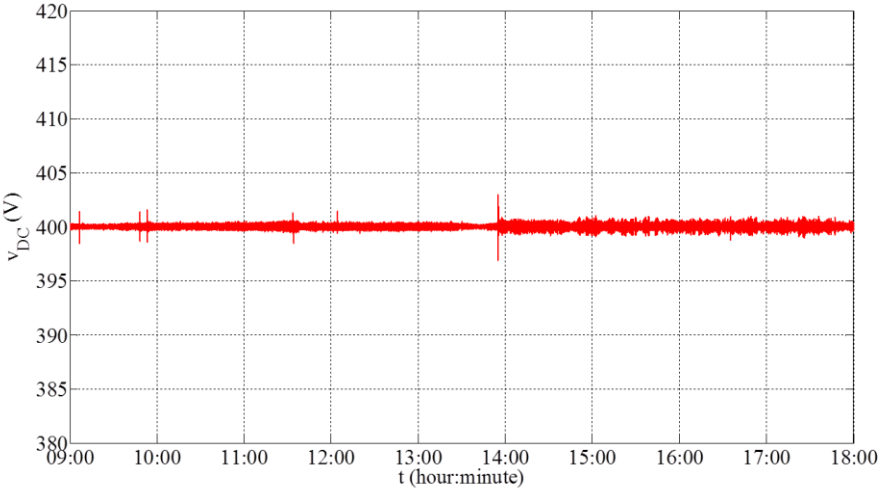

Figure 85. DC bus voltage.

IV.4.2. Test 2

The weather condition is shown in Figure 65 and the PV power and load power profile in this experiment are shown in Figure 66.

Figure 86 shows the power evolutions during the nine hours. At noon, since the excess PV power goes beyond the batteries absorbing capacity, the PV power is restrained afterwards. This is case 2. The SC is recharged several times while the batteries absorb power and discharge power dynamically.

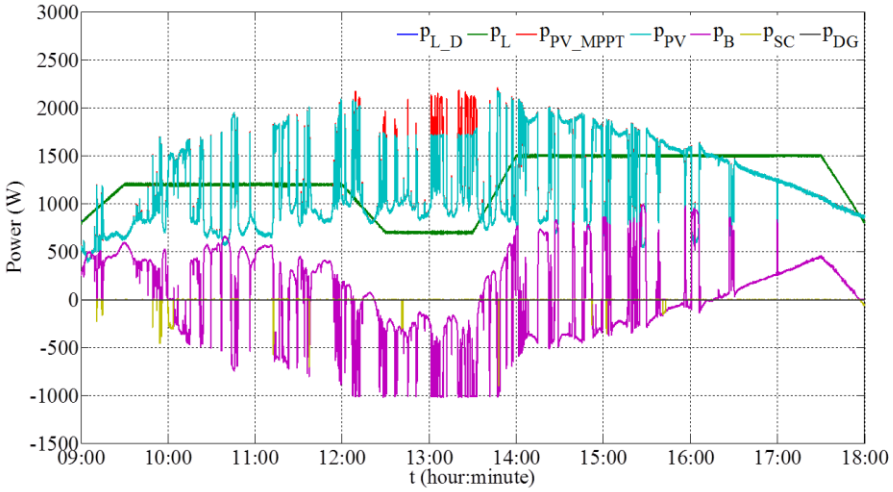

Figure 86. DC microgrid power evolutions.

Figure 87 and Figure 88 show that both SOC_B and SOC_{SC} have respected their dedicated restrictions. Since the PV power fluctuates severely and frequently, the DC bus voltage fluctuates with acceptable range (less than 2% of the rated DC bus voltage), as shown in Figure 89. Since the DG has not been started in this test, there is no analysis about the DG power.

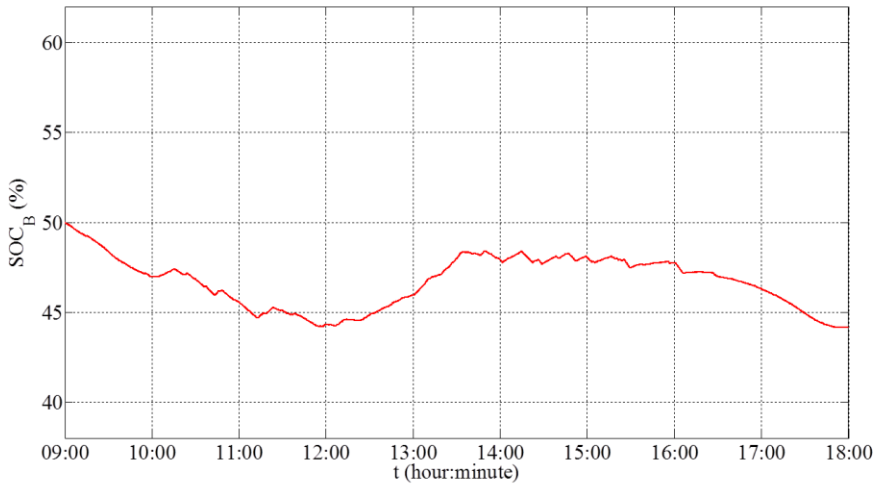

Figure 87. *SOC* evolution of electrochemical batteries.

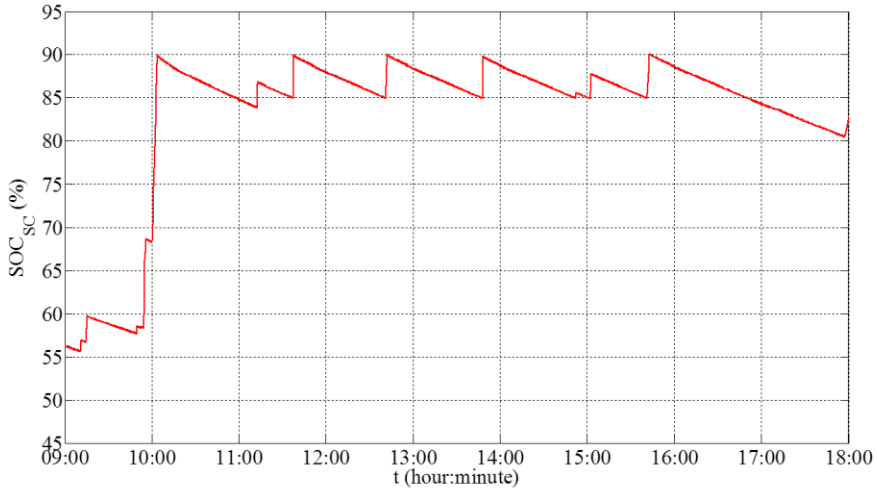

Figure 88. *SOC* evolution of supercapacitor.

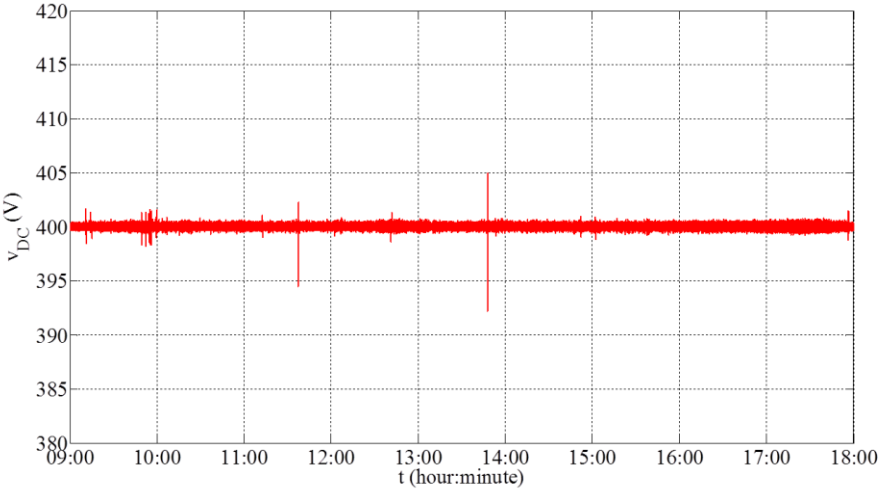

Figure 89. DC bus voltage.

IV.4.3. Test 3

The weather condition is shown in Figure 71 and the PV power and load power profile in this experiment are shown in Figure 72.

Figure 90 shows the power evolutions during the nine hours. During the first interval ($9:00 \le t < 10:20$), the batteries and PV are the main suppliers (case 8). During the second interval ($10:20 \le t < 10:46$), there are excess PV power, which is preferentially recharged into the SC. This is case 4. Around $10:46$, the SC is full. Afterwards, in the third interval ($10:46 \le t < 13:41$), batteries begin to absorb power. This is case 3. During this interval, around the time $11:50$ and $12:58$, SC is recharged again when SOC_{SC} is under the value $SOC_{SC\_MAX\_MIN}$ and when there is excess PV power. This is case 4. In the next interval ($13:41 \le t < 15:42$), after the batteries are fully charged, the PV power shedding is executed to supply the load and the SC when SOC_{SC} falls below $SOC_{SC\_MAX\_MIN}$ around the time $14:03$ and $15:13$. In the last interval ($15:42 \le t \le 18:00$), the batteries bank supplies the deficient power. This is case 8.

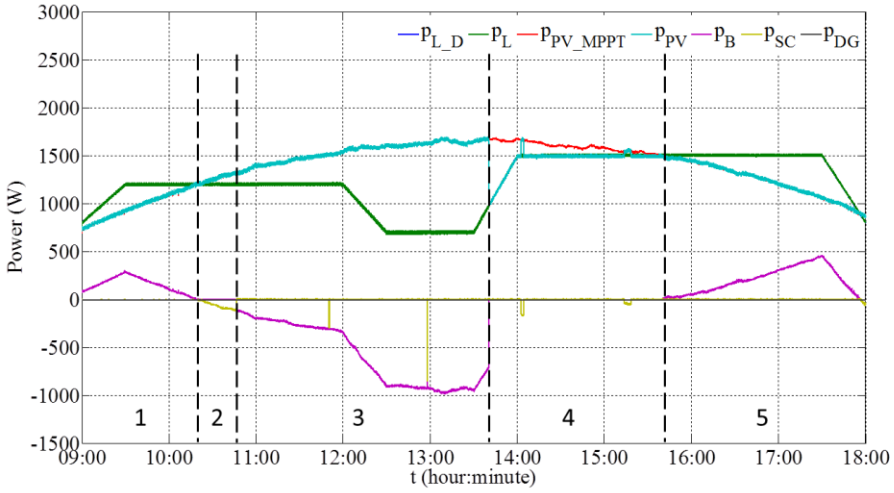

Figure 90. DC microgrid power evolutions.

Figure 91 and Figure 92 show that SOC_B and SOC_{SC} evolutions remain always within the constrained range. The DC bus voltage shown in Figure 93 is quite stable with the maximal fluctuation error less than 1.25% of the rated DC bus voltage. The different DG operation modes are not compared in this test because there is no need for the DG power in this day.

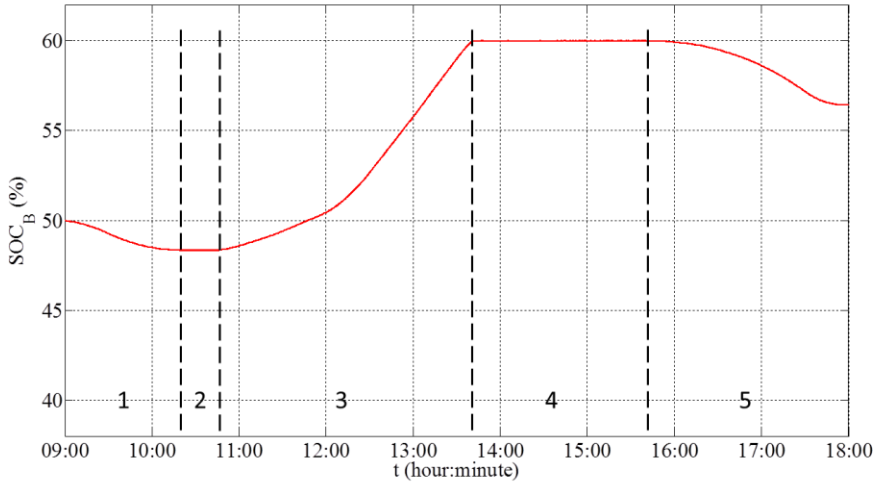

Figure 91. *SOC* evolution of electrochemical batteries.

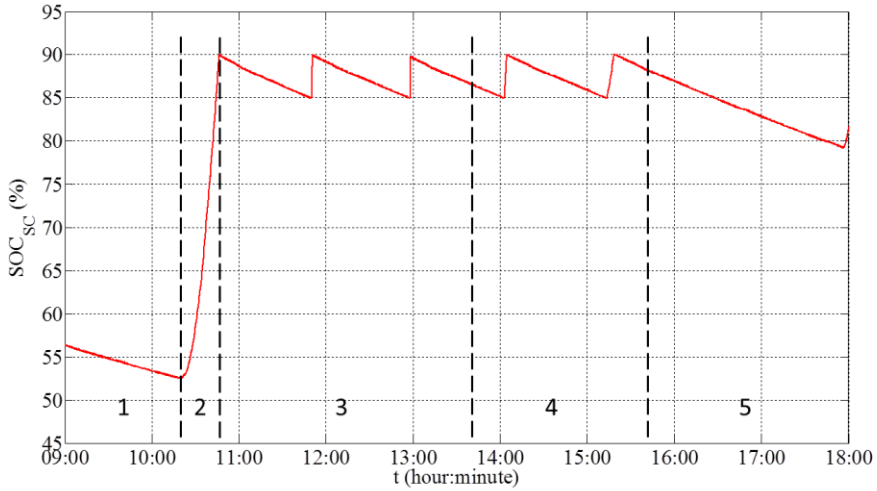

Figure 92. *SOC* evolution of supercapacitor.

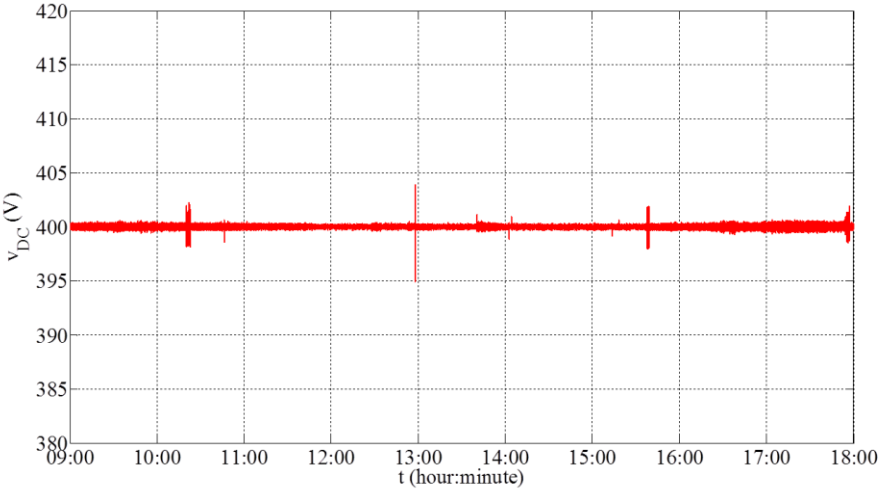

Figure 93. DC bus voltage.

IV.5. Economic analyses

Table 11 compares the energy cost between the DG duty cycle mode and DG load following mode during the three experimental tests.

Table 11. Costs comparison of the different DG mode: duty cycle and load following.

Day	C_{Total} **(euro)**		$(C_{DG\_Fuel} + C_{DG\_O\&M})$ **(euro)**	
	Duty cycle	**Load following**	**Duty cycle**	**Load following**
Test 1 - 8th July	9.20	10.19	8.58	10.05
Test 2 - 9th July	0.32	0.32	0	0
Test 3 - 10th July	0.38	0.38	0	0

As shown in this table, when the microgrid needs to start up DG, the DG energy cost in duty cycle mode is less than that in DG load following mode (the cost is cut down by 14.63%). Therefore, the total cost decreases from 10.19 euros to 9.20 euros. Compared with the DG duty cycle mode, the DG in load following mode outputs low power for long time and the DG energy efficiency would be higher when the output power is high.

In the two other days, since there is no need to start up the DG, the DG cost is zero and the total cost is same in both the duty cycle mode and load following mode. It's interesting to find that the total cost in the high solar irradiance day (Test 3) is higher than the solar irradiance with fluctuation day (Test 2). This is because in the Test 3, there is a period of PV shedding (more than 1 hour), which is counted into the cost.

IV.6. Conclusion

In this chapter, an improved power management strategy for considering the DG energy cost is proposed. The simulations are firstly done to verify the control strategy theoretically. Then, an experimental platform is set up and the power management strategy is implanted into the real-time control system.

The experimental tests validate the proposed power management, which can work under different weather condition for providing robust power balancing control strategy. Therefore, given the obtained experimental results, the feasibility of implementing the strategy in real operation, is validated.

In addition, in order to comparing the advantages and disadvantages between the two DG operating mode: load following mode and duty cycle mode, the energy tariff of each element of each element is defined and the total cost of the whole system is calculated. Compared with the DG load following mode, the fuel cost is reduced in the newly proposed strategy with a reasonable operation mode of DG, which is good from economic point of view.

General conclusions and perspectives

Under the duel pressures of the conventional fossil energises shortage and the environmental pollution by the utilization of them, transformation and upgrading of energy industry attracts more and more people's attention. In terms of electrical power industry, governments and electric companies all over the world regard the smart grid as the future direction of the development of power systems, to achieve the upgrading of the traditional power grid. As the local level of smart grid, microgrid is believed to bring advantages in incorporating renewable energies, improving the overall energy efficiency and improving reliability by self-operating in isolated mode in case of grid fault. DC microgrid is just one kind of microgrid; it has some advantages compared with the AC microgrid, such as easy control and conversion efficiency. The increase of DC load in the daily life will also drive the rapid development of DC microgrid.

In islands, mountains and remote areas where the conventional power distribution system is difficult to reach, standalone microgrid is utilizing its own distributed power generation to meet the requirements of the user's electricity demand. In view of the PV, wind and other renewable energy affected by the environment, this microgrid is generally equipped with energy storage system to suppress the power fluctuations of renewable energy. On the other hand, it is possible that the energy storage is used up because of the long-term bad weather. Therefore, back-up power, like DG, is very important to start up to continue to supply the users. However, when we want to start up DG, it needs some time to reach the stable output power. During this period, the users' demand cannot be met and the DC bus voltage will decrease to further influence the power quality.

In microgrid studies, DG is mostly considered to immediately supply the power when needed and the power management strategy of the whole system is mostly carried out by simulation. Besides, the fuel consumption and energy cost of DG is mostly calculated by a rough function, which is not precise as possible. In addition, the economical operating mode of DG can contribute the reducing of total cost of the whole system and the decreasing of NOx emissions and carbon emissions. However, there is little research work in this area. This thesis attempted to cover the research gap by studying the start-up characteristic of DG, the energy cost of DG and its use in the power management of a microgrid power system, which is tested by experimental tests.

This thesis firstly studied the DG start-up characteristic and the self-discharging characteristic of SC. Based on the experimental and technical notice date, DG and SC models are presented. Then, a power control strategy is proposed to achieve coordination between DG and SC, so that the SC can supply the load demand during the period of DG start-up and the load demand can be supplied continuously and smoothly without interruption. This control strategy is verified by both simulation and experimental tests.

The proposed standalone DC microgrid consists of a power system and a power management strategy for the real time control. The power system is composed of PV source, battery storage, SC, DG and controllable DC load, which simulate the energy consumption of buildings. The electrical power system relies on the power management strategy to keep the instantaneous power supply and power balance. The first strategy proposed in this thesis which has twelve cases, can ensure voltage stabilization and increase reliability by actively ensuring power balance, which are verified by experimental tests. However, the DG operates in load following mode, which only supplies the load demand and do not recharge the batteries and SC storages. In addition, the fuel cost is not considered in this strategy. But the power management strategy should also minimize the energy cost and at the same time respect the multi sources constraints.

Therefore, aiming at analysing the fuel consumption of DG, several experiments has been done to study the temperature influence on the DG and diesel fuel consumption rate under different output power value. The obtaining results are applied to a newly proposed power management strategy which has nine cases. Meanwhile, algorithms for PV power limiting and load shedding management are also developed and applied into the power management strategy to fulfill power control strategy. The DG operates in duty cycle mode with an optimal running time and an ideal output power. The experimental tests have been done to verify the feasibility of the proposed strategy. The more important improvement and contribution from this thesis comes from the creation and practical development of an experimental platform for microgrid based on PV sources emulator, which allows the repeatability conditions and reproducibility. Based on this test bed, another experiment has been done, in which the DG operates in load following mode with the same solar irradiation and environmental temperature. Therefore, under the same weather condition, the cost analyses and comparisons between these two modes have highlighted the benefits of applying the DG energy cost into the power management strategy when

aiming to ensure cost reduction to the end user. Furthermore, both the fuel cost of DG and total cost of the whole system are reduced when the DG operates in duty cycle mode.

After concluding the main research work of this thesis, the originality of this thesis concludes as given below.

Firstly, in order to continuously supply the load, DG start-up is compensated by supercapacitor. The proposed power control strategy can well supply the load demand during the operation without interrupting the power balancing. This method is verified by the experiments in the real environment. Therefore, DG and SC can also be used together in the emergency back-up power in case of the utility power failure in the important facilities, such as hospital and data center.

Secondly, the DG fuel cost function is found according to the experimental results, which is much more precise then the past research work. Thus, the lower limit generating power is confirmed so that the generation tariff of the DG is kept in a low status. In addition, it studies the temperature influence on the start-up stage of DG, resulting that these is little influence of temperature on the research DG object in this thesis.

Thirdly, this thesis proposes a power management strategy for the real time control, applied into a standalone DC microgrid, consisting of PV building-integrated sources, a battery storage system, SC and DG to supply the building appliances. The proposed strategy is a local centralized approach where all the available data about the microgrid system are concentred in one main system. The strategy is flexible and can be implemented in a microcontroller or a computer so that real-time power balancing control can be executed.

Fourthly, the DG different operating modes (load following and duty cycle) are analyzed and compared. The fuel cost of the DG and the total cost of the whole power system are calculated. Compared with the DG load following mode, the fuel cost is reduced in the duty cycle mode with a reasonable operation mode of DG (practical DG running time and optimal DG output power), which is good from economic point of view and environmental point of view. This reasonable operation mode of DG is applied to the proposed DC microgrid architectures, even though this solution itself is not limited to the DC microgrid case.

Fifthly, the proposed microgrid is a DC microgrid with DC bus. DC microgrid is believed to be the trend of future development, which provides more advantages for energy efficiency. As microgrid research is initiated by AC microgrid or grid-connected DC microgrid, the standalone DC microgrid has not been studied as much as possible. This thesis contributes the standalone DC microgrid study from an ensemble view combining power balancing, storage capacity power limits and energy cost saving.

Last but not least, all the power control strategies are verified through simulation in the first place. Then experimental platforms are built up to further verify and realize functions of the proposed strategies, which have been seldom reported in literature. Fairly good performance of one-day experimental test

proves that the energy management strategy can be employed in a real hybrid PV/DG/battery/SC power system. Furthermore, the strategy can be programmed into Digital Signal Processor or Field Programmable Gate Array to replace the real-time simulation system (dSPACE), so that it can have application in industrial field.

The accomplished work during this thesis opens up several perspectives, which are also the key points needed to be improved.

Firstly, the future work will focus on joint-optimization of operation and component-sizing for the standalone DC microgrid. Before constructing a real electrical power system, it should be solved the sizing optimization problem with multiple objectives including the minimization of investment cost, the maximization uses of renewable energy, the minimization of pollutant emissions and so on. The sizing problem should also follow the constraints such as the peak load demand, the environment condition, the peak day solar irradiation, the annual user's energy consumption, the annual solar irradiation and so on. With the optimal sizing and design of the power system, the energy management can be designed from day-ahead to 10 minutes ahead to further minimize the total cost.

Secondly, the proposed strategy is a rule based power management. Even though for a standalone microgrid, a rule based power management is enough to enhance the power system stability and load supply continuity, future work should focus on enhancing optimization performance. It is possible that the present research work combines with the other PhD' research in our laboratory, such as operational optimization. The different optimization techniques based on artificial intelligence or machine learning, can be applied to the energy management.

Thirdly, the energy management strategy will be incorporated with day-ahead or even several days-ahead PV forecasting, so that the running time of DG can be decided by the next several days' weather condition, to further save the fuel cost. In addition, the load demand can also influence the fuel cost. Therefore, the energy management strategy can be combined with the prediction algorithm, which gives the prediction of PV production and load consumption in the next several days. This prediction algorithm can be designed as a prediction layer, which is mainly responsible for the interpretation of the load demand plan and Météo France's data which includes the load predication and the PV power calculation. They are used to help to calculate the optimal running time of DG. The algorithmic method is also an optimization aspect, which is related with the first perspective.

Fourthly, the demand side management strategy which is based on a critical load limit and on a load shedding/restoration optimization algorithm, can also be studied. Regarding the demand side management, since not all the electrical appliances of users have an ON/OFF characteristic, the development of an approach being able to perform a partial load shedding/restoration, controlling each appliance is a good research aspect. This demand side management strategy can work together with the load prediction mechanism, which is related with the second perspective, to further optimize the electrical power consumption and to improve users power utilization experience.

Fifthly, further study will also take into account the electrical noises injected by DG that need to be filtered. Due to the fast turn-on and turn-off of the IGBT (AC/DC converter), high-frequency electrical noises are injected into the DC bus, which can be seen through the noises of DC bus voltage. While the third order LCL filter could obtain better high frequency attenuation capability with small inductance, it gradually becomes the mainstream filter to meet regulatory requirements. Current control of AC generator connecting to DC microgrid by rectifier with LCL filter based on passive damping or active damping can be another research aspect.

To sum up, the proposed standalone DC microgrid control structure combines energy cost consideration and power management with power balancing control. Although the microgrid only refers to an off-grid mode and involves only a few sources, the idea of parameterizing power balancing, power supply reliability and continuity, can be generalized and thus can be used as solution for advanced energy management for other microgrids to supply local power demand, to serve as emergency back-up power and to improve future renewable energy penetration.

References

[1] United Nations Framework Convention on Climate Change. The Paris Agreement - main page. Paris Agreem 2016:1. http://unfccc.int/paris_agreement/items/9485.php (accessed September 18, 2017).

[2] Howell S, Rezgui Y, Hippolyte JL, Jayan B, Li H. Towards the next generation of smart grids: Semantic and holonic multi-agent management of distributed energy resources. Renew Sustain Energy Rev 2017;77:193–214.

[3] Wissner M. The Smart Grid - A saucerful of secrets? Appl Energy 2011;88:2509–18.

[4] Yoldaş Y, Önen A, Muyeen SM, Vasilakos A V., Alan İ. Enhancing smart grid with microgrids: Challenges and opportunities. Renew Sustain Energy Rev 2017;72:205–14.

[5] Sechilariu M, Wang B, Locment F. Building Integrated Photovoltaic System With Energy Storage and Smart Grid Communication. IEEE Trans Ind Electron 2013;60:1607–18.

[6] Saad W, Han Z, Poor HV, Başar T. Game-theoretic methods for the smart grid: An overview of microgrid systems, demand-side management, and smart grid communications. IEEE Signal Process Mag 2012;29:86–105.

[7] Haase P. Intelligrid: A smart network of power. EPRI J 2005:26–32.

[8] United States Department of Energy O of ET and D. “ Grid 2030 ” a national vision for electricity’s second 100 years. 2003.

[9] European Technology Platform SmartGrids. strategic research agenda for europe's electricity networks of the future. 2007.

[10] Future strategic research agenda for europe's electricity networks of the. SmartGrids SRA 2035 Strategic Research Agenda Update of the SmartGrids SRA 2007 for the needs by the year 2035. 2012.

[11] Sechilariu M, Locment F. Chapter 1 – Connecting and Integrating Variable Renewable Electricity in Utility Grid. Urban DC Microgrid, 2016, p. 1–33.

[12] Bangchao Wang. Intelligent control and power flow optimation of microgrid. Energy management strategies. Université de Technologie compiègne, 2013.

[13] Rajesh KS, Dash SS, Rajagopal R, Sridhar R. A review on control of ac microgrid. Renew Sustain Energy Rev 2017;71:814–9.

[14] Chakraborty S, Weiss MD, Simoes MG. Distributed Intelligent Energy Management System for a Single-Phase High-Frequency AC Microgrid. IEEE Trans Ind Electron 2007;54:97–109.

[15] Dragicevic T, Lu X, Vasquez JC, Guerrero JM. DC Microgrids Part I: A Review of Control Strategies and Stabilization Techniques. Power Electron IEEE Trans 2016;31:4876–91.

[16] Dragicevic T, Lu X, Vasquez JC, Guerrero JM. DC Microgrids Part II: A Review of Power Architectures, Applications, and Standardization Issues. Power Electron IEEE Trans 2016;31:3528–49.

[17] Unamuno E, Barrena JA. Hybrid ac/dc microgrids—Part II: Review and classification of control strategies. Renew Sustain Energy Rev 2015;52:1123–34.

[18] Unamuno E, Barrena JA. Hybrid ac/dc microgrids—Part I: Review and classification of topologies. Renew Sustain Energy Rev 2015;52:1251–9.

[19] Pierri E, Binder O, Hemdan NGA, Kurrat M. Challenges and opportunities for a European HVDC grid. Renew Sustain Energy Rev 2017;70:427–56.

[20] Dragicevic T, Vasquez JC, Guerrero JM, Skrlec D. Advanced LVDC Electrical Power Architectures and Microgrids: A step toward a new generation of power distribution networks. IEEE Electrif Mag 2014;2:54–65.

[21] Sivakumar S, Sathik MJ, Manoj PS, Sundararajan G. An assessment on performance of DC?DC converters for renewable energy applications. Renew Sustain Energy Rev 2016;58:1475–85.

[22] ABB Company. ABB's Hybrid HVDC Circuit Breaker n.d. http://new.abb.com/grid/events/cigre2014/hvdc-breaker (accessed June 15, 2017).

[23] Hassanpoor A, Hafner J, Jacobson B. Technical Assessment of Load Commutation Switch in Hybrid HVDC Breaker. IEEE Trans Power Electron 2015;30:5393–400.

[24] Gerber DL, Vossos V, Feng W, Marnay C, Nordman B, Brown R. A simulation-based efficiency comparison of AC and DC power distribution networks in commercial buildings. Appl Energy 2017.

[25] Tarif EDF (Tarif réglementé) n.d. https://www.fournisseurs-electricite.com/edf/tarifs/bleu-reglemente (accessed October 10, 2017).

[26] Global Petrol Prices. France Diesel Price n.d. http://www.globalpetrolprices.com/France/diesel_prices/ (accessed September 18, 2017).

[27] Wang B, Sechilariu M, Locment F. Intelligent DC Microgrid With Smart Grid Communications: Control Strategy Consideration and Design. IEEE Trans Smart Grid 2012;3:2148–56.

[28] Petrollese M, Valverde L, Cocco D, Cau G, Guerra J. Real-time integration of optimal generation scheduling with MPC for the energy management of a renewable hydrogen-based microgrid. Appl Energy 2016;166:96–106.

[29] Ogunjuyigbe ASO, Ayodele TR, Akinola OA. Optimal allocation and sizing of PV/Wind/Split-diesel/Battery hybrid energy system for minimizing life cycle cost, carbon emission and dump energy of remote residential building. Appl Energy 2016;171:153–71.

[30] Sechilariu M, Locment F, Sechilariu M, Locment F. Chapter 3 – Backup Power Resources for Microgrid. Urban DC Microgrid, 2016, p. 93–132.

[31] Dufo-López R, Bernal-Agustín JL, Yusta-Loyo JM, Domínguez-Navarro JA, Ramírez-Rosado IJ, Lujano J, et al. Multi-objective optimization minimizing cost and life cycle emissions of stand-alone PV-wind-diesel systems with batteries storage. Appl Energy 2011;88:4033–41.

[32] Saheb Koussa D, Koussa M, Rennane A, Hadji S, Boufertella A, Balehouane A, et al. Hybrid diesel-wind system with battery storage operating in standalone mode: Control and energy management – Experimental investigation. Energy 2017;130:38–47.

[33] Roy TK, Mahmud MA, Oo AMT, Haque ME, Muttaqi KM, Mendis N. Nonlinear adaptive backstepping controller design for controlling bidirectional power flow of BESSs in DC microgrids. IEEE Ind. Appl. Soc. 52nd Annu. Meet. IAS 2016, Portland, OR, USA: IEEE; 2016, p. 1–8.

[34] Mendis N, Mahmud MA, Roy TK, Haque ME, Muttaqi KM. Power management and control strategies for efficient operation of a solar power dominated hybrid DC microgrid for remote power applications. 2016 IEEE Ind. Appl. Soc. Annu. Meet., IEEE; 2016, p. 1–8.

[35] Rahmani R, Moser I, Seyedmahmoudian M. Multi-agent based operational cost and inconvenience optimization of PV-based microgrid. Sol Energy 2017;150:177–91.

[36] Kusakana K. Optimal scheduling for distributed hybrid system with pumped hydro storage. Energy Convers Manag 2016;111:253–60.

[37] Ameen AM, Pasupuleti J, Khatib T. Simplified performance models of photovoltaic/diesel generator/battery system considering typical control strategies. Energy Convers Manag 2015;99:313–25.

[38] Xiao J, Bai L, Li F, Liang H, Wang C. Sizing of energy storage and diesel generators in an isolated microgrid Using Discrete Fourier Transform (DFT). IEEE Trans Sustain Energy 2014;5:907–16.

[39] Tankari MA, Camara MB, Dakyo B, Lefebvre G. Use of ultracapacitors and batteries for efficient energy management in wind-diesel hybrid system. IEEE Trans Sustain Energy 2013;4:414–24.

[40] Kusakana K. Operation cost minimization of photovoltaic-diesel-battery hybrid systems. Energy 2015;85:645–53.

[41] Mendis N, Muttaqi KM, Perera S, Kamalasadan S. An Effective Power Management Strategy for a Wind–Diesel–Hydrogen-Based Remote Area Power Supply System to Meet Fluctuating Demands Under Generation Uncertainty. IEEE Trans Ind Appl 2015;51:1228–38.

[42] Choe S, Son YK, Sul SK. Control and Analysis of Engine Governor for Improved Stability of DC Microgrid Against Load Disturbance. IEEE J Emerg Sel Top Power Electron 2016;4:1247–58.

[43] Pourmousavi SA, Nehrir MH, Sharma RK. Multi-Timescale Power Management for Islanded Microgrids Including Storage and Demand Response. IEEE Trans Smart Grid 2015;6:1185–95.

[44] Craparo E, Karatas M, Singham DI. A robust optimization approach to hybrid microgrid operation using ensemble weather forecasts. Appl Energy 2017;201:135–47.

[45] Lee JH, Lee SH, Sul SK. Variable-speed engine generator with supercapacitor: Isolated power generation system and fuel efficiency. IEEE Trans Ind Appl 2009;45:2130–5.

[46] Abdel-baqi O, Nasiri A, Miller P. Dynamic Performance Improvement and Peak Power Limiting Using Ultracapacitor Storage System for Hydraulic Mining Shovels. IEEE Trans Ind Electron 2015;62:3173–81.

[47] Bortolini M, Gamberi M, Graziani A, Pilati F. Economic and environmental bi-objective design of an off-grid photovoltaic-battery-diesel generator hybrid energy system. Energy Convers Manag 2015;106:1024–38.

[48] Tazvinga H, Zhu B, Xia X. Optimal power flow management for distributed energy resources with batteries. Energy Convers Manag 2015;102:104–10.

[49] Ismail MS, Moghavvemi M, Mahlia TMI. Techno-economic analysis of an optimized photovoltaic and diesel generator hybrid power system for remote houses in a tropical climate. Energy Convers Manag 2013;69:163–73.

[50] Dufo-López R, Pérez-Cebollada E, Bernal-Agustín JL, Martínez-Ruiz I. Optimisation of energy supply at off-grid healthcare facilities using Monte Carlo simulation. Energy Convers Manag 2016;113:321–30.

[51] Hijjo M, Felgner F, Meiers J, Frey G. Energy management for islanded buildings integrating renewables and diesel generators. 2016 IEEE PES PowerAfrica, 2016, p. 62–6.

[52] Nemati M, Braun M, Tenbohlen S. Optimization of unit commitment and economic dispatch in microgrids based on genetic algorithm and mixed integer linear programming. Appl Energy 2017.

[53] Diesel Service and Supply. Approximate Diesel Fuel Consumption Chart 2013. http://www.dieselserviceandsupply.com/Diesel_Fuel_Consumption.aspx (accessed September 18, 2017).

[54] Sachs J, Sawodny O. A Two-Stage Model Predictive Control Strategy for Economic Diesel-PV-Battery Island Microgrid Operation in Rural Areas. IEEE Trans Sustain Energy 2016;7:903–13.

[55] Merei G, Berger C, Sauer DU. Optimization of an off-grid hybrid PV–Wind–Diesel system with different battery technologies using genetic algorithm. Sol Energy 2013;97:460–73.

[56] Jeyaprabha SB, Selvakumar AI. Optimal sizing of photovoltaic/battery/diesel based hybrid system and optimal tilting of solar array using the artificial intelligence for remote houses in India. Energy Build 2015;96:40–52.

[57] Zhao B, Zhang X, Li P, Wang K, Xue M, Wang C. Optimal sizing, operating strategy and operational experience of a stand-alone microgrid on Dongfushan Island. Appl Energy 2014;113:1656–66.

[58] Yin C, Sechilariu M, Locment F. Diesel generator slow start-up compensation by supercapacitor for DC microgrid power balancing. 2016 IEEE Int. Energy Conf. ENERGYCON 2016, Leuven: IEEE; 2016, p. 1–6.

[59] Tani A, Camara MB, Dakyo B. Energy Management in the Decentralized Generation Systems Based on Renewable Energy Ultracapacitors and Battery to Compensate the Wind/Load Power Fluctuations. IEEE Trans Ind Appl 2015;51:1817–27.

[60] Inthamoussou FA, Pegueroles-Queralt J, Bianchi FD. Control of a Supercapacitor Energy Storage System for Microgrid Applications. IEEE Trans Energy Convers 2013;28:690–7.

[61] Ghazanfari A, Hamzeh M, Mokhtari H, Karimi H. Active Power Management of Multihybrid Fuel Cell/Supercapacitor Power Conversion System in a Medium Voltage Microgrid. IEEE Trans Smart Grid 2012;3:1903–10.

[62] Yoo H, Sul S-K, Park Y, Jeong J. System Integration and Power-Flow Management for a Series Hybrid Electric Vehicle Using Supercapacitors and Batteries. IEEE Trans Ind Appl 2008;44:108–14.

[63] Maxwell Technologies. http://www.maxwell.com/products/ultracapacitors/downloads n.d.

[64] Sechilariu M, Wang B, Locment F. Building-integrated microgrid: Advanced local energy management for forthcoming smart power grid communication. Energy Build 2013;59:236–43.

[65] Fantauzzi M, Lauria D, Mottola F, Scalfati A. Sizing energy storage systems in DC networks: A general methodology based upon power losses minimization. Appl Energy 2017;187:862–72.

[66] Legrand. Electrical energy supply. 2009.

[67] Xu L, Chen D. Control and Operation of a DC Microgrid With Variable Generation and Energy Storage. IEEE Trans Power Deliv 2011;26:2513–22.

[68] Balog RS, Weaver WW, Krein PT. The Load as an Energy Asset in a Distributed DC SmartGrid Architecture. IEEE Trans Smart Grid 2012;3:253–60.

[69] Liu X, Wang P, Loh PC. A Hybrid AC/DC Microgrid and Its Coordination Control. IEEE Trans Smart Grid 2011;2:278–86.

[70] Kanchev H, Lu D, Colas F, Lazarov V, Francois B. Energy Management and Operational Planning of a Microgrid With a PV-Based Active Generator for Smart Grid Applications. IEEE Trans Ind Electron 2011;58:4583–92.

[71] Yin C, Wu H, Locment F, Sechilariu M. Energy management of DC microgrid based on photovoltaic combined with diesel generator and supercapacitor. Energy Convers Manag 2017;132:14–27.

[72] Wang B, Houssamo I, Sechilariu M, Locment F. A simple PV constrained production control strategy. 2012 IEEE Int. Symp. Ind. Electron., Hangzhou, China: IEEE; 2012, p. 969–74.

[73] Houssamo I, Locment F, Sechilariu M. Maximum power tracking for photovoltaic power system: Development and experimental comparison of two algorithms. Renew Energy 2010;35:2381–7.

[74] Houssamo I, Locment F, Sechilariu M. Experimental analysis of impact of MPPT methods on energy efficiency for photovoltaic power systems. Int J Electr Power Energy Syst 2013;46:98–107.

[75] Wang B, Houssamo I, Sechilariu M, Locment F. A simple PV constrained production control strategy. 2012 IEEE Int. Symp. Ind. Electron., Hangzhou, China: IEEE; 2012, p. 969–74.

[76] Ma T, Yang H, Lu L. Development of hybrid battery-supercapacitor energy storage for remote area renewable energy systems. Appl Energy 2015;153:56–62.

[77] Wen S, Lan H, Hong YY, Yu DC, Zhang L, Cheng P. Allocation of ESS by interval optimization method considering impact of ship swinging on hybrid PV/diesel ship power system. Appl Energy 2016;175:158–67.

[78] Jin X, Mu Y, Jia H, Wu J, Jiang T, Yu X. Dynamic economic dispatch of a hybrid energy microgrid considering building based virtual energy storage system. Appl Energy 2017;194:386–98.

[79] Adefarati T, Bansal RC. Reliability and economic assessment of a microgrid power system with the integration of renewable energy resources. Appl Energy 2017;206:911–33.

[80] Cooper AR, Mcgowan DJ, Morrow DJ, Chambers KDR. Temperature-dependant voltage regulator operation for optimal load acceptance of a diesel generator. IET Electr Power Appl 2012;6:553–60.

[81] The Engineering ToolBox. Liquids and Densities n.d. http://www.engineeringtoolbox.com/liquids-densities-d_743.html (accessed September 18, 2017).

[82] Yang Q, Li J, Le Blond S, Wang C. Artificial Neural Network Based Fault Detection and Fault Location in the DC Microgrid. Energy Procedia, vol. 103, 2016, p. 129–34.

[83] Maxwell Technologies. Maxwell supercapacitor 75V module datasheet n.d.:1–4. http://www.maxwell.com/products/ultracapacitors/75v-power-modules/documents (accessed September 18, 2017).

[84] Sonnenschein Solar. Batterie solaire gel SONNENSCHEIN S12/ 130A n.d.:1–2. https://www.solaris-store.com/381-batterie-solaire-gel-sonnenschein-solar-s12-130a.html (accessed September 18, 2017).

[85] Yin C, Wu H, Sechilariu M, Locment F. Energy Management of Standalone DC Microgrid. ELECTRIMACS 2017 (International Conf. theory Appl. Model. Simul. Electr. power Eng. Incl. Electr. Mach. power Electron. Convert. power Syst., Toulouse: 2017, p. 1–6.

Appendices

Appendix 1: Parameters of Solar-Fabrick series SF 130/2

Appendix 2: Parameters of Sonnenschein Solar: S12/130A

Appendix 3: Parameters of Maxwell 75V modules: BMOD0094 P075 B02

Appendix 4: Parameters of SDMO Technic 6500E AVR

Appendix 5: Parameters of programmable electric load PL-6000-A Puissance+

Appendix 6: Parameters of the insulated gate bipolar transistor (IGBT) module SEMIKRON SKM100GB063D

Appendix 7: Parameters of industrial driver (SEMIKRON SKHI22A) for IGBT

Appendix 1: Parameters of Solar-Fabrick series SF 130/2

Module Photovoltaïque

Solar-Fabrik Série SF 130/2

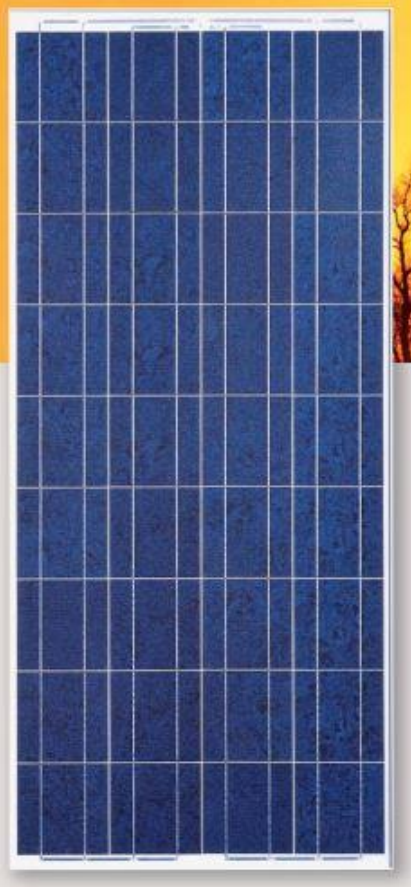

Une qualité optimale de série:

- Stabilité dans le temps grâce au verre solaire spécial transparent, équipé de filtre UV
- Présélection et tri des cellules à 100 %
- Rendement énergétique élevé grâce à l'utilisation de composants de qualité appairés avec précision (cf. l'étude « Power Check » de l'institut Fraunhofer ISE)
- Techniques de production de pointe et système de gestion de la qualité certifié (ISO 9001), pour la garantie d'une qualité produit « made in Germany »
- Cadre de module en aluminium spécialement développé en option; montage rapide et facile avec le système de fixation breveté Profilink; esthétique avantageuse grâce aux fixations intégrées
- Charge du panneau jusqu'à: 5400 Pa selon la norme IEC 61215
- Critères de tri très sélectifs de seulement +/- 2,5 W (= 1,9 %) pour éviter une première sélection des modules.
- Contrôles réguliers des modules de calibrage pour la mesure de la puissance à l'Institut Fraunhofer de systèmes à énergie solaire (ISE)

Dimensions

Série SF 130/2	Sans cadre	Cadre alu
l x L (mm)	1485 x 663	1491 x 669
Épaisseur (mm)	5	35
Poids (kg)	10,5	12,5

Homologations/Certifications

EN IEC 61215 ed. 2
Classe de protection II
Directive 89/336/CEE (CE)
Directive 73/23/CEE (CE)

solar fabrik

Caractéristiques module Solar-Fabrik Série SF 130/2

Type de module		SF 130/2-125	SF 130/2-130	SF 130/2-135
Nombre de cellules (polycristallin)		36	36	36
Tension max. système		840 V	840 V	840 V

Caractéristiques électriques en STC (Standard Test Conditions: 1000 W/m², 25 °C, AM 1,5)

Puissance nominale*	P_{max}	125 W	130 W	135 W
Limites de tri puissance		+/- 2,5 W	+/- 2,5 W	+/- 2,5 W
Tension appr.	U_{MPP}	17,50 V	17,72 V	17,94 V
Tension circuit ouvert appr.	U_{OC}	21,53 V	21,69 V	21,86 V
Courant appr.	I_{MPP}	7,14 A	7,34 A	7,52 A
Courant de court-circuit appr.	I_{SC}	7,84 A	7,96 A	8,08 A

Caractéristiques électriques sous 800 W/m², NOCT, AM 1,5

Puissance en MPP appr.	P_{max}	96 W	100 W	104 W
Tension appr.	U_{MPP}	17,67 V	17,90 V	18,12 V
Tension circuit ouvert appr.	U_{OC}	21,26 V	21,42 V	21,59 V
Courant appr.	I_{MPP}	5,43 A	5,58 A	5,72 A
Courant de court-circuit appr.	I_{SC}	5,88 A	5,97 A	6,07 A

Sous un ensoleillement de 200 W/m² et une température de 25 °C, le rendement diminue de 7 % environ par rapport au rendement en conditions standard STC.

Températures

Coefficient de température tension	$T_K(U_{OC})$	-72 mV/K
Coefficient de température courant	$T_K(I_{SC})$	5,45 mA/K
NOCT		45 °C +/-4K

Autres caractéristiques

Test haute tension	Tension d'essai 3200 V_{DC}/max. 60µA
Tenue à la grêle **	Jusqu'à 25 mm de diamètre à 23 m/s
Résistance à la tempête **	Vitesse du vent jusqu'à 130 km/h = 800 Pa et facteur de sécurité 3
Charge de neige supportée **	Sans cadre: 2400 Pa ≙ 245 kg/m²
Contrainte testée selon IEC 61215	Avec cadre: 5400 Pa ≙ 550 kg/m²

* (tolérance +/- 5 %)

** en combinaison avec notre système de fixation breveté Profilink installé selon les recommandations (BP)
Sous réserve de modifications techniques.

Garantie de puissance: 25 ans conformément à nos conditions de garantie supplémentaires, envoyées sur demande.

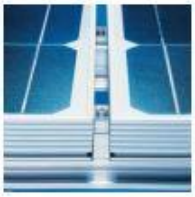

Un système de fixation efficace: Profilink

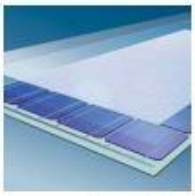

Structure du module: verre spécialement trempé à faible teneur en fer/film vinyl transparent en acétate d'éthyle (EVA)/ cellules photovoltaïques/ EVA/ feuille arrière en Tedlar

Certifié par le VDE (Association des électrotechniciens allemands) selon les normes DIN EN ISO 9001, Reg.Nr. 5002983/QM11.2003 / DIN EN ISO 14001, Reg.Nr. 5002983/UM11.2003

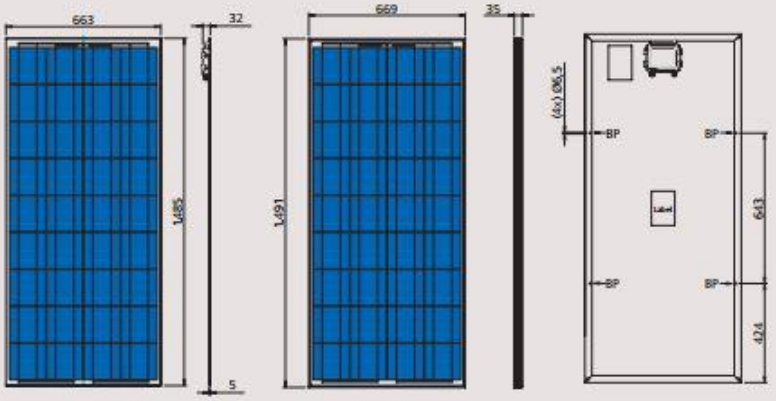

SF 130/2 sans cadre SF 130/2 avec cadre

Solar-Fabrik AG
Munzinger Straße 10
79111 Freiburg / Allemagne
tél. +49-(0)761-4000-0
fax +49-(0)761-4000-199
www.solar-fabrik.de

État: 15.12.2006, Solar-Fabrik AG
Document n° 0612MD8153

Appendix 2: Parameters of Sonnenschein Solar: S12/130A

Sonnenschein

The compact alternative for smaller solar applications.

Sonnenschein Solar batteries are specially designed for small to medium performance requirements in leisure and consumer applications. The advantages of the maintenance free VRLA-batteries are enhanced by the worldwide high reputation and technical image of the dryfit technology. Typical applications are weekend and holiday houses without mains supply, street solar stations, information signs, parking meters, wireless emergency phone boxes and also other safety equipment power supplies.

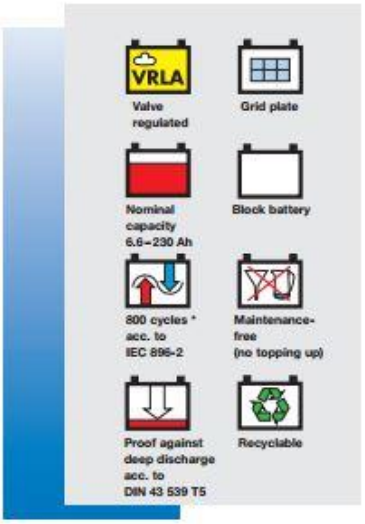

2

Sonnenschein

Technical characteristics and data

Type	Part number	Nominal voltage V	Nominal capacity C_{100} 1.8 V/C Ah	Discharge current I_{100} A	Length (l) max. mm	Width (b/w) max. mm	Height up to top of cover (h1) max. mm	Height incl. connectors (h2) max. mm	Weight approx. kg	Terminal	Terminal position
S12/6.6 S	NGSO1206D6HS0SA	12	6.6	0.066	151.7	65.5	94.5	98.4	2.6	S-4.8	3
S12/17 G5	NGSO120017HS0BA	12	17.0	0.170	181.0	76.0	–	167.0	6.1	G-M5	1
S12/27 G5	NGSO120027HS0BA	12	27.0	0.270	167.0	176.0	–	126.0	9.7	G-M5	1
S12/32 G6	NGSO120032HS0BA	12	32.0	0.320	197.0	132.0	160.0	184.0	11.2	G-M6	2
S12/41 A	NGSO120041HS0CA	12	41.0	0.410	210.0	175.0	–	175.0	14.8	A-Terminal	1
S12/60 A	NGSO120060HS0CA	12	60.0	0.600	261.0	136.0	208.0	230.0	19.0	A-Terminal	1
S12/85 A*	NGSO120085HS0CA	12	85.0	0.850	353.0	175.0	–	190.0	27.3	A-Terminal	1
S12/90 A	NGSO120090HS0CA	12	90.0	0.900	330.0	171.0	213.0	236.0	31.3	A-Terminal	2
S12/130 A	NGSO120130HS0CA	12	130.0	1.300	286.0	269.0	208.0	230.0	39.8	A-Terminal	4
S12/230 A	NGSO120230HS0CA	12	230.0	2.300	518.0	274.0	216.0	238.0	70.0	A-Terminal	3

Fig.1

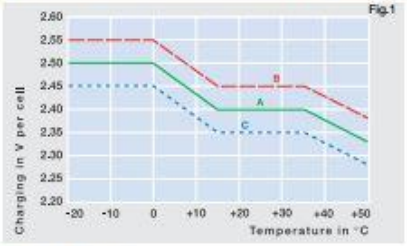

Charge mode (to Fig.1):

1.) with switch regulator (two-step controller)
- charge on curve B (max.charge voltage) for max.2 hrs/day then switch over to continous charge - curve C

2.) Standard charge (without switching) - curve A

3.) Boost charge (Equalizing charge with external generator)
- charge on curve B for max. 5 hrs/month, then switch over to curve C

Fig.2

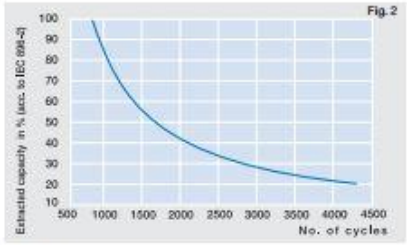

(to Fig. 2)
Endurance in cycles according to IEC 896-2
* S12/85 A = 400 cycles

Capacities C_1 – C_{100} (20°C)

Type	C_1 1.70 V/C	C_5 1.70 V/C	C_{10} 1.70 V/C	C_{20} 1.75 V/C	C_{100} 1.80 V/C
S12/6.6 S	2.9	4.6	5.1	5.7	6.6
S12/17 G5	9.3	12.6	14.3	15.0	17.0
S12/27 G5	15.0	22.1	23.5	24.0	27.0
S12/32 G6	16.9	24.4	27.0	28.0	32.0
S12/41 A	21.0	30.6	34.0	38.0	41.0
S12/60 A	30.0	42.5	47.5	50.0	60.0
S12/85 A	55.0	68.5	74.0	76.0	85.0
S12/90 A	50.5	72.0	78.0	84.0	90.0
S12/130 A	66.0	93.5	104.5	110.0	130.0
S12/230 A	120.0	170.0	190.0	200.0	230.0

Drawings with terminal position, terminal and torque

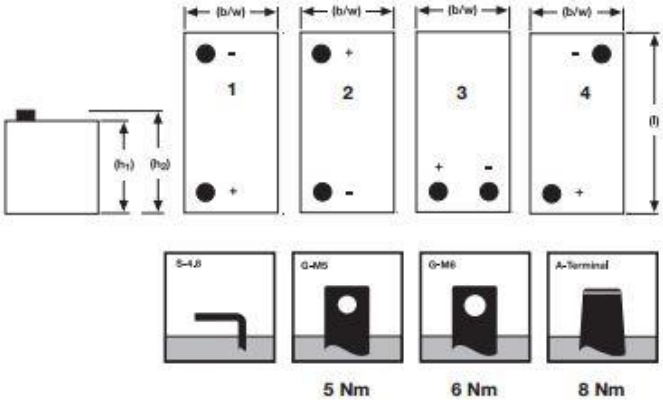

Not to scale!

3

Appendix 3: Parameters of Maxwell 75V modules: BMOD0094 P075 B02

DATASHEET **75V MODULE**

FEATURES AND BENEFITS*

- Up to 15 year DC life
- 75V DC working voltage
- Resistive cell balancing
- Temperature outputs
- High power density

TYPICAL APPLICATIONS

- Wind turbine pitch control
- UPS systems

PRODUCT SPECIFICATIONS

ELECTRICAL	BMOD0094 P075 B02
Rated Capacitance[1]	94 F
Minimum Capacitance, initial[1]	94 F
Maximum Capacitance, initial[1]	113 F
Maximum ESR_{DC}, initial[1]	13 mΩ
Test Current for Capacitance and ESR_{DC}[1]	100 A
Rated Voltage	75 V
Absolute Maximum Voltage[2]	91 V
Absolute Maximum Current	1,900 A
Leakage Current at 25°C, maximum [3]	50 mA
Maximum Series Voltage	750 V
Capacitance of Individual Cells[9]	3,000 F
Maximum Stored Energy, Individual Cell[9]	3.0 Wh
Number of Cells	32
TEMPERATURE	
Operating Temperature (Cell Case Temperature)	
Minimum	-40°C
Maximum	65°C
Storage Temperature (Stored Uncharged)	
Minimum	-40°C
Maximum	70°C

*Results may vary. Additional terms and conditions, including the limited warranty, apply at the time of purchase. See the warranty details for applicable operating and use requirements.

Maxwell TECHNOLOGIES Enabling Energy's Future™

PRODUCT SPECIFICATIONS (Cont'd)

PHYSICAL	BMOD0094 P075 B02
Mass, typical	25 kg
Power Terminals	M8/M10
Recommended Torque - Terminal	20/30 Nm
Vibration Specification	SAE J2380
Shock Specification	N/A
Environmental Protection	IP54
Cooling	Natural Convection
MONITORING / CELL VOLTAGE MANAGEMENT	
Internal Temperature Sensor	RTD
Temperature Interface	Analog
Cell Voltage Monitoring	N/A
Connector	Harting
Cell Voltage Management	Passive
POWER & ENERGY	
Usable Specific Power, P_d[4]	2,100 W/kg
Impedance Match Specific Power, P_{max}[5]	4,300 W/kg
Specific Energy, E_{max}[6]	2.9 Wh/kg
Stored Energy, E_{stored}[7]	73 Wh
SAFETY	
Short Circuit Current, typical (Current possible with short circuit from rated voltage. Do not use as an operating current.)	5,800 A
Certifications	RoHS
High-Pot Capability[10]	2,500 VDC

TYPICAL CHARACTERISTICS

THERMAL CHARACTERISTICS	BMOD0094 P075 B02
Thermal Resistance (R_{ca} All Cell Cases to Ambient), typical[8]	0.50°C/W
Thermal Capacitance (C_{th}), typical	19,000 J/°C
Maximum Continuous Current (ΔT = 15°C)[8]	48 A_{RMS}
Maximum Continuous Current (ΔT = 40°C)[8]	78 A_{RMS}
LIFE	
DC Life at High Temperature[1] (held continuously at Rated Voltage and Maximum Operating Temperature)	1,500 hours
Capacitance Change (% decrease from minimum initial value)	20%
ESR Change (% increase from maximum initial value)	100%
Projected DC Life at 25°C[1] (held continuously at Rated Voltage)	15 years
Capacitance Change (% decrease from minimum initial value)	20%
ESR Change (% increase from maximum initial value)	100%
Shelf Life (Stored uncharged at 25°C)	4 years

ESR AND CAPACITANCE VS TEMPERATURE

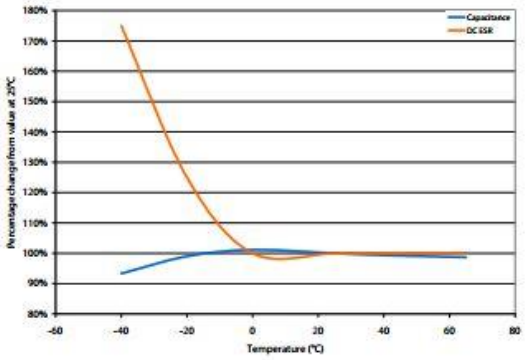

Maxwell TECHNOLOGIES Enabling Energy's Future™

NOTES

1. Capacitance and ESR_{DC} measured at 25°C using specified test current per waveform below.
2. Absolute maximum voltage, non-repeated. Not to exceed 1 second.
3. After 72 hours at rated voltage. Initial leakage current can be higher.
4. Per IEC 62391-2, $P_d = \frac{0.12V^2}{ESR_{DC} \times mass}$
5. $P_{max} = \frac{V^2}{4 \times ESR_{DC} \times mass}$
6. $E_{max} = \frac{½\ CV^2}{3{,}600 \times mass}$
7. $E_{stored} = \frac{½\ CV^2}{3{,}600}$
8. $\Delta T = I_{RMS}^2 \times ESR \times R_{ca}$
9. Per United Nations material classification UN3499, all Maxwell ultracapacitors have less than 10 Wh capacity to meet the requirements of Special Provisions 361. Both individual ultracapacitors and modules composed of those ultracapacitors shipped by Maxwell can be transported without being treated as dangerous goods (hazardous materials) under transportation regulations.
10. Duration = 60 seconds. Not intended as an operating parameter.

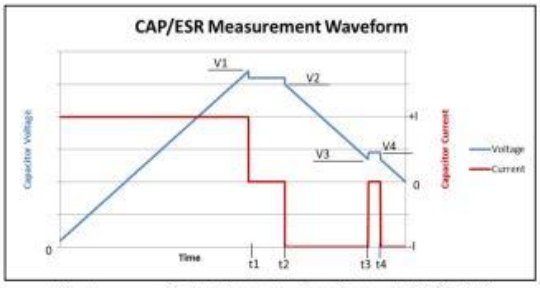

$V1 = V_{rated}$ t2 - t1 = 15 seconds Capacitance = I x (t3-t2)/(V2-V3)
$V3 = 0.5 \times V_{rated}$ t4 - t3 = 5 seconds ESR = (V4 - V3)/I

MOUNTING RECOMMENDATIONS

Please refer to the user manual for installation recommendations

MARKINGS

Products are marked with the following information: Rated capacitance, rated voltage, product number, name of manufacturer, positive and negative terminal, warning marking, serial number.

BMOD0094 P075 B02

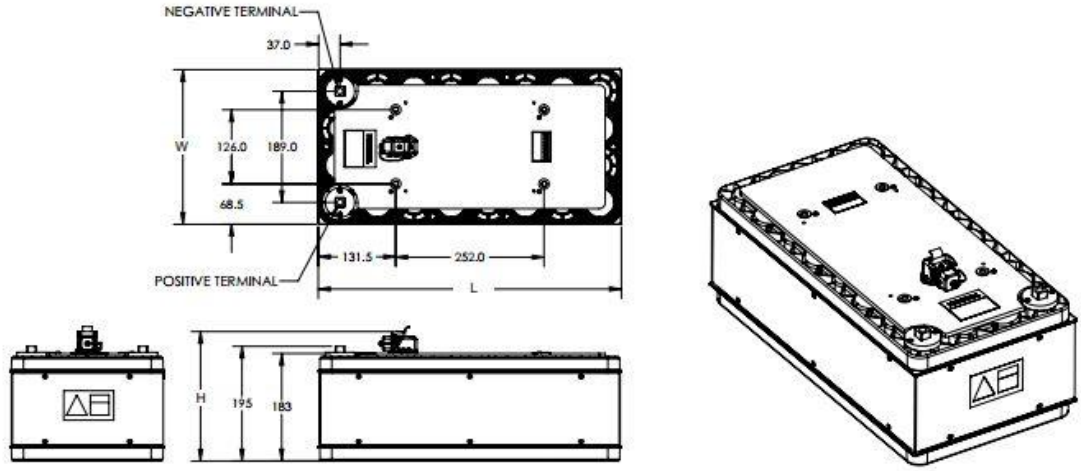

Part Description	Dimensions (mm) L (±0.3mm)	W (±0.2mm)	H (±0.7mm)	Package Quantity
BMOD0094 P075 B02	515	263	220	1

Product dimensions are for reference only unless otherwise identified. Product dimensions and specifications may change without notice.
Please contact Maxwell Technologies directly for any technical specifications critical to application. All products featured on this datasheet are covered by the following U.S. patents and their respective foreign counterparts: 6643119, 7295423, 7342770, 7352558, 7384433, 7440258, 7492571, 7508651, 7791860, 7791861, 7859826, 7883553, 7935155, 8072734, 8098481, 8279580, and patents pending.

Maxwell Technologies, Inc.
Global Headquarters
3888 Calle Fortunada
San Diego, CA 92123
USA
Tel: +1 858 503 3300
Fax: +1 858 503 3301

Maxwell Technologies SA
Route de Montena 65
CH-1728 Rossens
Switzerland
Tel: +41 (0)26 411 85 00
Fax: +41 (0)26 411 85 05

Maxwell Technologies, GmbH
Leopoldstrasse 244
80807 München
Germany
Tel: +49 (0)89 / 4161403 0
Fax: +49 (0)89 / 4161403 99

Maxwell Technologies, Inc.
Shanghai Trading Co. Ltd.
Unit A2,C 12th Floor
Huarun Times Square
500 Zhangyang Road,
Pudong New Area
Shanghai 200122,
P.R. China
Phone: +86 21 3852 4000
Fax: +86 21 3852 4099

Maxwell Technologies Korea Co., Ltd.
Room 1524, D-Cube City
Office Tower, 15F #662
Gyeongin-Ro, Guro-Gu,
Seoul, 152-706
South Korea
Phone: +82 10 4518 9829

Maxwell TECHNOLOGIES
Enabling Energy's Future™

Appendix 4: Parameters of SDMO Technic 6500E AVR

KOHLER
SDMO

TECHNIC 6500 E AVR

PORTABLE POWER

Generating Sets Range TECHNIC

PRODUCT ADVANTAGES

- Entire group guaranteed 3 years
- KOHLER air-cooled industrial engine
- Connection interface equipped with an hour meter
- Electric starter with batteries without maintenance
- AVR : Automatic tension regulation

QUAD CLEAN AIR FILTER The Cyclonic Quad Clean air filters provide 4 levels of filtration which effectively filter out large particles and capture the finest particles. They ensure a continuous supply of clean air to the engine, fuel economies, increase the engine performance and extend its lifetime
AVR By regulating the voltage electronically by ±2%, depending on the model, the AVR eliminates all risk of damage to boilers or certain kinds of electronic equipment.

Range TECHNIC
A long run time equipment that can withstand extreme conditions, for daily professional use.

TECHNIC 6500 E AVR

GENERAL SPECIFICATIONS

Range	TECHNIC
Frequency (Hz)	50 Hz
Max power LTP (kW) *	6.50
Nominal voltage (V)	230
Number of Phase	Single phase
Fuel	Petrol
Tank (L)	18
75% cons. (l/h) *	2.60
75% Autonomy (h) *	6.90
Sound power level guaranteed LwA dB(A)	97
Acoustic pressure level @1m in dB(A)	83
Acoustic pressure level @7m in dB(A)	69

ENGINE SPECIFICATIONS

Engine brand	KOHLER
Engine type	CH440E
Distribution	O.H.V.
Start	Electrical Starter
Oil shutdown	Oui
Displacement (cm3)	429
Oil system capacity including filters (L)	1.30

ALTERNATOR SPECIFICATIONS

Technology	Collar and brush
AVR Regulation	Yes
Indication of protection	IP 23
Insulation class	H

PLUGS AND PANEL DESCRIPTIVE

1 230V 10/16A socket - circuit breaker + 1 230V 32A socket - circuit breaker + hour meter

DIMENSIONS AND WEIGHT

Lenght (cm)	81
Width (cm)	55.50
Height (cm)	59
Dry Weight (kg)	101

PACKAGING

Packaging type	Box
Length (cm)	82
Width (cm)	56.50
Height (cm)	60
Weight (kg)	104
Pallet type	120/80
Number of box by pallet	6
Pallet height (cm)	193
weight of the packaged Pallet (kg)	634

KOHLER
SDMO

10/30/2017

Appendix 5: Parameters of programmable electric load PL-6000-A Puissance+

GENERAL SPECIFICATIONS:

INPUT RATING

Voltage range:	230V+6%/-10%
Frequency range:	47-65Hz

PROGRAMMATION VALUE

Voltage accuracy:	0.05%FS+0.05%V
Voltage resolution:	12 bits
Current accuracy:	0.01%FS+0.01%V
Current resolution:	12 bits
Power accuracy:	0.05%FS+0.05%V
Power resolution:	12 bits

REGULATION

Voltage line regulation:	0.01%
Voltage load regulation:	0.05%
Current line regulation:	0.1%
Current load regulation:	0.05%
Power line regulation:	0.5%
Power load regulation:	0.1%
Sense:	2V

DYNAMIC MODE

Bandwidth:	2kHz
Rise & fall time:	<20µs
Overshoot:	<5%
Recovery time:	<20 µs

SIGNAL QUALITY

Voltage Ripple & Noise (rms)	0.2%
Voltage Ripple & Noise (Pk-Pk)	2%
Current Ripple & Noise (rms)	0.2%
Current Ripple & Noise (Pk-Pk)	2%

MEASUREMENT

Voltage accuracy:	0.1%FS
Current accuracy:	0.1%FS

PROTECTION

Over voltage/Over current/Over temperature/Reverse current

ISOLATION

Line/output:	100 MΩ @ 500Vdc
Output to case:	10 MΩ @ 500Vdc

DIELECTRIC

Line to output:	2500Veff-50Hz
Line to case:	1500Veff

ENVIRONMENT

Operating temperature:	-10°C/40°C
Storage temperature:	-25°C/80°C
Humidity:	10-90%
Protection:	IP30

CONFORMITY

CE

STANDARD REMOTE CONTROL

HMI:	touchscreen display
	Waveform storage

ANALOG
ETHERNET
RS232

OPTION

Power analyzer	POW-ANA-PL
Specific range	SR-PL
Double range	DR-PSA
10kHz bandwidth	WBW-PL
Control Resistance	CR-PL
IEEE remote control	IEEE
Last configuration data save	MEM
MASTER configuration	PSAM
SLAVE configuration	PSAS

SOFTWARE option

Arbitrary function generator	OPS1
Advanced Sequence	OPS4
MPP tracking	MPP

Appendix 6: Parameters of IGBT module SEMIKRON SKM100GB063D

SKM 100GB063D

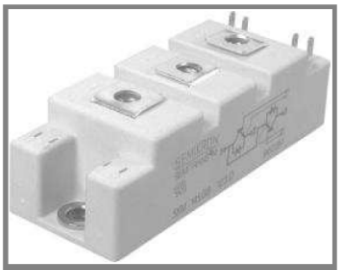

SEMITRANS® 2

Superfast NPT-IGBT Module

SKM 100GB063D

Features

- N channel, homogeneous Silicon structure (NPT- Non punch through IGBT)
- Low tail current with low temperature dependence
- High short circuit capability, self limiting if term. G is clamped to E
- Pos. temp.-coeff. of V_{CEsat}
- Very low C_{ies}, C_{oes}, C_{res}
- Latch-up free
- Fast & soft inverse CAL diodes
- Isolated copper Bonding Technology without hard mould
- Large clearance (10 mm) and creepage distances (20 mm)

Typical Applications*

- Switching (not for linear use)
- Switched mode power supplies
- UPS
- Three phase inverters for servo / AC motor speed control
- Pulse frequencies also above 10 kHz

Absolute Maximum Ratings			T_c = 25 °C, unless otherwise specified	
Symbol	**Conditions**		**Values**	**Units**
IGBT				
V_{CES}	T_j = 25 °C		600	V
I_C	T_j = 150 °C	T_{case} = 25 °C	130	A
		T_{case} = 70 °C	100	A
I_{CRM}	I_{CRM}=2xI_{Cnom}		200	A
V_{GES}			± 20	V
t_{psc}	V_{CC} = 300 V; $V_{GE} \leq$ 20 V; V_{CES} < 600 V	T_j = 125 °C	10	µs
Inverse Diode				
I_F	T_j = 150 °C	T_{case} = 25 °C	100	A
		T_{case} = 80 °C	75	A
I_{FRM}	I_{FRM}=2xI_{Fnom}		200	A
I_{FSM}	t_p = 10 ms; sin.	T_j = 150 °C	720	A
Module				
$I_{t(RMS)}$			200	A
T_{vj}			- 40 ... + 150	°C
V_{isol}	AC, 1 min.		2500	V

Characteristics			T_c = 25 °C, unless otherwise specified			
Symbol	**Conditions**		**min.**	**typ.**	**max.**	**Units**
IGBT						
$V_{GE(th)}$	V_{GE} = V_{CE}, I_C = 2 mA		4,5	5,5	6,5	V
I_{CES}	V_{GE} = 0 V, V_{CE} = V_{CES}	T_j = 25 °C		0,1	0,3	mA
V_{CE0}		T_j = 25 °C		1,05		V
		T_j = 125 °C		1		V
r_{CE}	V_{GE} = 15 V	T_j = 25°C		10,5		mΩ
		T_j = 125°C		14		mΩ
$V_{CE(sat)}$	I_{Cnom} = 100 A, V_{GE} = 15 V	T_j = 25°C$_{chiplev.}$		2,1	2,5	V
		T_j = 125°C$_{chiplev.}$		2,4	2,8	V
C_{ies}	V_{CE} = 25, V_{GE} = 0 V	f = 1 MHz		5,6		nF
C_{oes}				0,6		nF
C_{res}				0,4		nF
Q_G	V_{GE} = 0V - +15V			240		nC
R_{Gint}	T_j = °C			0		Ω
$t_{d(on)}$	R_{Gon} = 10 Ω	V_{CC} = 300V		50		ns
t_r		I_C= 100A		40		ns
E_{on}		T_j = 125 °C		4		mJ
$t_{d(off)}$	R_{Goff} = 10 Ω	V_{GE} = ±15 V		300		ns
t_f				35		ns
E_{off}				3		mJ
$R_{th(j-c)}$	per IGBT				0,27	K/W

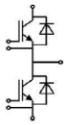

GB

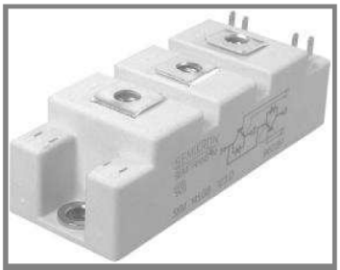

SEMITRANS® 2

Superfast NPT-IGBT Module

SKM 100GB063D

Characteristics						
Symbol	**Conditions**		**min.**	**typ.**	**max.**	**Units**
Inverse Diode						
$V_F = V_{EC}$	I_{Fnom} = 100 A; V_{GE} = 0 V	T_j = 25 °$C_{chiplev.}$		1,55	1,9	V
		T_j = 125 °$C_{chiplev.}$		1,55		V
V_{F0}		T_j = 125 °C			0,9	V
r_F		T_j = 125 °C		8	10	mΩ
I_{RRM}	I_F = 100 A	T_j = 125 °C		44		A
Q_{rr}				6		µC
E_{rr}	V_{GE} = -15 V; V_{CC} = 300 V					mJ
$R_{th(j-c)D}$	per diode				0,6	K/W
Module						
L_{CE}					30	nH
$R_{CC'+EE'}$	res., terminal-chip	T_{case}= 25 °C		0,75		mΩ
		T_{case}= 125 °C		1		mΩ
$R_{th(c-s)}$	per module				0,05	K/W
M_s	to heat sink M6		3		5	Nm
M_t	to terminals M5		2,5		5	Nm
w					160	g

Appendix 7: Parameters of industrial driver (SEMIKRON SKHI22A) for IGBT

SKHI 22 A / B (R) ...

SEMIDRIVER™

Hybrid Dual IGBT Driver

SKHI 22 A / B (R)

Features

- Double driver for halfbridge IGBT modules
- SKHI 22A is compatible to old SKHI 22
- SKHI 22B has additional functionality
- CMOS compatible inputs
- Short circuit potection by V_{CE} monitoring and switch off
- Drive interlock top / bottom
- Isolation by transformers
- Supply undervotage protection (13 V)
- Error latch / output

Typical Applications

- Driver for IGBT modules in bridge circuits in industrial applications

1) see fig. 6

2) At R_{CE} = 18 kΩ, C_{CE} = 330 pF

Absolute Maximum Ratings

Symbol	Conditions	Values	Units
V_S	Supply voltage prim.	18	V
V_{iH}	Input signal volt. (High) SKHI 22A	V_S + 0,3	V
	SKHI 22B	5 + 0,3	V
$Iout_{PEAK}$	Output peak current	8	A
$Iout_{AVmax}$	Output average current	40	mA
f_{max}	max. switching frequency	50	kHz
V_{CE}	Collector emitter voltage sense across the IGBT	1200	V
dv/dt	Rate of rise and fall of voltage secondary to primary side	50	kV/µs
V_{isolIO}	Isolation test voltage input - output (2 sec. AC)	2500	Vac
V_{isol12}	Isolation test voltage output 1 - output 2 (2 sec. AC)	1500	V
R_{Gonmin}	Minimum rating for R_{Gon}	3	Ω
$R_{Goffmin}$	Minimum rating for R_{Goff}	3	Ω
$Q_{out/pulse}$	Max. rating for output charge per pulse	4[1)]	µC
T_{op}	Operating temperature	- 40 ... + 85	°C
T_{stg}	Storage temperature	- 40 ... + 85	°C

Characteristics T_a = 25 °C, unless otherwise specified

Symbol	Conditions	min.	typ.	max.	Units
V_S	Supply voltage primary side	14,4	15	15,6	V
I_{SO}	Supply current primary side (no load)		80		mA
	Supply current primary side (max.)			290	mA
V_i	Input signal voltage SKHI 22A on/off		15 / 0		V
	SKHI 22B on/off		5 / 0		V
V_{iT+}	Input threshold voltage (High) SKHI 22A			12,5	V
	SKHI 22B			3,9	V
V_{iT-}	Input threshold voltage (Low) SKHI 22A	4,5			V
	SKHI 22B	1,5			V
R_{in}	Input resistance SKHI 22A		10		kΩ
	SKHI 22B		3,3		kΩ
$V_{G(on)}$	Turn on gate voltage output		+ 15		V
$V_{G(off)}$	Turn off gate voltage output		- 7		V
R_{GE}	Internal gate-emitter resistance		22		kΩ
f_{ASIC}	Asic system switching frequency		8		MHz
$t_{d(on)IO}$	Input-output turn-on propagation time	0,85	1	1,15	µs
$t_{d(off)IO}$	Input-output turn-off propagation time	0,85	1	1,15	µs
$t_{d(err)}$	Error input-output propagation time		0,6		µs
$t_{pERRRESET}$	Error reset time		9		µs
t_{TD}	Top-Bot Interlock Dead Time SKHI 22A		4,3		µs
	SKHI 22B	no interlock		4,7	µs
V_{CEsat}	Reference voltage for V_{CE}-monitoring		5[2)]	10	V
C_{ps}	Coupling capacitance primary secondary		12		pF
MTBF	Mean Time Between Failure T_a = 40°C		2,0		10^6 h
w	weight		45		g

This technical information specifies semiconductor devices but promises no characteristics. No warranty or guarantee expressed or implied is made regarding delivery, performance or suitability.